UNIVERSIDAD COMPLUTENSE DE MADRID

FACULTAD DE CIENCIAS BIOLÓGICAS

DEPARTAMENTO DE BIOQUÍMICA Y BIOLOGÍA MOLECULAR

DESIGN AND BIOMEDICAL APPLICATIONS OF FUNCTIONALIZED BIOMATERIALS BASED ON BACTERIAL POLYESTERS

DISEÑO Y APLICACIONES BIOMÉDICAS DE BIOMATERIALES FUNCIONALIZADOS BASADOS EN POLIÉSTERES DE ORIGEN BACTERIANO

TESIS DOCTORAL DE:

NADIA DINJASKI

BAJO LA DIRECCIÓN DE:

MARÍA AUXILIADORA PRIETO JIMÉNEZ

Madrid, 2013

UNIVERSIDAD COMPLUTENSE DE MADRID

FACULTAD DE CIENCIAS BIOLÓGICAS
DEPARTAMENTO DE BIOQUÍMICA Y BIOLOGÍA MOLECULAR

Design and biomedical applications of functionalized biomaterials based on bacterial polyesters

TESIS DOCTORAL

NINA DINJASKI

Madrid, 2013

UNIVERSIDAD COMPLUTENSE DE MADRID
FACULTAD DE CIENCIAS BIOLÓGICAS
DEPARTAMENTO DE BIOQUÍMICA Y BIOLOGÍA MOLECULAR

Design and biomedical applications of functionalized biomaterials based on bacterial polyesters

TESIS DOCTORAL

NINA DINJASKI

DIRECTORA:

MARÍA AUXILIADORA PRIETO JIMÉNEZ

CONSEJO SUPERIOR DE INVESTIGACIONES CIENTÍFICAS
CENTRO DE INVESTIGACIONES BIOLÓGICAS

Madrid, 2013

Summary

INTRODUCCIÓN

Los polihidroxialcanoatos (PHA), conocidos comúnmente como “bioplásticos”, son polímeros biodegradables que se acumulan en forma de gránulos en el interior celular de algunas bacterias. Son biopolímeros sintetizados a partir de fuentes renovables, que pueden ser biodegradados en condiciones controladas, y que presentan características físico-químicas similares a las de los plásticos derivados de la industria petroleoquímica (Rehm, 2010). Dado que los PHA no son tóxicos, son biodegradables y biocompatibles, estos compuestos tienen un gran potencial para múltiples aplicaciones debido a su posible uso como biomateriales. Por tanto, la síntesis de nuevos PHA es de gran interés desde los puntos de vista industrial y biomédico, ya que los nuevos biopolímeros, así como los monómeros que los componen, presentan propiedades físico-químicas y mecánicas diferentes a los PHA convencionales.

Las infecciones asociadas a los implantes y un incremento alarmante de la resistencia a los antibióticos justifica la necesidad de generar nuevas superficies antimicrobianas para el desarrollo de los biomateriales en el campo de la ingeniera de los tejidos. Los poliésteres bacterianos, PHA, son una de las clases más importantes de biomateriales debido a sus propiedades biocompatibles y biodegradables. Entre otras, una de las posibles aplicaciones requeridas para algunos materiales de uso clínico o alimentario, es su capacidad para actuar como materiales bacteriostáticos o bactericidas, de tal manera que los objetos, embases o dispositivos construidos con estos materiales puedan evitar la proliferación de las bacterias (propiedad bacteriostática) o puedan incluso provocar la muerte de las bacterias en contacto (propiedad bactericida). Los polímeros antimicrobianos representan una clase de biocidas cada vez más importante como una alternativa a los biocidas existentes y en algunos casos incluso a los antibióticos (Siedenbiedel y Tiller, 2012).

En este sentido, en esta Tesis Doctoral se han utilizado dos estrategias para la funcionalización de PHA con alto valor añadido con aplicaciones en los sectores industrial y biomédico. La primera estrategia consiste en la producción bacteriana *in vivo* de nano-particulas functionalizadas, las cuáles han sido diseñadas para exponer

proteínas de fusión en su superficie. Los gránulos de PHA pueden ser utilizados como nano-particulas para inmovilización de proteínas recombinantes mediante el sistema BioF, previamente establecido en el laboratorio. Este sistema se basa en el uso del N-terminal de fasina PhaF de *Pseudomonas putida* KT2440 como tag de afinidad, lo que permite anclar proteínas recombinantes al granulo de PHA (Moldes et al., 2004). Uno de los inconvenientes del sistema BioF para purificar e inmovilizar proteínas es el bajo rendimiento, dado que no toda la proteína fusionada se une al gránulo, y que gran parte de la superficie del gránulo está ocupada por las fasinas naturales. Este sistema ha sido mejorado mediante el estudio del proceso de unión del tag al gránulo de PHA y la identificación de los requerimientos mínimos que permiten la formación y segregación del gránulo del PHA entre las células hijas durante la división celular.

La segunda estrategia aplicada se basa en el uso de la ingeniería metabólica para diseñar las cepas bacterianas capaces de producir nuevos poliésteres. Se estudiaron las propiedades de los nuevos PHA obtenidos por fermentación, denominados PHACOS, que contienen monómeros con grupos tioéster en la cadena lateral (Escapa et al., 2011).

Resultados y discusión

Para optimizar el sistema BioF de inmovilización de proteínas *in vivo* a gránulos de PHA se ha estudiado primeramente la función fisiológica de fasina PhaF, determinándose que interviene en la segregación de los gránulos durante la división celular y en la localización de los gránulos en el citoplasma. Se han identificado dos funciones diferentes de los dominios C- y N-terminal de esta proteína. Se demostró que el C-terminal que contiene AAKP-like tandem repeats y se une a ADN de forma inespecífica, lo que está de acuerdo con su similitud con la famila de Histonas tipo H1. El N-terminal es responsable de la unión al gránulo y coincide con la secuencia del tag de afinidad BioF. Mediante microscopía electrónica de transmisión (TEM), láser confocal y multidimensional *in vivo*, se ha demostrado en las primeras fases de crecimiento de células que producen PHA, que la fasina PhaF dirige los gránulos al centro de la célula generando una distribución característica en forma de aguja en el citoplasma de *P. putida* KT2440. Además nuestros estudios de citometria de flujo en células mutantes en el gen *phaF* han demostrado la existencia de dos populaciones diferentes de células (la que contiene

y la que no contiene PHA). Estudios de complementación han demostrado que, además de su función en la localización celular de los gránulos, PhaF está implicada en segregación de los gránulos entre las células hijas durante la división celular. Los estudios *in vivo* de la proteína de fusión entre la proteína fluorescente verde (GFP) y el C-terminal de PhaF mediante microscopía confocal han demostrado la unión de C-terminal al nucleoide. Por lo tanto se ha hipotetizado el mecanismo de esta fasina en su función distribuidora de gránulos mediante la interacción del C-terminal con el cromosoma que se está segregando, y de forma simultánea, su unión al gránulo de PHA mediante el N-terminal o dominio BioF.

En esta Tesis doctoral, también se ha estudiado la implicación de la otra fasina de *P. putida* KT2440, la proteína PhaI, en la maquinaria de formación del gránulo de PHA. La fasina PhaI completa y el módulo BioF de la fasina PhaF son similares en su estructura primaria. En este trabajo se demuestra una función coordinada de los módulos de las fasinas (PhaI y N-terminal de PhaF) para la formación y distribución óptima de los gránulos de PHA. Por una parte, se estudió la producción de las proteínas recombinantes en distintas condiciones de crecimiento, tanto en la estirpe salvaje como en diferentes mutantes en fasinas de *P. putida*. Las construcciones de estos mutantes se llevaron acabo mediante la técnica de deleción con el plásmido pK18mobsac. Este sistema tiene la ventaja de que provoca deleciones géneticas dirigidas sin incorporar marcadores antibióticos, lo cual conlleva una ventaja desde el punto de vista medioambiental. Por otra, se estudió la localización de las fasinas fusionadas a la proteína GFP en presencia y ausencia del gránulo de PHA. Estas construcciones se llevaron acabo en el plásmido pCNB5 que contiene un mini-transposon, lo que facilita la inserción estable de la construcción genética en monocopia en el cromosoma de *P. putida*. Estos experimentos nos permitieron seleccionar la cepa y las condiciones más idóneas para la producción *in vivo* de nanopartículas de bioplásticos activas. Los estudios hechos mediante microscopía epifluorescente y citometria de flujo de los mutantes en fasinas de *P. putida* que producen la proteína recombinante BioF::GFP han demostrado que la distribución equilibrada después de la división celular se recupera cuando PhaF, y BioF o PhaI son sintetizados al mismo tiempo, demostrando la propiedad intercambiable de los módulos de las fasinas. Mediante western blot se ha confirmado que concentraciones muy bajas de la fasina natural PhaF son suficientes para asegurar la segregación de los gránulos entre las células hijas durante la división celular. Todos estos estudios han permitido construir y diseñar la cepa huésped óptima para ser utilizada en el sistema BioF, derivada de la cepa modelo *P. putida* KT2440 con las modificaciones genéticas mínimas que le han hecho idónea para producir nanopartículas de bioplásticos activas. La cuantificación de la proteína recombinante se llevo acabo mediante

citometria de flujo y fluorimetría. Este sistema representa una herramienta muy útil para la inmovilización *in vivo* de las proteínas activas a un soporte biodegradable para su uso en diagnóstico, liberación de antígenos y otros.

La segunda estrategia aplicada en esta Tesis doctoral para diseñar biomateriales funcionalizados consiste en el estudio de las propiedades de los nuevos PHA obtenidos por fermentación bacteriana, denominados PHACOS, que contienen monómeros con grupos tioéster en la cadena lateral. Se conoce muy poco sobre si los monómeros derivados de los PHAs convencionales pueden poseer actividad antibacteriana. Así por ejemplo, se ha descrito que algunos hidroxiácidos monoméricos derivados de PHAs tienen actividad sobre *Staphylococcus aureus* (Ruth et al., 2007). Sin embargo, la potencia antibacteriana de estos compuestos es baja ya que presentan unas MICs (Concentración Mínima Inhibitoria) muy altas, del orden de 1-5 mM.

Para investigar posible actividad antibacteriana de PHACOS, se produjo el poliéster siguiendo el protocolo de fermentación bacteriana previamente descrito (Escapa et al., 2011). La actividad antibacteriana de PHACOS y el PHA control no funcionalizado (PHO) frente diferentes cepas bacterianas se determino según la norma ISO 22196:2007 (E) (Medida de la actividad antibacteriana en superficies de plástico) con ciertas modificaciones. El resultado obtenido indicó que PHACOS inhibe el crecimiento de las cepas de *S. aureus* incluyendo tres aislados clínicos MRSA, de forma que sólo sobreviven un 10% de las células cuando se comparan con el control.

Además, se estudió la capacidad de PHACOS para evitar la formación de biopelículas bacterianas en su superficie en comparación con otros materiales. A tal fin se utilizó como modelo las bacterias *S. aureus* CECT 86 y *P. aeruginosa* CECT 4122 que son capaces de formar biopelículas en la superficie de distintos materiales. La capacidad de las bacterias para formar biopelículas en las superficies de los materiales biopoliméricos, se examinó mediante dos procedimientos: i) la tinción de la biopelícula con el colorante cristal violeta; y ii) el contaje de las unidades formadoras de colonia (UFC) de bacterias adheridas a los discos. Los resultados obtenidos demostraron que la presencia de PHACOS provoca una disminución de dos veces en la formación de biopelículas de *S. aureus* y no de *P. aeruginosa* comparado con el polímero control. Además, se estudió la capacidad de PHACOS para matar las bacterias adheridas a su superficie en comparación con otros materiales. El número y la viabilidad de las bacterias adheridas a la superficie de los biopolímeros se determinaron por microscopía de fluorescencia utilizando la prueba de viabilidad bacteriana el BacLightTM LIVE / DEAD

(Invitrogen L13152). Los resultados demostraron que el 80% de las células de *S. aureus* no fueron viables, es decir, mueren tras entrar en contacto con PHACOS. Sin embargo, tan solo un 17 % de las células no son viables tras entrar en contacto con polímero control. El número total de bacterias (viables y no viables) adheridas a discos recubiertos de PHACOS comparadas con las bacterias presentes en los discos controles recubiertos con PHO fue similar, lo que demuestra que la adhesión bacteriana no está disminuida, pero sí que se afecta la supervivencia de las bacterias.

Por otro lado, se estudió la biocompatibilidad y actividad antimicrobiana de PHO y PHACOS *in vivo* en ratones BALB c mediante el uso de una sonda fluorescente (H-ICG). Este trabajo se realizó en colaboración con el grupo del Dr. Andrés García (Georgia Institute of Technology, Atlanta, USA). Se demostró tanto la biocompatibilidad de PHO y PHACOS como la actividad antimicrobiana de PHACOS *in vivo*. Por lo tanto, se concluyó que el PHACOS es un material con capacidad antibacteriana intrínseca, tal cual se obtiene de la fermentación bacteriana, sin tener que modificarlo químicamente.

En general, se pueden distinguir tres tipos de polímeros antimicrobianos: biocidas poliméricos, polímeros biocidas y polímeros liberadores de biocidas. Los biocidas poliméricos son polímeros que constan de unidades de repetición bioactivas, es decir, los polímeros son múltiples biocidas interconectados, que actúan de manera similar a los monómeros. No siempre, la polimerización de monómeros biocidas conduce a polímeros antimicrobianos activos, ya sea, debido a que los polímeros son insolubles en agua o las funciones biocidas no llegan a su destino. Los polímeros biocidas son usualmente macromoléculas cargadas positivamente que interactúan con las células microbianas que generalmente llevan una carga negativa neta en la superficie debido a sus proteínas de membrana, a los ácidos teicoicos en las bacterias Gram-positivas, y a los fosfolípidos cargados negativamente en la membrana externa de las bacterias Gram-negativas. Los últimos experimentos que forman parte de esta Tesis doctoral demuestran la actividad microbiana de los monómeros que componen el polímero PHACOS, por lo que se propone que PHACOS es un biocida polimérico.

Abbreviations

3HA	(*R*)-3-hydroxyalkanoate
3HD	(*R*)-3-hydroxydecanoate
3HDD	(*R*)-3-hydroxydodecanoate
3HHx	(*R*)-3-hydroxyhexanoate
3HO	(*R*)-3-hydroxyoctanoate
3MB	3-mercaptobutyrate
3MP	3-mercaptopropionate
6-ATH	6-acetylthiohexanoic acid
mcl-OHAs	medium-chain-length oligo(3-hydroxyalkanoates)
OH-4ATB	3-hydroxy-4-acetylthiobutanoate
OH-6ATH	3-hydroxy-6-acetylthiohexanoate
OHAs	oligo(hydroxyalkanoates)
OHB	oligo(3-hydroxybutyrate)
OHB-*co*-4HB	oligo(3-hydroxybutyrate-*co*-4-hydroxybutyrate)
OHB-*co*-HHx	oligo(3-hydroxybutyrate-*co*-3-hydroxyhexanoate)
OH-C6	3-(*R*)-hydroxyhexanoate
OH-C8	3-(*R*)-hydroxyoctanoate
OH-C10	3-(*R*)-hydroxydecanoate
P4HB	poly(4-hydroxybutyrate)
PBS	phosphate buffer saline
PEG	polyethylene glycol
PHA	polyhydroxyalkanoate
PHACOS	poly((*R*)-3-hydroxyacilthioalkanoate-*co*-3- hydroxyalkanoate)
PHB	poly((*R*)-3-hydroxybutyrate)
PHB-*co*-HHx	poly((*R*)-3-hydroxybutyrate-*co*-(*R*)-3-hydroxyhexanoate)
PHB-*co*-HV	poly((*R*)-3-hydroxybutyrate-*co*-(*R*)-3-hydroxyvalerate)
PHD	poly(3-hydroxydecanoate)
PHO	poly((*R*)-3-hydroxyoctanoate)
PHO-*co*-HHx	poly(3-hydroxyoctanoate-*co*-3-hydroxyhexanoate)
PHO-*co*-HU	poly(3-hydroxyoctanoate-*co*-3-hydroxyundecenoate)
PLA	poly-lactic acid
RHAs	*(R)*-hydroxyalkanoic acids

INDEX

I. Introduction

1. Polyhydroxyalkanoates (PHA) historical outline

Bacterial polyhydroxyalkanoates (PHA) constitute a family of biopolyesters composed of range of different polymers, mainly discovered during the past 20 years (Steinbüchel, 1991). The exception is the simplest member of the class, poly((*R*)-3-hydroxybutyrate) (PHB), that was first identified in 1926 in *Bacillus megaterium* (Lemoigne, 1926) and is the most well-known PHA polymer.

During the 1980´s, many companies have tried to produce various PHA at pilot or industrial scales. The British company, Imperial Chemical Industries (ICI), developed a commercial process to produce PHB, and the copolymer poly((*R*)-3-hydroxybutyrate-*co*-(*R*)-3-hydroxyvalerate) (PHB-*co*-HV) (Chen, 2009). Over the past years, PHA as polymeric materials have been designed for biomedical application, as drug delivery carriers, nutritional supplements, drugs, fine chemicals and others (Chen and Wu, 2005). More recent interest in the medical application as implants has arisen, primarily in response to the emerging needs of the field of tissue engineering. In fact, in the past two years PHA has become one of the leading classes of biomaterials under investigation for the development of tissue-engineered cardiovascular products, due to their properties not available in existing synthetic absorbable polymers. Although most products containing these materials have yet to be approved for *in vivo* medical use, some companies are currently engaged in the development of diverse tissue-engineered products based on PHA polymers (*e.g*. Tepha, Inc., USA). PHA draw particular interest since they were shown to be biodegradable and biocompatible (Brandl et al., 1995; Brandl et al., 1990). The best approach for achievement of those properties is by production in bacteria, thus, guaranteeing complete stereospecificity (all chiral carbon atoms in the back-bone are in the *R* configuration), which is essential for their biodegradability and biocompatibility. Both, the type of bacterium and growth conditions determine the chemical composition of PHA as well as the molecular weight, which typically ranges from 2×10^5 to 3×10^6 Da (Byrom, 1987; Lee, 1996).

Apart from immense potential for medical applications, due to the biodegradable properties and natural origin, PHA is being also considered as bioplastics, an alternative to the plastic materials derived from petrochemicals. Since bacteria utilize

renewable sources for the production of PHA, dependency on fossil resources can be reduced (Chen, 2009; Chen and Patel, 2011). Currently the production costs of bioplastics synthesis is 5–10 times higher compared to the cost of synthesis of plastics derived from petrochemicals, which is up to date a major hindrance for the successful commercialization of bioplastics (Rehm, 2010).

This work will focus on design and application of added value PHA using different approaches for polymer functionalization. The strategy is founded on seizing the advantages of intrinsic polymer features and adding modifications that confer new properties to the biomaterial for medical applications. The work is based on the processes developed in bacterial model strain *Pseudomonas putida* KT2440 and therefore in many aspects will be centered on PHA produced by this strain.

2. Occurrence of PHA

PHA are synthesized by many bacteria as carbon and energy storage in response to the excess of carbon source, when growth is limited due to starvation of other nutrients as for instance nitrogen and phosphorus (Madison and Huisman, 1999; Preito et al., 2007; Escapa et al, 2012). PHA is accumulated in a form of intracellular inclusions with an amorphous, hydrophobic PHA core mainly enveloped by proteins involved in PHA metabolism (see section 3; Potter and Steinbüchel, 2005) (Figure 1).

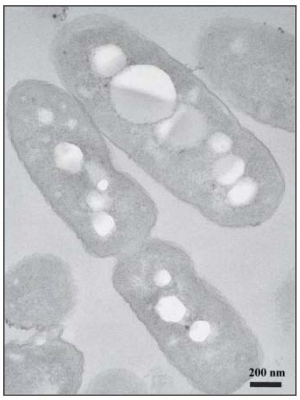

Figure 1. Transmission electron microscopy (TEM) image of mcl-PHA producing *P. putida* KT2442 cells. PHA reserve granules are located intracellularly. The number and the size of granules is specie dependent ranging from 100-500nm and 2-8 granules per cell.

This accumulation is subject to extensive regulation (i) at enzymatic level, by cofactor inhibition and availability of metabolites (Escapa et al., 2012; de Eugenio et al., 2010a), (ii) at transcriptional level by specific and global transcriptional regulatory factors (De Eugenio et al., 2010a and 2010b) and (iii) at translational level driven by global post-transcriptional regulators (Olearly 2012; de Eugenio PhD-thesis). Moreover, new investigations of PHB granules revealed that granules isolated in native form can perform their function autonomously of the rest of the cell content since they harbour all proteins required for PHA metabolism (Jendrossek, 2009). Therefore, they are considered as subcellular organelles, named carbonosomes, performing at least tree functions (PHA synthesis, storage and mobilization).

PHA have been classified according to various criteria: i) their monomer size as short-chain-length PHA (scl-PHA), with C4-C5 monomers and medium-chain-length PHA(mcl-PHA) with C6-C14 monomers, (Anderson et al., 1990) ii) their functional substituents found in the radical chain (such as double bonds or aromatic groups), or iii) the structure of the polymer (formed by homogenous, random or block copolymers) (Olivera et al. 2010a) (Figure 2).

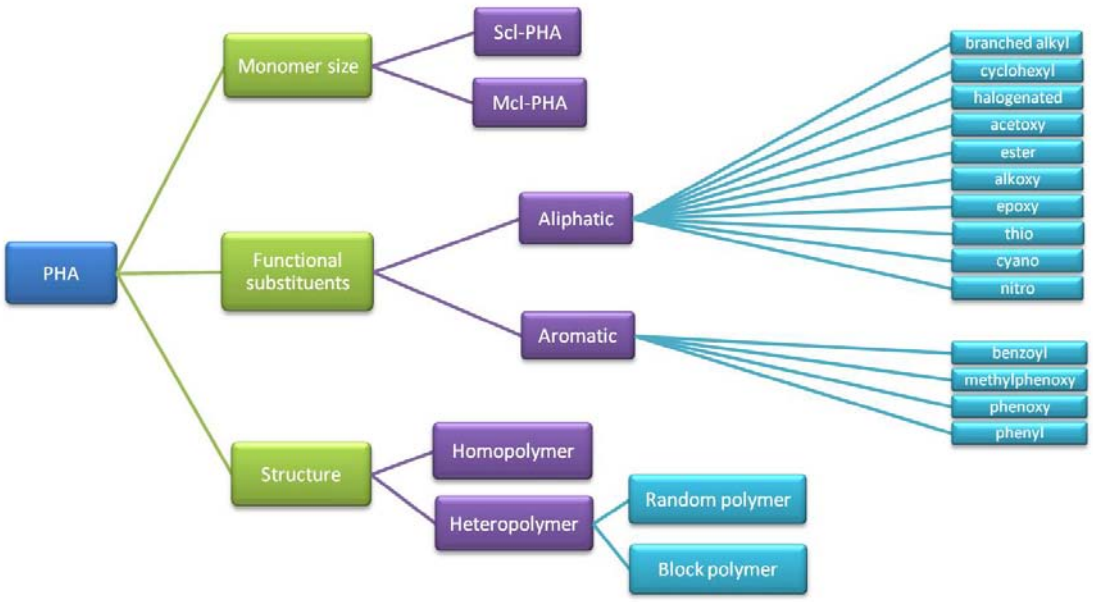

Figure 2. Classification of PHA according to different criteria.

Scl-PHA such as PHB and its copolymers PHB-*co*-HV are being produced on a commercial scale, and they have been extensively applied for packaging, molding, fibers and other commodities (Chen, 2009). Mcl-PHA mainly produced by bacteria belonging to genera *Pseudomonas,* are currently considered promising candidates for bioplastic applications owing the properties derived from their longer side-chains and altered crystalline structure, such as elasticity, hydrophobicity, low oxygen permeability, water resistance and biodegradability. They can be molded and processed into compostable packaging and resorbable materials for medical applications and have also been used as food coatings, pressure-sensitive adhesives, paint binders and biodegradable rubbers (Zinn et al., 2001, Elbahloul and Steinbüchel, 2009).

Furthermore, unconventional mcl-PHA bearing different functional moieties in their side chains can be produced through different biotechnological strategies that will be revised in detail in the following section. These reactive groups allow tuning of physical and chemical properties of the polymer, and represent potential targets for post-biosynthetic modifications (Escapa et al., 2011).

3. Granule associated proteins (GAPs): The PhaF Phasin

As previously mentioned, PHA constrain the hydrophobic core of intracellular inclusions surrounded by proteins involved in PHA metabolism (Potter and Steinbüchel, 2005). These granule associated proteins (GAPs), have been designated into following classes, namely, PHA synthases, depolymerases, regulatory proteins, acyl synthetase (ACS1) and phasins (Figure 3). *Pseudomonas* strains genes encoding GAPs proteins are organized in the *pha* cluster (Prieto et al., 2007). The organization of the *pha* gene cluster for the synthesis of mcl-PHA was partially reported in 1991 in the strain *Pseudomonas putida* GPo1 (Huisman *et al*., 1991) and completed in 1999 with the discovery of the genes encoding the phasins (Prieto *et al*., 1999) (Figure 4).

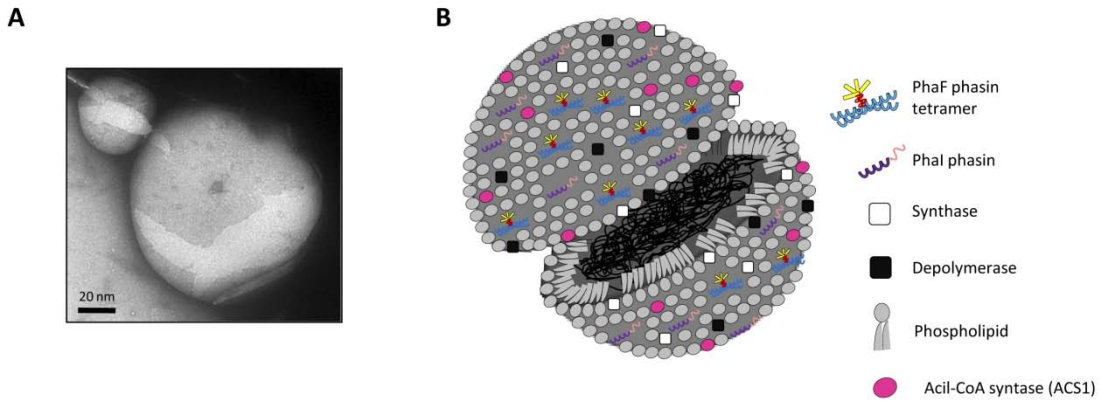

Figure 3. TEM image of *P. putida* KT2442 PHA granule (A) and a model of PHA granule structure (B). B, The PHA granule is composed of PHA core coated with phospholipid monolayer where granule-associated proteins GAPs (phasins, synthases, depolymerase, ACS1) are embedded or attached. Among GAPs phasins are the most aboundant proteins.

Phasins, the major GAPs, were described as amphiphilic proteins which generate an interphase between the cytoplasm and the hydrophobic core of PHA granules (Steinbüchel *et al*., 1995). They also play a role in controlling the size and the number of the granules per cell (Pieper-Furst *et al*., 1995; Wieczorek *et al*., 1995; Grage *et al*., 2009). Other functions proposed for phasins are prevention of protein misfolding on the granule surface (Steinbüchel *et al*., 1995) and a storage source of nitrogen (McCool and Cannon, 1999).

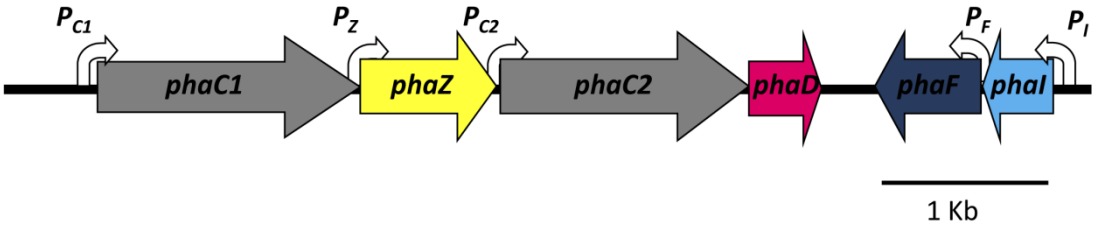

Figure 4. Genetic organization of *pha* cluster in *P. putida* KT2442. Arrows indicate different genes involved in PHA metabolism, their relative size and transcriptional direction. Promoter regions are indicated as curved white arrows. The *pha* is composed of two synthase coding genes, *phaC1* and *phaC2* (grey), interspersed by depolymerase coding gene *phaZ* (yellow), *phaD* gene coding for transcriptional regulator not classified as GAP (pink) and two genes coding for the phasins, *phaF* (dark blue) and *phaI* (light blue) transcribed divergently to the other *pha* genes.

They are widespread among bacteria, sharing similar functions but differing in their primary structures (Grage *et al*., 2009). It is generally accepted that phasins are composed of a hydrophobic domain associated to the PHA granules surface and a hydrophilic domain exposed to the cytoplasm. The amphiphilic layer stabilizes the PHA granules and prevents them from coalescing (Wieczorek *et al*., 1995).

P. putida strains contain two phasins PhaI (15 kDa) and PhaF (26 kDa) (Prieto *et al*., 1999). The PhaF is a nucleoid-associated protein involved in the transcriptional regulation of genes linked to PHA metabolism (Prieto et al., 1999; Galan et al., 2011). According to the structural three-dimensional model prediction, PhaF is an elongated protein, composed of long, amphipathic N-terminal helix with PHA binding capacity, followed by a short leucine zipper proposed as protein oligomerization linker, and a superhelical C-terminal domain wrapped around the chromosomal DNA (Maestro et al., 2013)(Figure 5). C-terminal half contains AAKP-like tandem repeats characteristic of the histone H1-family (Prieto *et al*., 1999).

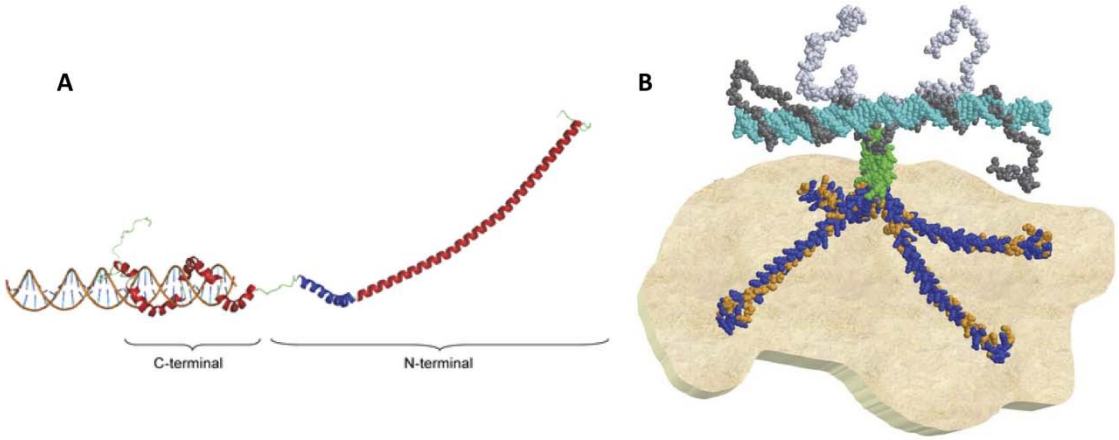

Figure 5. A structural model of PhaF phasin and a model of the interaction between PHA granules, phasins and chromosomal DNA in *P. putida* KT2440. A, Joint model structure of monomeric PhaF complex with DNA. The leucine zipper is shown in blue; B, PhaF tetramer is depicted interacting with the PHA granule while also attached to a fragment of nucleoid DNA. The hydrophobic residues in N-terminal domain are shown in orange, while the polar ones are colored blue. The leucine zipper is colored green and the DNA in cyan (Maestro et al., 2013).

Several evidences support the structural and functional independence of the domains. First, the PhaI phasin, which shares considerable sequence similarity with the

N-terminal region of PhaF (57% similarity, 38% identity) (Prieto et al., 1999) is capable of acquiring a folded, stable and functional structure by itself (Moldes et al., 2004). Also, the N-terminal domain is conserved in other PHA-binding phasins with a different C-terminal part (Moldes et al., 2004; Maestro et al., 2013). Moreover, very diverse fusion proteins containing the N-terminal moiety of PhaF (the BioF affinity tag, see below) can be adsorbed on PHA granules without compromising their function (Moldes et al., 2004; Moldes et al., 2006).

4. Peptide functionalized PHA using GAPs

PHA granules are becoming increasingly recognized as potential functionalized beads for biotechnological and medical applications. Recently, granules formed inside recombinant bacterial cells were used as tailor-made functionalized micro- or nano-beads where specific proteins attached to the PHA core have been engineered to display various functions. The application performance of engineered PHA beads in high-affinity bioseparation (Lewis and Rehm, 2009), enzyme immobilization (Moldes et al., 2004; Peters and Rehm, 2006), protein delivery to natural environments (Moldes et al., 2006), diagnostics (Baeckstroem et al., 2007) and as an antigen delivery system (Parlane et al., 2009) has been demonstrated. To that end, different strategies using GAP proteins located on the surface of PHA granules, as for instance synthase, depolymerase and phasins were employed (see below).

Moreover, the approach using GAPs can be applied *in vitro* or *in vivo*. Namely, for *in vitro* technology PHA extraction is followed by *in vitro* bead production and using the advantage of GAPs-bead strong hydrophobic interaction, fusion proteins are *in vitro* purified/immobilized (Yao *et al*., 2008). The *in vivo* approach consists of GAP fusion immobilization onto the PHA granule surface while the granules are being formed inside the PHA producer cell (Moldes et al., 2004).

Among GAPs, PHA granule binding proteins phasins are very attractive due to their diversity compared to the other GAPs. Thus, phasins were utilized as affinity tags to design recombinant protein purification system based on *in vitro* approach. This

method allowed low cost production and purification of high value added proteins in a continuous way (Wang *et al*., 2008). Significant improvements in bio-separation technology were made by upgrading the system interconnecting phasins and target proteins via self-cleaving intein (Banki *et al*., 2005). This approach allowed *in vivo* immobilization onto the granule and the release of purified recombinant proteins once the native PHB particles are recovered which in turn pushed bio-separation technology several steps forward in the direction towards convenience and cheapness. A receptor mediated drug delivery system was developed based on PhaP phasin. The system consists of *in vitro* synthesized PHA nanoparticles, PhaP and polypeptide or protein ligands (e.g. mannosylated human α1-acid glycoprotein (hAGP) and human epidermal growth factor (hEGF)) (Yao *et al*., 2008). Moreover, *in vivo* immobilized correctly folded eukaryotic proteins on the surface of PHA granules via phasin protein were used for fluorescence activated cell sorting (FACS) based diagnostics which is a powerful technique for the qualitative and quantitative detection of biomolecules used widely in both basic research and clinical diagnostic applications. Beads displaying a specific antigen are used to bind antibodies which are then fluorescently labeled using secondary antibodies (Backstrom *et al*., 2007).

Similarly, applying *in vitro* approach the substrate binding domain of PHA depolymerase has been used to anchor fusion proteins to PHA microbeads (Lee *et al*., 2005). Another example of successful GAPs application is for enzyme immobilization on the *in vivo* PHA granule surface using N-terminus of PHA synthase from *Pseudomonas aeruginosa* as a tag (Peters and Rehm, 2006).

The convenience of *in vitro* technology is best spotted in medical applications such as drug targeting where is preferable the use of endotoxin free PHA for coating with GAPs fusions (see below). However, other applications as for instance protein delivery to natural environments do not necessary acquire extremely pure PHA and can beneficiate from *in vivo* approach. Thus, a system for protein immobilization/purification was designed, based on the use of PHA granules and the N-terminal domain of the protein PhaF (BioF tag) (Moldes et al., 2004). BioF system constitutes specific biotechnological tool for producing mcl-PHA beads (Figure 6). Once, the fermentation under optimal mcl-PHA production conditions is accomplished

in *P. putida*, the granules carrying the BioF-proteins fusions can be isolated from the crude cell lysate by a simple centrifugation process and directly used for further applications. This approach was used for *in vivo* immobilization of Cry1Ab derived insect-specific toxin protein into mcl-PHA granules. Generating BioF insect-specific toxin immobilized to bioplastics, suggested that the BioF tag could be exploited as a new tool for spreading active polypeptides to the environment (Moldes et al., 2006) (Figure 6).

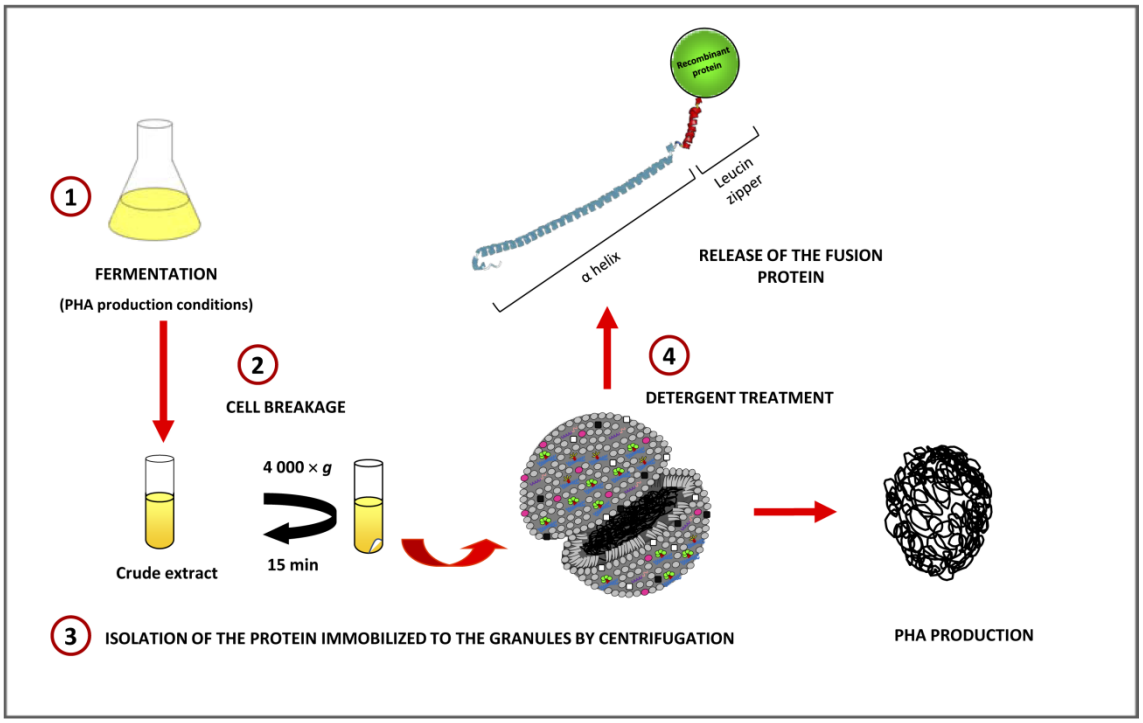

Figure 6. *In vivo* immobilization of fusion proteins to bioplastics by BioF tag. The procedure consists of the fermentation under optimal PHA production conditions in *P. putida*, isolation of the granules carrying the BioF-proteins fusions from the crude cell lysate by a simple centrifugation step and release of fusion proteins via detergent treatment (modified from Moldes et al., 2004).

5. PHA metabolic network and polyester functionalization

In most bacteria, such as the paradigmatic *Ralstonia eutropha* H16 strain, PHB is synthesized in three-step reaction starting with acetyl-CoA (Peoples and Sinskey, 1989)

(Figure 7). In the first step two acetyl-CoA molecules are condensed in a reaction catalysed by a 3-ketothiolase. Then, generated acetoacetyl-CoA is stereoselectively reduced to (*R*)-3-hydroxybutyryl-CoA by a NADPH-dependent acetoacetyl-CoA reductase. Finally, the (*R*)-3-hydroxybutyryl-CoA monomers are polymerized by a PHB synthase, releasing PHB and free CoA as end-products.

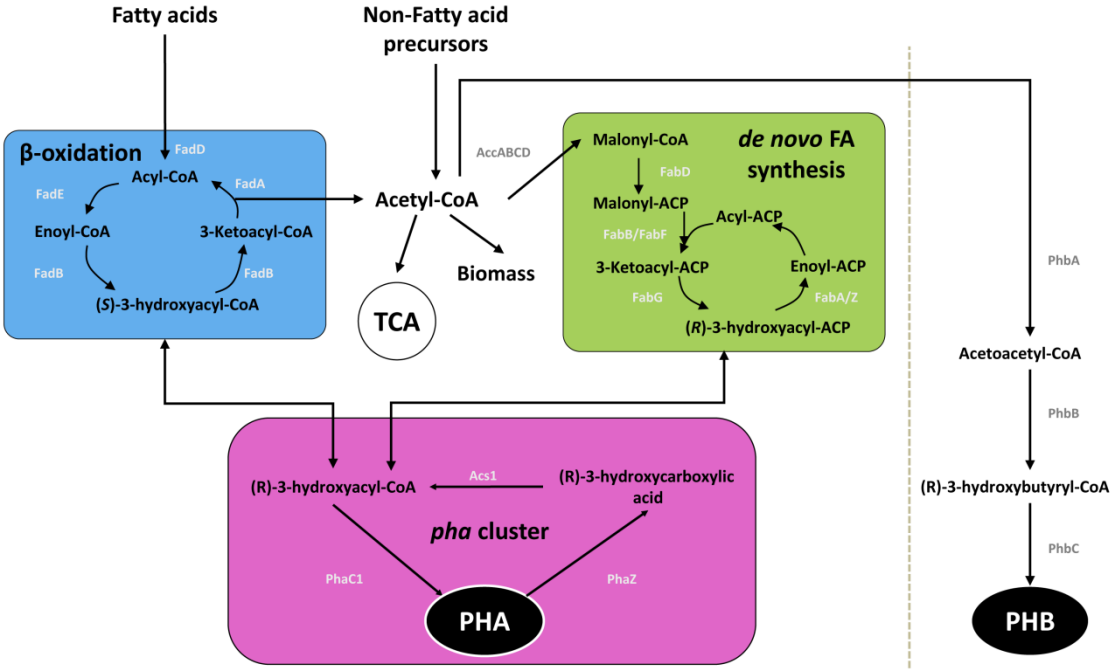

Figure 7. Metabolic pathways involved in PHA biosynthesis. Intermediates for PHA synthesis are derived from pathways connected with central carbon metabolism (β-oxidation and *de novo* fatty acid synthesis*)*. Acetyl-CoA is the key intermediate in the PHA synthesis, as the connection between catabolic and anabolic pathways involved in this system. PHA cycle is continuous process of synthesis (PhaC1) and degradation (PhaZ) of the polymer in which acyl-CoA synthetase (ACS1) is encarged for transformation of the depolymerization products. Resulting products of ACS1 activity, (*R*)-3-hydroxyacyl-CoA, are potencial substrates for polymerase or enzyms of fatty acid metabolism. PHB is syntesized from acetyl-CoA in 3 succesive steps invoplving the activity of β-ketoacil-CoA tiolase (PhbA), acetoacetyl-CoA dehydrogenase (PhbB) and PHB polymerase (PhbC) (Escapa et al., 2013).

Pseudomonas species rely on β-oxidation pathway and *de novo* fatty acid synthesis to convert fatty acid or carbohydrate intermediates, respectively, into different (*R*)-3-hydroxyacyl-CoAs. These metabolites are used as substrates by PHA synthases which

catalyze the committed step of mcl-PHA biosynthesis and finally end up in PHA polymer (Prieto et al., 2007).

The β-oxidation pathway involves the participation of a transport system coupled to an acyl-CoA synthetase (FadD) which catalyses the activation of n-alkanoic acid to their acyl-CoA derivates. Later, an acyl-CoA dehydrogenase (FadF), which requires the participation of an electron-transferring protein (FadE), catalyses the formation of a double bond in the β-position. Finally, a protein complex (FadBA) with five enzymatic activities (enol-CoA-hydratase, 3-OH-acyl-CoA dehidrogenase, cis-Δ^3-*trans*- Δ^2-enoyl-CoA isomerase, 3-OH-acyl-CoA epimerase and 3-ketoacyl-CoA thiolase) catalyses the removal of two carbon units of the acyl-chain being processed (Olivera *et al*., 2001) (Figure 7). Concerning the fatty acids β-oxidation protein complex (FadAB), two set of *fadAB* genes have been described in the strain *P. putida* KT2442, *fadB* and *fadA* (PP_2136 and PP_2137) and *fadBx* and *fadAx* (PP_2214 and PP_2215). Apparently, the first set plays a more important role in fatty acid degradation, since *fadB* and *fadA* deletion mutants did not show completely blocked β-oxidation, but production of PHA with higher content of longer chain monomers, possibly due to their defective β-oxidation pathway (Escapa et al., 2011; Ouyang et al., 2007; Chung et al, 2009).

Non-fatty acid precursors can be oxidized to acetyl-CoA and channeled into PHA by *de novo* synthesis pathway, via (*R*)-3-hydroxyacyl-acyl carrier protein (ACP) intermediates. In this process, malonyl-CoA and its precursor, acetyl-CoA, are activated by transacylation to acyl-carrier protein (ACP). Malonyl and acyl-ACP derivatives are condensed by ketoacyl-ACP synthetase, reduced losing a ketone group, dehydrated and saturated to the corresponding (*R*)-3-hydroxyacyl-ACP chain that may be further elongated in two-carbon growing chains. Acyl-ACP intermediates can be then re-transformed in (*R*)-3-hydroxyacyl-CoAs by a specific transacylase, PhaG, present in most Pseudomonads (Fiedler et al., 2000) (Figure 7). Interestingly, unsaturated monomers such as 3-hydroxy-5-dodecenoate and 3-hydroxy-7-tetradecenoate are also generated by fatty acid *de novo* synthesis (Huijberts et al., 1992).

Due to the broad substrate specificity of PHA synthase (PhaC), many organic molecules containing a carboxyl and a hydroxyl group in the position 3, can be

converted to the respective CoA thioester and can, in principle, be incorporated into a high-molecular-mass PHA. The biosynthesis pathways of the activated PHA precursor, (*R*)-3-hydroxyacyl-CoA, have been extensively studied and exploited through metabolic engineering, leading to the production of modified PHA that is a range of heteropolymers and homopolymers containing (*R*)-3-hydroxy fatty acids (Rehm and Steinbüchel, 1999).

5.1. Functionalized PHA through metabolic engineering strategies

Over the past decade, a better understanding of the molecular mechanisms and regulatory processes underlying the synthesis of biopolymers has emerged. Genome sequencing, functional genomics and System Biology studies, cloning and characterization of biosynthesis genes have all had a substantial impact on understanding of biosynthesis pathways in organisms that produce commercially relevant polymers and also lead to the discovery of new biopolymer-producing bacteria (Pohlmann *et al*., 2006; Kalia *et al*., 2003; Lee, 2006; Escapa et al., 2012; Follonier; Pobletes etc). This knowledge provided a powerful tool to engineer bacteria that are capable of, not only efficient biopolymer production, but also the production of modified and even unnatural polymers exhibiting unique material properties for specific high-value applications. Since the discovery that some bacteria can incorporate (*R*)-3-hydroxyalkanoates (3HA) bearing functional groups from related substrates (Lenz et al., 1992), research has led to structural diversification of PHA by biosynthesis and post-biosynthesis chemical modifications (Hazer and Steinbüchel, 2007; Scholz, 2010). Structural and functional diversity is readily addressed in bacterial polyesters, as they are produced by modulated fermentation processes.

This concept has been exploited to produce a plethora of tailor-designed mcl-PHA, with highly diverse structures that include acetylthioester, acetoxy, alkoxy, amino, cyano, cyclohexyl, epoxy, halogenated, hydroxy or propylthiol groups (Table 1) (Kim et al., 2007; Scholz, 2010). A larger variety of PHA compositions with varying molar amounts of functional groups can be generated in most of the cases, by altering the ratio of co-substrates. Functional groups prone to chemical modifications have been

introduced, mainly in *P. oleovorans* and *P. putida*, such as thiol, bromine, chlorine and fluorine radicals, cyano and epoxy groups. The introduction of such groups also modifies the thermal properties, and thus the processing requirements of the resulting polymers, enabling higher melting and lower glass-transition temperatures, or modified biological activities (see below).

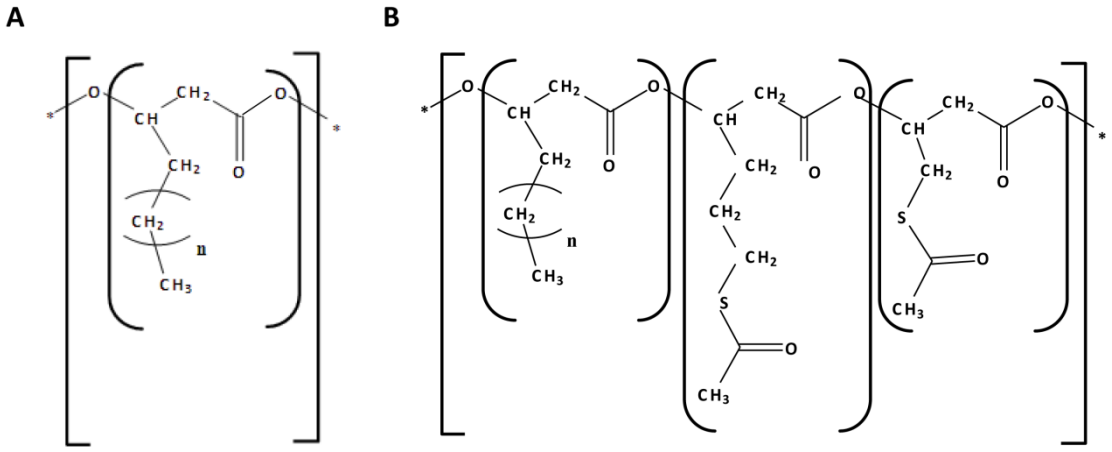

Figure 8. Schematic representation of medium chain lenght PHAs (mcl-PHAs) chemical structure. A, PHO-*co*-HHx composed of non-functionalized monomers OH-Alk (3-(*R*)-hydroxyoctanoate (OH-C8) and 3-(*R*)-hydroxyhexanoate (OH-C6)); B, PHACOS composed of functionalized monomers (3-hydroxy-6-acetylthiohexanoate (OH-6ATH) and 3-hydroxy-4-acetylthiobutanoate (OH-4ATB)) and of non-functionalized monomers OH-Alk ((OH-C8), 3-(*R*)-hydroxydecanoate (OH-C10), and traces (OH-C6)).

Recently in our laboratory we produced poly((*R*)-3-hydroxyacilthioalkanoate-*co*-3-hydroxyalkanoate) (PHACOS) (Figure 8), a new second generation family of polymers containing thioester groups in the side chain. PHACOS is composed of 6-acetylthio-3-hydroxyhexanoic acid (OH-6ATH) and the shorter derivative 4-acetylthio-3-hydroxybutanoic acid. Previous studies described the biosynthesis of PHA containing sulphur groups in side chains, comprising either thiophenoxy functional groups (Takagi et al., 1999) or thioether groups (Ewering et al., 2002). Moreover, biopolymers with thioester linkages in the polymer backbone were isolated from PHA-accumulating bacterium *R. eutropha*, containing 3-metrcaptopropionate (3MP) or 3-mercaptobutyrate (3MB) as constituents (Lütke-Eversloh et al., 2002; Lütke-Eversloh and Steinbüchel, 2004).

PHACOS were obtained applying 6-acetylthiohexanoic acid (6-ATH) as precursor in a co-feeding strategy with decanoic acid as co-substrate. *P. putida* KT2442 and its *fadB* mutant were used for PHACOS synthesis. The necessity of adding mcl-fatty acids to the medium for promoting PHA synthesis in the presence of 6-ATH was clearly demonstrated. Decanoic acid was confirmed to be a good PHA precursor in cultures containing 6-ATH. However, results showed that PHACOS cannot be efficiently produced in mutant strain under conventional one-stage culture process as a consequence of KT42FadB strain inability to use 6-ATH and incorporate thioester groups in the side chain of polymer. Two-stage culture process was optimal for efficient production of PHACOS in both strains. The procedure consists of two consecutive cultivation stages. In first stage cells were grown in LB medium for biomass production. In the second stage, cells were incubated in minimal medium in the presence of 6-ATH as precursor in a co-feeding strategy with decanoic acid as co-substrate. When the derived strain KT42FadB, mutated in the *fadB* gene from the β-oxidation pathway, is used, the polymer is overproduced and contains mainly OH-6ATH units (Escapa et al., 2011).

Although most of functionalized mcl-PHA intermediates are obtained through β-oxidation of fatty-acids, non-related carbon sources such as acetate, ethanol, fructose, glucose, gluconate or glycerol are channeled to PHA by the *de novo* fatty acid pathway, yielding a fraction of unsaturated monomers (3-hydroxy-5-dodecenoate and 3-hydroxy-7-tetradecenoate, see above and Figure 7). The molar fraction of unsaturated monomers usually ranges from 5 to 10 mol% depending on the strain (Sanchez et al., 2003; Silva-Queiroz et al., 2009) and can be increased by diminishing the culture temperature (Huijberts et al., 1992). The use of carbohydrate-related sources is advantageous in terms of substrate cost and diversity of monomer composition. However, PHA yields are generally lower in comparison to yields obtained when using fatty acids as substrates. Besides carbohydrates, glycerol has also been considered as an attractive raw material for PHA production due to its availability as by-product of biodiesel industry (Gómez et al, 2012). In *Pseudomonas* strains, glycerol is converted to glycerol-3-phosphate and then to dihydroxyacetone phosphate, which is further on catabolized by a branch of Entner–Doudoroff (ED) pathway (Schweizer et al., 1997;

Cuskey et al., 1985). Glycerol use is hindered by a prolonged lag phase, caused by the transcriptional repressor GlpR. GlpR knock-out mutants resulted in faster consumption of glycerol, together with improved PHA accumulation, possibly as a consequence of the larger availability of intermediates generated by *de novo* fatty acid synthesis (Escapa et al., 2013).

Table 1. Precursors used in the literature to produce functionalized mcl-PHA (branched alkyl, cyclohexyl, halogenated, acetoxy, ester, alkoxy, epoxy, thio, cyano, nitro, aromatics) (Modified from Tortajada et al., 2013)

Precursor	%Mol functional groups	Strain	Ref.
Branched alkyl			
Citronellol	>99.0	*P. citronellolis* ATCC 13674	Choi et al., (1994)
Alkylhydroxyoctanoates	5.0	*P. oleovorans* ATCC 29347	Scholz et al.,(1994)
Methyloctanoates	3.0-96.4	*P. oleovorans* ATCC 29347	Fritzsche et al., (1990)c, Lenz et al., (1992)
Cyclohexyl			
Cyclohexylbutyric acid	>99.0	*P. cichorii* YN2	Honma et al., (2004)
Cyclohexylvaleric/ butytic acid	13.2-100.0	*P. oleovorans* ATCC 29347	Andújar et al., (1997), Kim et al., (2001)
Unsaturated			
Alkenes (C7-C9)	45.0-55.0	*P. oleovorans* ATCC 29347	Lageveen et al., (1988)
Undecenoic acid	27.1-100.0	*P. putida* KCTC 2407	Kim et al., (2000)
Undecenoic	5.0-99.0	*P. oleovorans* ATCC 29347	Kim et al., (1995b), Park et al., (1998), Sparks et al., (2008)
Hydroxyoctenoic acids	63.5-81.6	*P. oleovorans* ATCC 29347	Fritzsche et al., (1990)b
Dicarboxylic acids (C4-C10)	4.7-11.7	*P. citronellolis* ATCC 13674	Choi et al., (1994)
Undecynoic acid	32.0-100.0	*P. oleovorans* ATCC 29347	Kim et al., (1998)

Undecynoic acid	22.0-100.0	*P. putida* KCTC 2407	Kim et al., (1998)
Halogens			
Bromoalkanoic acids (C6-C11)	3.7-38.0	*P. oleovorans* ATCC 29347	Kim et al., (1992), Lenz et al., (1992)
Chlorooctane	69.0	*P. oleovorans* ATCC 29347	Doi et al., (1990)
Fluorohexanoic/ nonanoic acids	1.9-8.8	*P. oleovorans* ATCC 29347	Kim et al., (1996)a
Fluorohexanoic/ nonanoic acids	1.0-17.3	*P. putida* KT2440	Kim et al., (1996)a
Fluorophenoxyundecanoic acid	>99.0	*P. putida* 27N01	Takagi et al., (2004)
Acetoxy			
Octanone , octylacetate	3.3-10.3	*P. oleovorans* ATCC 29347	Jung et al., (2000)
Ester, Alkoxy, Epoxy			
Alkylheptanoate	2.5-60.0	*P. oleovorans* ATCC 29347	Scholz et al.,(1994)
Alkxyhexanoic/octanoic/ undecanoic acids	31-100.0	*P. oleovorans* ATCC 29347	Kim et al., (2003)
10-epoxyundecanoic acid	25.0-75.0	*P. oleovorans* ATCC 29347	Bear et al., (1997)
C7-C12 alkenes	4.2-20.0	*P. cichorii* YN2	Imamura et al., (2001)
Soybean oil	63.0	*P. stutzeri* 1317	He et al., (1998)
Thio, sulfanyl			
Acetylthiohexanoic acid	16.5-78.5	*P. putida* KT2442, KT24FadB	Escapa et al., (2011)
Propylthiohexanoic acid	14.5-17.5	*R. eutropha* DSM541	Ewering et al., (2002)
Propylthioundecanoic acid	6.02% w/w S	*P. putida* KT2440	Ewering et al., (2002)
Methylsulfanylphenoxyvaleric acid	12.2-35.6	*P. cichorii* H45, YN2	Kenmoku et al., (2002)
Methylsulfanylphenoxyvaleric acid	18.4	*P. jessenii* P161	Kenmoku et al., (2002)
Thiophenoxyundecanoic acid	>99.0	*P. putida* 27N01	Takagi et al., (1999)

Cyano, nitro			
Cyanoundecanoic acid	17.0-32.0	*P. oleovorans* ATCC 29347	Lenz et al., (1992)
Cyanophenoxyhexanoi acid	0-2.2	*P. oleovorans* ATCC 29347	Kim et al., (1996)a
Cyanophenoxyhexanoi acid	0.0-34.0	*P. putida* KT2440	Gross et al., (1996), Kim et al., (1995)a
Nitrophenoxyhexanoc acid	4.2-5.1	*P. oleovorans* ATCC 29347	Kim et al., (1996)a
Nitrophenoxyhexanoic acid	1.0-4.8	*P. putida* KT2440	Kim et al., (1996)a
Dinitrophenylvaleric acid	1.2-6.9	*P. oleovorans* ATCC 29347	Aróstegui et al., (1999)
Aromatics (benzoyl, methylphenoxy, phenoxy, phenyl)			
Benzoylalkanoic acids (C4-C8)	8.3-79.8	*P. cichorii* YN2	Honma et al., (2004)
Methylphenoxyalkanoic acids (C6, C8)	40-65	*P. putida* KCTC 2407	Kim et al., (2000)
Methylphenoxyalkanoic acids (C6, C8) (PVA, NA)	68-100	*P. oleovorans* ATCC 29347	Kim et al., (1999)
Methylphenoxyalkanoic acids (C6, C8)	24-100	*P. putida* KCTC 2407	Kim et al., (1999)
Phenoxyundecanoic Acid	>99	*P. oleovorans* ATCC 29347	Ritter et al., (1994)
Phenoxyalkanoic acids (C6,C8,C11)	100	*P. oleovorans* ATCC 29347	Kim et al., (1996)b
Phenoxyundecanoic acid	12-100	*P. putida* BM01	Song et al., (1996)
Phenylvaleric acid	13.7-19.5	*P. putida* BM01	Song et al., (2001)
Phenylvaleric acid	>99	*P. oleovorans* ATCC 29347	Curley et al.,(1996)b

Phenyl, tolylvaleric/ octanoic acids	3-64	*P. oleovorans* ATCC 29347	Curley et al., (1996)a
Phenylalkanoic acids (C4-C8)	>95	*P. jessenii* C8	Tobin et al., (2005)
Phenylalkanoic acids (C4-C8)	>95	*P. putida* S12, CA-1, H4, F6, D5	Tobin et al., (2005)
Phenylalkanoic acids (C6-C11)	>99	*P. putida* U fadA-, ΔFadBA-PhaZ	Abraham et al., (2001), García et al., (1999), Olivera et al., (2001)
Phenylvaleric acid	>99	*P. oleovorans* ATCC 29347	Fritzsche et al., (1990)a
Phenylvaleric acid	12.6-40.6	*P. oleovorans* ATCC 29347	Kim et al., (1991)

5.2. Properties of PHA carrying functionalized groups

The physical and material properties of PHA are significantly influenced by their monomer composition and chemical structure (Chen, 2009). On one hand, scl-PHA may be too rigid and brittle and lack the superior mechanical properties required for biomedical and packaging film applications. Poly-(*R*)-3-hydroxybutyrate-*co*-(*R*)-3-hydroxyhexanoate (PHB-*co*-HHx) copolymers with low 3-hydroxyhexanoate (OH-C6) fraction are most commonly used PHA because of its appropriate mechanical properties for use as flexible films, compared with PHB (Noda, 1996). On the other hand, mcl-PHA may be elastomeric but at the same time characterized by very low mechanical strength. Therefore, for packaging materials, tissue engineering and other specific applications, the physical and mechanical properties of microbial polyesters need to be diversified and improved (Hazer *et al*., 2012). To date, more than 100 different monomers such as linear, branched, saturated, unsaturated and aromatic (Huijberts et al. 1992; Olivera et al. 2001b; Scholz 2010; Scholz et al. 1994) have been reported as PHA constituents (Steinbüchel and Valentin, 1995). The length of the side chain and its functional group considerably influence the properties of the polymer. Of special interest are functionalized groups in the side chain that allow further chemical

modification, *e.g*. halogens, carboxyl, hydroxyl, epoxy, phenoxy, cyanophenoxy, nitroin phenoxy, thiophenoxy, and methylester groups (Kim and Lenz, 2001).

Table 2. PHA monomer composition (%mol) of the polymers obtained from *P. putida* KT2442 and *P. putida* KT42FadB 24 h cultures

Carbon source	Strain	Culture procedure	Monomer composition (mol%)						
			OH-C6	OH-C8	OH-C10	Σ Alk.	OH-4ATB	OH-6ATH	Σ Thio.
15 mM SO	KT2442	One-stage	8.5	91.5	-	100	-	-	-
12 mM DA	KT2442	One-stage	2	36.6	61.4	100	-	-	-
2.4 mM DA + 12 mM 6ATH	KT2442	One-stage	1.5	11.2	6.6	19.3	26.5	51	77
2.4 mM DA + 12 mM 6ATH	KT42FadB	One-stage	0.9	19.6	60.9	81.4	2.5	14	16.5
2.4 mM DA + 12 mM 6ATH	KT2442	Two-stage	2.1	13.6	7.1	22.8	31.5	47	78.5
2.4 mM DA + 12 mM 6ATH	KT42FadB	Two-stage	0.6	15.5	19.1	35.2	7.5	58	65

OH-C6, OH-C8 and OH-C10 (percentages were estimated by GC-MS. OH-6ATH and OH-4ATB percentages were estimated by NMR. SO (Sodium octanoate), DA (Decanoic acid).

PHACOS, the family of PHA carrying thioester group in the side chain, generally show an amorphous behavior due to the inability of the polymer backbone to fold tight enough and organize to form crystals. This property is caused by the presence of bulky side chains and functional groups that leads to stiffer and less mobile chains. Moreover, PHACOS show good thermal stability up to 200 °C. This could result in a good processing ability for these materials and potentially interesting mechanical properties. The molecular weights (Mn and Mw) of PHACOS are in the typical range observed for mcl-PHA (Witholt and Kessler, 1999). Regarding PHACOS elaboration, neither the culture procedure nor the bacteria strain (mutant or wild type) had

significant influence on the molecular weight. However, PHACOS have tunable thermal properties as a result of different glass transition temperatures derived from the different possibilities of monomer composition. The *fadB* mutant strain led to PHACOS with lower content in thioester-based monomers, but inserted monomers showed longer side chains (Table 2) that resulted in polymer having much lower glass transition temperature. This amorphus mcl-PHA with low values of glass transition (Tg) are expected to display relatively high softness and marked elasticity which are very interesting properties for materials dedicated to biomedical applications (Escapa *et al*., 2011).

Concerning mcl-PHA obtained from non-fatty acid precursors, it is observed that the higher the molar fraction of unsaturated constituents in the monomers, the lower the resulting melting and glass transition temperatures, very likely due to crystallization inhibition by unsaturated side chains (Ashby and Foglia, 1998). Double bonds are also easily attacked in chemical reactions, allowing even higher diversification of the polymer properties (Lageveen et al., 1988; Hazer and Steinbüchel, 2007). A number of treatments have been described for crosslinking of unsaturated PHA, namely electron-beam irradiation, UV-irradiation or even autoxidation (De Koning et al., 1994; Bassas et al., 2008a; 2008b; Silva-Queiroz et al., 2009) and in some cases those PHA can be transformed into rubbers (De Koning et al., 1994). Moreover, chemical epoxidation of the pendant vinyl groups has been applied to decrease melting temperature and increase glass transition temperature (Park et al., 1998). In addition, new plastic properties can also be achieved by blending PHA with other polymers.

6. PHA as scaffold biomaterial in tissue engineering

Any material, natural or man-made, biodegradable and biocompatible, that comprises the whole or part of a living structure or a biomedical device which performs, augments, or replaces a function that has been lost through disease or injury is known as a "biomaterial". They have played an important role in the treatment of disease and the improvement of health care (Langer and Tirrell, 2004). Among them, PHA polymers are promising materials for biomedical applications because they are natural, renewable, biodegradable and biocompatible thermoplastics (Hazer and Steinbüchel, 2007).

Elastomeric mcl-PHA and its copolymers offer an extensive design space with a large range of properties that opened a new incites of polymer application and subsequently accelerated research in the past few years (Chen, 2009). However, the lack of availability of these polymers in large quantities still limits the investigation. Hence, most of the current research is concentrated on poly-(*R*)-3-hydroxyoctanoate (PHO) and PHB-*co*-HHx copolymer due to their large quantities production and improved mechanical and elastomeric properties compared to scl-PHA (Wiliams et al., 2000; Chen et al., 2001).

Many successful studies using various animal models have clearly demonstrated that PHA, represented by PHB, poly-4-hydroxybutyrate (P4HB), PHO and PHB-*co*-HV and PHB-*co*-HHx copolymers possesses the biodegradability, biocompatibility and thermoprocessibility for not only implant applications but also controlled drug release uses (Chen and Wu, 2005). The application performance of those PHA as different biomedical devices has been studied (*e.g.* sutures, repair devices, repair patches, slings, cardiovascular patches, orthopedic pins, adhesion barriers, stents, guided tissue repair/regeneration devices, articular cartilage repair devices, nerve guides, tendon repair devices, bone marrow scaffolds, artificial oesophagus and wound dressings) (revised in Chen and Wu, 2005) (Table 3). Among them, P4HB has been approved by FDA (The Food and Drug Administration agency of the United States Department of Health and Human Services) for suture application with a trade name TephaFLEX marketed by Tepha Inc., of Cambridge, Mass., USA. Tepha specializes in manufacturing

pericardial patches, artery augments, cardiological stents, vascular grafts, heart valves, implants and tablets, sutures, dressings, dusting powders and prodrugs (Figure 9). With successful approval of P4HB as an implant biomaterial, more PHA based biomaterials are expected to go into clinical trials soon. With the diversity of PHA materials, they are expected to become a family of bioimplant materials with rich applications (Chen, 2009). Herein the most outstanding possible applications of PHA in biomedical field will be revised.

Potential use of PHA in the construction of the devices for cardiovascular applications has been intensively studied. One of the most advanced application of PHB has been the development of regenerative pericardial patch (Bowald and Johansson-Rudel, 1997) used to close pericardium after surgery without adhesion between heart and sternum. Following the *in vivo* study on animal models, clinical testing on human patients has been successfully performed (Duvernoy et al., 1995). In addition, PHB was successfully used for arterial septal defect repair (Malm et al, 1992) and construction of cardiovascular stents (Behrend et al., 1998). Furthermore, PHA were tested in vascular grafting studies for repair or replacement of malfunctioning blood vessels in the arterial or venous systems due to damage or disease.

Table 3. PHA used in biomedical field

Modified/unmodified PHA	Medical application	Reference
PHB	Subcutanous patches	Baptist et al. (1965)
PHB	Peripheral nerve guide	Hazari et al. (1992), Moshahebi et al. (2002)
PHB	Regenerative pericardial patch	Bowald et al. (1997), Duvernoy et al. (1995)
PHB	Pulmonary artery regeneration	Malm et al. (1994)
PHB	Arterial septal defect repair	Malm et al. (1992)

PHB	Cardiovascular stents	Behrend et al. (1998)
PHB	Stomach wall patch	Löbler et al. (2002)
PHB	Drug delivery, chemoembolization	Kassab et al. (1999)
PHB	Spinal cord injury	Navikov et al. (2002)
PHB-*co*-HV	Guided tissue regeneration	Leenstra et al. (1995)
PHB-*co*-HV	Bone regeneration	Cool et al. (2008)
tricalcium phosphate reinforced PHB, PHB-*co*-HV	Internal bone fixation	Jones et al. (2000)
PHB-*co*-HV	Urethral reconstruction	Bowald et al.(1990)
PHB-*co*-HV	Subcutanous patches	Gogolewski et al. (1993)
PHB-*co*-HV	Myocardial patch	Kenar et al.
PHB-*co*-HV	Bone regeneration	Cool et al. (2008)
PHB-*co*-HV	Auricular implant for drug delivery	Jones et al. (1994)
PHB-*co*-HV	Rods, drug delivery	Hasirci et al. (1998), Korkusuz et al. (2001)
PHB-*co*-HV	Cartilage proliferation	Kose et al. (2005)
PHB/PHB-*co*-HV	Suture	Shishatskaya et al. (2004)
PHBHHx	Vessel stent	Qu et al. (2006)
PHBHHx	Nerve conduit	Chen et al. (2009)

PHBHHx	Bone regeneration	Wang et al. (2004)
PHBHHx	Cartilage proliferation	Wang et al.(2005)
PHB/PHBHHx	Cartilage proliferation	Ye et al. (2009)
PHB-*co*-HV,PHB-4HB	Drug delivery	Turesin et al. (2001)
PHB-*co*-HV-PLGA	Nerve guide	Yücel et al. (2010)
HA reinforced PHB	Bone regeneration	Shishatskaya et al. (2006)
HA reinforced PHB/VA	Bone regeneration	Luklinska et al. (2003)
PHO	Pulmonary valve	Stock et al. (2000)
PHO	Pulmonary heart valve	Sodian et al. (2000)
PHO-*co*-HHx-PGA	Abdominal aorta scaffold	Tim et al. (1999), Stock et al. (2000)
PHO-Sy	Subcutaneous patches	Hazer et al. (2009)
PHOU-Au	Subcutaneous patches	Hazer et al. (2011)
PHACOS	Antimicrobial polymer	Dinjaski et al. (2013)

PHA monomers (R3HB)	therapeutic effects on Alzheimer's and Parkinson's diseases, osteoporosis and even memory improvement	Massieu et al. (2003), Zou et al. (2009), Kashiwaya et al. (2000)
PHA monomers and oligomers	nutritional and energy supplements Ca2+ stimulation effect	Qu et al. (2006), Cheng et al. (2005), Cheng et al. (2006)

The elastomeric polymer PHO-*co*-HHx has been evaluated for a two components scaffold for abdominal aorta tissue engineering in a lamb model (Tim et al., 1999; Stock et al., 2000a). Perhaps the most remarkable results with PHA polymers have been obtained in the development of cell-seeded tissue-engineered heart valves. P4HB and PHO heart valve scaffolds were constructed and tested *in vivo* (see below; Sodian *et al*, 2000a) (Figure 9).

In dental and maxillofacial field PHB-*co*-HV was utilized for guided tissue regeneration, where polymer barrier membranes were constructed to encourage regeneration of new periodontal ligament by creating a space that excludes gingival tissue from healing wound. Their performance *in vivo* was found to be satisfying (Leenstra et al., 1995). Moreover, PHB-*co*-HV was used for guided bone regeneration (Cool et al., 2008). When used in orthopedic for internal bone fixation PHB and PHB-*co*-HV polymers were usually reinforced with hydroxyapatite (HA), glass or tricalcium phosphate (Jones et al., 2000). Obtained results showed favorable overall tissue responses, some indication of osteogenic activity was noted as well and therefore it was concluded that they can serve as alternative to corticocancellous bone grafts.

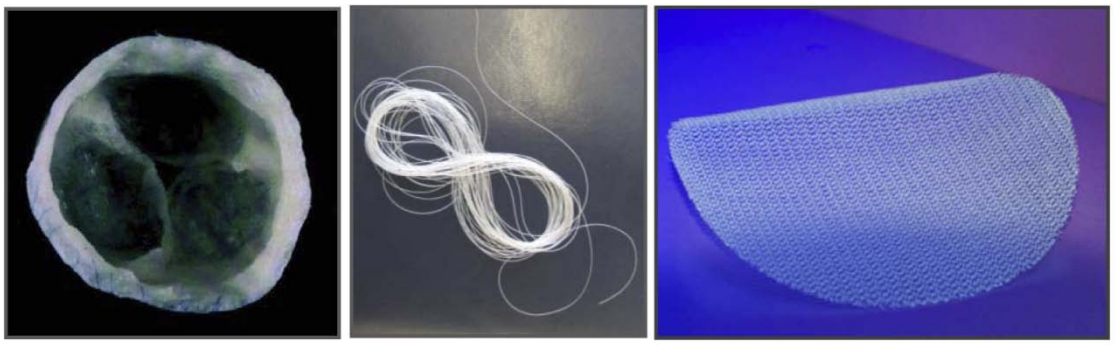

Figure 9. Examples of possible applications of PHA in biomedical field. From left to right PHO heart valve scaffolds, PHB-*co*-HV suture and TephaFLEX® surgical mesh (used for soft tissue reinforcement in plastic and reconstructive surgery, for temporary wound support, reinforcement of soft tissues and hernia repair).

Another possible application of PHB-*co*-HV copolymer was reported in urology for urethral reconstruction where the polymer scaffold was reported to support regeneration to fully functional urethra tissue (Bowald and Johansson, 1990). Moreover, wound management is one of the well studied areas where PHA found many applications. PHB and PHB-*co*-HV sutures were proven to feature necessary strength for the healing of muscle-fascial wounds not causing any acute vascular reaction at the site of implantation or any adverse events (Shishatskaya *et al*., 2004) (Figure 9). Finally, it has been verified that PHB shows a good polymer characteristics for soft tissue defect repair, especially for the closure of lesions in the gastrointestinal tract (Löbler et al., 2002).

The use of PHB and PHB-*co*-HV for drug delivery was evaluated in numerous studies that included investigation of their performance as subcutaneous implants (Jones et al., 1994), compressed tablets for oral administration (Hasirci et al., 1998; Korkusuz et al., 2001) and microparticles for intravenous use (Kassab et al., 1999). The therapeutic potential of P4HB was investigated and it was found to have possible beneficial effects in narcolepsy treatment and others (Williams and Martin, 2001).

Oligomeric forms of ketone body hydroxybutyrate (HB) were evaluated as an alternative to the sodium salt of the monomer that could provide controlled release systems for monomers and overcome the problem associated with administering large

amounts of sodium ion *in vivo*. This system could find application in seizure control, reduction of protein catabolism, appetite suppression, metabolic disease control, treatment of diabetes and insulin resistant states and others (Martin et al., 2000).

Due to the elastomeric behavior and biodegradability of mcl-PHA they can be used as promising base polymers for developing biodegradable pressure synthetic adhesives (PSA). Such PSA can find applications in wound coverings and closures, surgical drapes, electrocardiograph electrode mounts and transdermal drug delivery (Babu et al. 1993). For the development of PSA, PHO, poly-(*R*)-3-hydroxydecanoate (PHD) and mixtures of poly-(*R*)-3-hydroxyoctanoate-*co*-(*R*)-3-hydroxyundecenoate (PHO-*co*-HU) were used (Babu et al., 1993). Moreover, mcl-PHA like PHO and copolymers as PHB-*co*-HHx have been used as biopolymer scaffolds for the regeneration of nerve axons (Chen et al., 2010). Many other applications of PHA have been addressed with great potential for clinical use (Table 3).

7. Factors affecting PHA application

7.1. The pyrogen removal

For medical use, most PHA as attractive biopolyesters, have been sterilized using ethylene oxide, without causing significant physicochemical properties of the polymers. However, inappropriate extraction of PHA from bacterial biomass results in contamination with lipopolysaccharides (LPS) that form an integral part of the gram-negative bacteria outer membrane (Petsch and Anspach, 2000). Due to their high heat stability and insensitivity to pH changes they cannot be eliminated by simple sterilization step. Those cell-associated compounds, named endotoxins, are pyrogenic and cause fever and pathology when injected into animals. A special attention was paid to minimize the endotoxin contamination of PHA as a number of contaminants were reported in industrial samples of PHB-*co*-HV (Rouxhet et al., 1998; Garrido, 1999).

Endotoxin levels are measured in endotoxin units (EU) because their molecular weight may vary a great deal (10 000 to 1 000 000 Da). One EU is approximately equivalent to 100 pg of *Escherichia coli* lipopolysaccharide—the amount present in around 10^5 bacteria. Humans can develop symptoms when exposed to as little as 5 EU/kg body weight. These symptoms include, but are not limited to fever, low blood pressure, increased heart rate, low urine output. Even smaller doses of endotoxin in the blood stream are often fatal.

A conventional industrial sample of PHB was found to contain more than 120 EU/g (Williams et al., 1999). Several methods have been reported for endotoxin removal, such as depyrogenation based on the use of peroxide (Williams et al., 1999) and sodium hydroxide (Lee et al., 1999). FDA permits concentration of less than 20 EU/g of PHA or per medical device. This can be successfully achieved by a heat driven PHA extraction with a solvent followed by non solvent precipitation. Another method is temperature-controlled recovery of PHO-*co*-HHx from *P. putida* GPo1. In contrast to other methods, precipitation of PHO was triggered by cooling the hot solution to a particular temperature. Applying this method a minimal endotoxicity of 2 EU/g PHO can be achieved and a purity of close to 100% (w/w) (Furrera et al., 2007).

7.2. Biocompatibility

There were many attempts to define biocompatibility related to the behavior of biomaterials in various contexts. The term refers to the ability of a material to perform its desired function generating an appropriate host response in a specific situation (Black, 2006). The ambiguity of the term reflects the ongoing development of insights into how biomaterials interact with the human body and eventually how those interactions determine the clinical success of a medical device. Indeed, the main objective when using biomaterials is to generate the most appropriate beneficial cellular or tissue response without eliciting any undesirable local or systemic effects in the recipient or beneficiary of the therapy. However, since the immune response and repair functions in the body are so complicated the biocompatibility of a material should not be describe in relation to a single cell type or tissue. Nevertheless,

considering *in vitro* cellular behavior is essential for a comprehensive biocompatibility evaluation of further on implanted polymers.

A high biocompatibility is essential for the acceptance of any incorporated object by humans and mammals. Several factors are shown to influence implant biocompatibility such as shape, surface porosity, surface hydrophilicity, surface energy, chemistry of the material, the environment (tissue) where it is incorporated and its degradation products (Zinn *et al*., 2001). PHA have the potential to become an important compound for medical applications. For instance, tests have shown PHB biocompatibility, which is not surprising when considering the fact that *R*-3-hydroxybutyric acid is a normal constituent of blood at concentrations between 0.3 and 1.3 mM (Wiggam *et al*., 1997) and is also found in the cell envelope of eukaryotes (Reusch, 2000).

7.2.1. *In vitro* effect of PHA on mammalian cells

In vitro investigations have been shown to be suitable for elucidating several aspects of cell interactions with biomaterials. They preclude the numerous events that might occur after implantation of a foreign material in an animal model and provide a simple environment to study cellular responses. As upon implantation of polymers, the local tissue reaction consists of an inflammatory response, which initiates tissue repair, and regeneration processes, many different mammalian cell lines have been used in *in vitro* studies. Most commonly used are fibroblasts, macrophages, polymorphonuclear leukocytes (PMNs) and endothelial cells (Saad et al., 1999).

Cytotoxicity and inflammation studies of PHA have been mainly focus on characterizing cell response to the extracts of the polymers, whereas few studies attempted to analyze cell response in direct contact with the polymer (Chaput et al., 1995). However, the results varied with the medium, surface-to-volume ratio, time and temperature.

Tissue response was characterized by seeding the cells on the polymers surface and evaluating their initial attachment, growth and morphology. Thus, the effect of

surface morphology of PHA, as one of the factors influencing biocompatibility, was studied *in vitro* on mouse fibroblast (Kai et al., 2002). The study demonstrated that films with a fairly regular and smooth surface as PHB-*co*-HHx/PHB blends with low crystallization allowed improved cell attachment and growth of the seeded mouse cell line L929, thereby increasing its biocompatibility (Kai et al., 2002). Moreover, good endothelial cell and myofibroblasts attachment to PHO-*co*-HHx was reported (Sodian et al., 1999). Interactions between PHA as for instance PHB-*co*-HV and human keratinocytes (Ji et al., 2008), allogeneic chondrocytes (Wang et al., 2008), glial cells (Xiao et al., 2008), fibroblast and osteoblast (Wang et al., 2005), were studied and results proved the ability of mentioned cell lines to adhere and proliferate.

In tissue engineering, apart from reaction to material itself, evaluation of the cellular behavior affected by the degradation products is very important and especially in the case of PHA that are considered to be biodegradable. To analyze the effect of PHA degradation products, oligo-hydroxyalkanoates (OHAs), studies were carried out on macrophages, Kupffer cells, fibroblasts, osteoblasts and others (Cardielli et al., 1995; Sun et al., 2007; Saad et al., 1996 a,b,c). Those studies demonstrated that OHAs in low concentration (10-20 mg/L) do not significantly affect cell viability, whereas higher concentrations (>40 mg/L) reduce cell viability with more cell apoptosis, more cell death, delayed cell cycle and reduced cell proliferation. Moreover, the cytotoxicity of OHA decreased with increasing OHA side chain length indicating that medium chain length OHAs and mcl-PHA are more biocompatible then scl-PHA (Sun et al., 2007).

Attempts to increase the biocompatibility of polymer scaffolds have been made using different approaches. Current strategies for improving implant biocompatibility may be grouped into two areas: i) passive coatings and ii) active release. Passive strategies rely on modification of the implant surface through chemical and physical means. Alternatively, active release is based on the release of molecules that may modify the host´s foreign body response, direct the wound healing process and favor tissue integration of the implant (Bridges and Garcia, 2008).

Because the surface chemistry at the tissue-implant interface has a large influence on the immune system activation, the outer surface of implant is of great importance.

One of passive strategies includes increasing the hydrophilicity of the polymer to enable better adherence of the cells on the scaffolds. To that end, graft copolymerisation of acrylamide onto the PHO films was carried out and allowed better ovary cells attachment (Kim et al., 2002). Coating the surface of the polymer with a biocompatible compound is another approach to increase the biocompatibility of the polymer. With that aim, the surface of PHB-*co*-HHx matrices was coated with a biocompatible silk fibroin protein (Mei et al., 2006), PHA granule binding protein PhaP fused with cell adhesion motif Arg-Gly-Asp, RGD (Dong et al., 2010) and others. Moreover, approaches such as cell deposition can increase biocompatibility (Sodian et al., 2000).

In another initiative, using active strategies different implant coatings that deliver active molecules (e.g. anti-inflammatory agents) and offer more interactive and direct approach to modulate cell behavior have been designed (Bridges and Garcia, 2008). Immunomodulatory agents can be immobilized onto the surface or delivered in soluble form. Possible strategies for the controlled release of agents include passive diffusion, bioerodible/degradable coatings, hydrolysable or enzyme-degradable linkages and many others.

7.2.2. *In vivo* tissue response

In spite the fact that investigation of *in vivo* response to implanted PHA has began in the mid 1960s (Baptis and Ziegler, 1965) it is still a controversial subject as multiple factors and wide range of tested PHA with different monomer composition influence in a specific way and produce distinctive tissue and inflammatory responses. In vicinity of some of implanted PHA presence of inflammatory cells has been reported (Gogolewski et al., 1993). However, care should be taken when interpreting these data, since some of the studies have been based on industrial and commercially available rather than medical grades of PHA polymers (Williams et al., 1999). Moreover, inflammation and other undesirable reactions of tested biomaterials can be related to polymer chemical composition, a particular implantation site, the shape of the implant, the degree of chemical purity of the material and others. The biocompatibility of the implants is

evaluated applying various criteria. Histological approach is based on determination of the degree of fibrotic reaction surrounding the samples and the presence of inflammatory or malign cells. Biochemical assays are used to reveal cellular and extracellular matrix formation (*e.g.* presence of collagen by 4-hydroxyproline assay). Imunocytochemical analysis is based on the use of antibodies for inflammatory cell detection. Many other assays can be performed depending on the specificity of scaffold function (*e.g.* thrombus formation, echocardiography for investigation of 3-leaflet heart valve proper functioning, scaffold vascularization, etc.).

Up on implantation of foreign body (biomaterial) host reactions occurs. This host reaction includes: i) blood-material interactions, ii) acute inflammation, iii) chronic inflammation, iv) granulation tissue development, and v) fibrosis/fibrous capsule development (Figure 10). In the very early process of implantation, proteins and other biomolecules present in the blood plasma and biological fluids rapidly adsorb onto the surface of biomaterial completing the first stage of the process, blood/material interactions. Adsorbed molecules (fibrinogen, IgG and complement fragments) mediate leukocyte biomaterial interactions and subsequent inflammatory reactions. During acute phase neutrophils are stimulated and recruited to implantation site. The biological role of the acute inflammatory response is to phagocytose foreign material. The attempt by inflammatory cells to engulf and degrade the implant leads to reduced analyte diffusion. Further on, neutrophils are replaced by macrophages and chroinc inflammation begins. Additionally, consumption of oxygen and glucose produces superoxide and peroxide. Moreover, local pH may drop due to this oxidative process, resulting in enzyme degradation. Differentiated macrophages secrete a variety of inflammatory mediators and often fuse to form multinucleated foreign body giant cells (FBGC) that is the hallmark of chronic response. FBGC further enhances degradation of the underlying implant surface. The extent of the chronic inflammatory response is dependent on not only the physical and chemical properties of the implant but also on mechanical stresses (i.e., movement) at the implant site. Granulation tissue is formed following resolution of the chronic inflammatory response due to the persistence of macrophages and infiltration of fibroblasts to the wound site. During the final step in the immune sequence, fibroblasts infiltrate to the site and generate a fibrous capsule

around the implant (Bridges and Garcia, 2008) (Figure 10). The severity and extent of the biological response to an implanted biomaterial or device influences the probability for its successful integration with surrounding tissue, as well as overall device performance. Initial phases of foreign body reaction are dictated largely by the extent of injury and surgical technique, implantation site, implant shape, size and local and systemic health of the recipient (Anderson, 2001). Significant research efforts have focused on modifying material properties to generate more biocompatible implants.

A small amount of information on PHO, PHO-*co*-HHX and P4HB is available, whereas most of current information relates to PHB and PHB-*co*-HB (reviewed in Hasiric, 2000) as previously discussed. One of the earliest *in vivo* studies on mcl-PHA was carried out on the copolymer PHO-*co*-HHx through subcutaneous polymer implantation in mice (Williams et al., 1999). No evidence of macrophages was found in the implant sites and the tissue response continued to be very mild even 40 weeks post-implantation. Histological analysis revealed that the implants were encapsulated by a thin layer of fibroblasts surrounded by collagen and the polymer proved to be particularly inert, and could be readily removed with little tissue adherent to the implants (Williams et al., 1999).

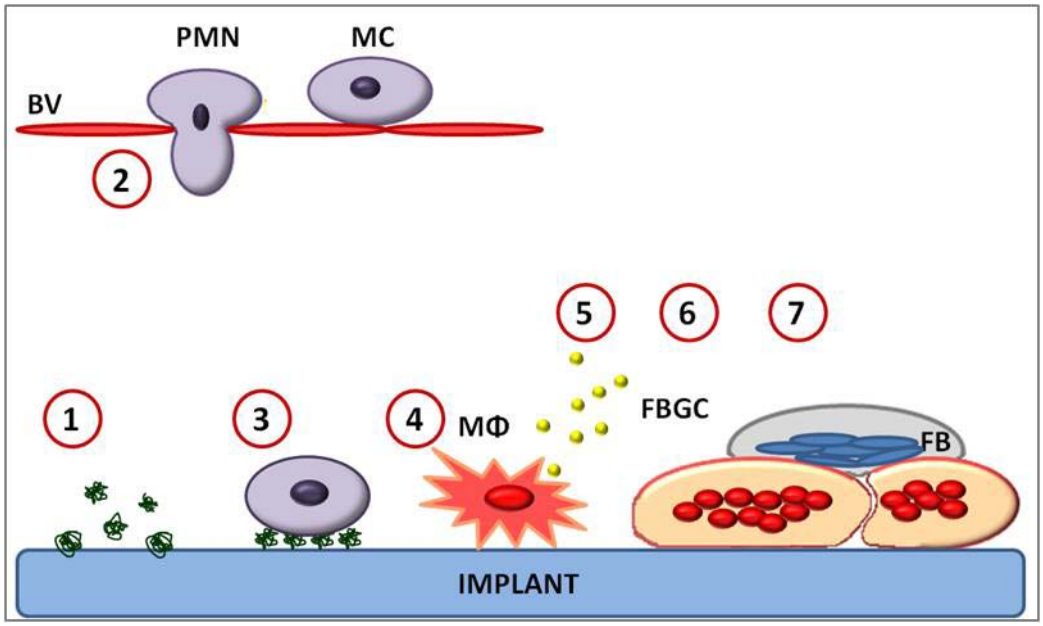

Figure 10. Events of host foreign body response to implanted materials. 1-3, Polymorphonuclear leukocytes (PMF) and monocytes (MC) recruited by stimulatory cues emigrate from blood vessels (BV) and adhere to the layer of adsorbed proteins on the implant;

4-6, Differentiated macrophages (MΦ) become activated, secreting a variety of inflammatory mediators, and often fuse into foreign body giant cell (FBGC); 7, Fibroblasts (FB) infiltrate to the site and generate a collagenous fibrous capsule around the implant.

One of the strategies to improve biocompatibility and implant integration is by their *in vitro* seeding with autologous cells. Thus, after the proper functioning of constructed PHO trileaflet heart valve scaffold tested in pulsatile bioreactor was confirmed by synchronous opening and closing (Sodian et al., 2002), scaffold was seeded with vascular cells harvested from vascular arteries (Sodian et al., 2000). This study demonstrated that tissue-engineered heart valve scaffolds fabricated from PHO can be used for implantation in the pulmonary position with an appropriate function for 120 days in lambs (Sodian *et al*., 2000). In another study the feasibility of creating PHO trileaflet pulmonary conducts seeded with autologus cells was evaluated (Stock et al., 2000). Based on obtained results, it was concluded that engineered scaffold can properly function in pulmonary circulation.

7.3. *In vitro* and *in vivo* biodegradation

PHA polymers are known as biodegradable, whose degradation might be triggered by different mechanisms. One of the well studied processes is enzymatic hydrolysis by microbial depolymerases. Many microorganisms can catabolize PHA through extracellular or intracellular degradation under aerobic or anaerobic conditions (Jendrossek and Handrick, 2002). Up to date, both extracellular scl-PHA (Jendrossek and Handrick, 2002) and intracellular mcl-PHA depolymerases have been characterized (de Eugenio et al., 2007). The interest in the study of the PHA hydrolysis lies not only in their potential use as bioplastics or biomaterials but also in the production of intermediates (3HA), as they can be used as chiral starting materials in fine chemical, pharmaceutical, and medical industries (Luengo et al., 2003; Ren et al., 2005). In addition, biodegradable materials have numerous applications in medicine and surgery. Those materials are designed to degrade *in vivo* in a controlled manner over a predetermined implantation period, such that degradation achieves or helps to achieve a particular function. The rates of PHA polymer degradation vary considerably and depend primarily upon chemical composition. It was demonstrated that PHA biodegradation is influenced by the presence of functional groups in the polymer chain, as well as by hydrophilicity/hydrophobicity balance (Mochizuki and Hirami, 1997; Tokiwa and Calabia, 2004). Moreover, stereoregularity, molecular mass, morphological properties and crystallinity affect the biodegradability of PHA (Mochizuki and Hirami, 1997; Tokiwa and Calabia, 2004). Other factors influencing *in vivo* degradation such as location, surface area, physical shape and form can be very important. Thus, *in vitro* studies are not always good indicators of *in vivo* polymer behavior. The specific material requirements will differ according to the nature of the application.

Studies on PHA polymers enzymatic hydrolysis in animal tissue are primarily based on *in vitro* investigation. With that aim, influence of different additives as for instance polysaccharides, polycaprolactone (PCL), lipases, PHA depolymerases and several extract on PHA degradation was examined.

PHA depolymerases are profoundly studied enzymes involved polymer degradation. However, even they are abundant in the environment, their PHA degradation activity is linked to soil and there are no evidences of their presence in animal tissue (Williams and Martin, 2002). However, characterization of PHA depolymerases gave some hints on the properties that other α/β hydrolases from animal tissue might harbor (Winkler et al., 1990; Jendrossek et al., 1996). Thus, to examine the involvement of lipases in degradation process, 16 different lipases were tested on 5 PHA polymers. It was demonstrated that lipases can hydrolyze PHA polymers decreasing in following order poly-3-hydroxypropionate (PHP)>P4HB > poly-5-hydroxyvaleriate (P5HV)>poly-6-hydroxyhexanoate (P6HH), whereas none of the lipases hydrolyzed PHB (Mukai et al., 1993). Moreover, some of the earliest studies suggest that microbial lipases neither degrade PHB (Tokiwa et al., 1986). However, two lipases have been detected in tissue adjacent to PHB implant raising the possibility of their involvement in PHB degradation (Lobler et al., 1999).

Moreover, possible participation of the gastrointestinal tract enzymes in the degradation process was studied *in vitro*. To that end, PHB was subjected to porcine pancreatin that contains a mixture of enzymes (lipase, amylase, α-chymotrypsin, trypsin and protease) and obtained results indicated a participation of enzymes in PHB hydrolysis (Freiera et al., 2002).

Effect of different extracts on PHB-*co*-HV degradation was tested *in vitro*. It was demonstrated that percentage of weight loss decreased in following order newborn calf serum > pancreatin > synthetic gastric juice > Hank´s buffer (Atkins and Peacock, 1996). Moreover, digestability of PHB-*co*-HV *in vivo* was demonstrated and it increased when polymer was treated with sodium hydroxide (Forni et al., 1999)

Studies have demonstrated that macrophages are able to phagocytize PHB *in vitro* (Saad et al., 1999) and free radicals, acidic products or enzymes produced by these cells may also accelerate the degradation (Tracy et al., 1999). Moreover, it was demonstrated that when biodegradable polymer is implanted *in vivo*, macrophages and foreign body giant cells phagocytize and resorb the polymer (Marios and Zang, 1999; Shishatskaya et al., 2008). However, unique mechanism and enzymes involved in

degradation process *in vivo* have not been identified, as they are shown to differ depending of the PHA polymer.

Another proposed mechanism of PHA degradation is based on non-enzymatic chemical hydrolysis. This type of degradation was studied on PHO in water and phosphate buffer saline, PBS *in vitro* (Marois et al., 1999). It was found that the hydrolytic degradation is characterized by water absorption that induces increase of porosity and crystallinity, which subsequently leads to polymer hydrolysis (Marois et al., 1999). In addition, physical appearance of polymer changes, surface gloss is lost and rugosity develops (Chaput et al., 1995).

Water uptake and chemical hydrolysis that lead to polymer swelling are the mechanisms proposed to initiate the degradation process of *in vivo* implanted PHA (Hazer and Hazer, 2011). In the studies carried out *in vivo* it was found that PHO-*co*-HHx degrades slowly. The subcutaneous implants of PHO-*co*-HHx in mice decreased in Mw from 137,000 at implantation to around 65,000 over 40 weeks, and there was no significant differences between the molecular weights of samples taken from the surfaces and interior of the implants. The latter finding suggests that slow, homogenous hydrolytic breakdown of the polymer occurs (Williams et al., 1999). For, PHB it was reported that hydrolysis starts from random chain scission as this kind of hydrolysis is followed by decrease in molecular weights with unimodal distribution and relatively narrow polydispersity (Williams and Martin, 2001). However, PHB-*co*-HHx increased its polydispersity accompanied by an increase of crystallinity followed by a drop over the period of 6 months. These phenomena are attributed to the difference in the degradation rate of crystalline and amorphous regions in the polymers. The fact that amorphous regions are more accessible to aqueous liquid usually leads in increase in crystallinity. When the chain scission occurs in crystallinity regions, reduction of overall crystalinity manifests. Possible reason of the difference in PHB and PHB-*co*-HHX degradation could be coexistence of two different degradation mechanisms: enzymatic and non-enzymatic catalyzed (Qu et al., 2006).

It is worth nothing that *in vivo* as most PHA polymers break down they release hydroxyl acids that are significantly less acidic and less inflammatory than many currently used synthetic absorbable polymers (Taylor et al., 1994).

Different approaches have been used to increase PHA degradability as for instance increasing hydrophilicity, polymer surface, crystallinity reduction and others. Thus, PHO-*co*-HHx was blended with gelatin and the degradation was accelerated (Wang et al., 2004). Blending of gelatin created a more porous polymer surface and subsequently more surface area of the polymer was exposed for hydrolysis attack (Wang et al., 2004). Studies have been carried out to increase the hydrophilicity of the polymer, either by incorporating more hydrophilic groups in the polymer chain or by grafting more hydrophilic molecules onto the polymer chain. Such modifications enable improved water uptake and swelling of the polymer matrix, thus leading to better hydrolysis (degradation) of the polymer. In one such study, efficient improvement of degradation was achieved by PLA and polyethylene glycol (PEG) grafting onto the backbone of PHO-*co*-HU (Renard et al., 2012).

II. OBJECTIVES

As it was previously mentioned, functionalization of PHA confers new properties to the polymer and subsequently open wide range of possibilities for industrial and biomedical application. Depending on the needs of designated application different strategies for polymer modification can be used. Moreover, due to the high hydrophobicity of the PHA and the presence of endotoxins, polymer modification processes need to be studied in detail and refined for specific application. Therefore, the main gol of this PhD Thesis was to study the components of PHA machinery that control granule formation and localization within the bacterial cell, as well as to address the key factors that drive phasin tag immobilization to the granule. Moreover, the new properties of functionalized PHA applying metabolic engineering approach were investigated. Therefore, this PhD Thesis was organized in following objectives:

- Design of natural PHA nano-beads engineered to display fusion proteins of interest by strategy for tailor-made functionalizing of PHA granules.
- Testing new properties of second generation bacterial polyesters carrying chemically modifiable functionalized side chain that confers new properties to the polymer.
- *In vivo* investigation of second generation mcl-PHA antibacterial properties and biocompatibility.
- Development of a noninvasive method for *in vivo* real-time monitoring of mcl-PHA implant associated infection and inflammation.

III. Materials and methods

1. Bacterial strains, plasmids, media and growth conditions

The bacterial strains used throughout this study are listed in Table 4. Unless otherwise stated *Escherichia coli* and *Pseudomonas putida* strains were grown in Luria-Bertani (LB) medium (Stambrook and Russell, 2001) with aeration at 37°C and 30°C respectively. The appropriate selection antibiotics, kanamycin (50 µg/mL), gentamycin (5 µg/mL), rifampicin (50 µg/mL) or ampicillin (100 µg/mL) were added when needed. The *P. putida* strain KT2442, a derivative strain of the parental strain KT2440 whose complete nucleotide sequence of the genome is accessible in the data bank (Nelson *et al.*, 2002), was used throughout this study. *Escherichia coli* DH10B (Invitrogen) and *E. coli* BL21 (DE3) (harboring the T7 RNA polymerase gene under control of the *lacUV5* promoter) were used as hosts for gene cloning and overexpression, respectively.

Table 4. Bacterial strains, plasmids and oligonucleotide primers

Strains		
P. putida		
KT2442	KT2440 derivative strain	Nelson *et al*. (2002)
KT42F	KT2442 derivative strain, *phaF* deletional mutant	Galan *et al*. (2011)
KT42I	KT2442 derivative strain, *phaI* deletional mutant	This work
KT42C1	KT2442 derivative strain, *phaC1* deletional mutant	Eugenio *et al*. (2010)
KT42C1ZC2	KT2442 derivative, *phaC1, phaZ, phaC2* deletional mutant	This work
KT42C1ZC2F	KT42C1ZC2 derivative strain, *phaF* deletional mutant	This work
KT42C1ZC2F-BG	KT42C1ZC2F derivative strain containing BioF-GFP	This work
KT42-BG	KT2442 derivative strain containing BioF-GFP	This work
KT42F-BG	KT42F derivative strain containing BioF-GFP	This work
KT42I-BG	KT42I derivative strain containing BioF-GFP	This work

KT42I-F	KT42I derivative strain containing *phaF*	This work
KT42I-BGF	KT42I-BG derivative strain containing *phaF*	This work
KT42I-GC	KT42I derivative strain containing GFP::C-PhaF	Galan *et al.* (2011)
KT42F-GC	KT42F derivative strain containing GFP::C-PhaF	Galan *et al.* (2011)
KT42-GC	KT2442 derivative strain containing GFP::C-PhaF	Galan *et al.* (2011)
Escherichia coli		
DH10B	Host for *E. coli* plasmids	Invitrogen
CC118λpir	Host for pVLT35 plasmids	Herrero *et al*. (1990)
SM10λpir	Host for pPF61 plasmids	Prieto *et al.* (1999)
SM10λpir (pKNGFdel)	Host for pKNGFdel plasmids	Galan *et al.* (2011)
Plasmids		
pMAB20-GFP-LYTAG	pMAB20 derivate harboring BioF-GFP-LYTAG	Biomedal S.L.
pKI18mobsacB	pK18mobsacB derivate containing fragments upstream and downstream *phaI* gene	This work
pCNB5	pUTminiTn*5*, *lacI*^{q}*::Ptrc*, Km^{r}, Ap^{r}	Lorenzo *et al*. (1993)
pCNB5-BioF-GFP-LYTAG	pCNB5 derivate containing BioF-GFP-LYTAG	This work
pCNB5-GFP-Cterm	pCNB5 derivate containing GFP-C-term	This work
pGEM-T	Ap^{r}, cloning vector	Invitrogen
pPF61	pJMT6, *lacI*^{q}*::Ptrc::phaF*	Prieto *et al.* (1999)
pKNGFdel	pKNG101 derivate containing fragments upstream and downstream *phaF* gene	Galan *et al.* (2011)
pGreenTIR	plasmid harbouring GFP cassette	Miller *et al*. (1997)

pUC18NotGFP	pUC18Not derivate containing GFP casstet	This work
pUC18NotGFP-Cterm	pUC18Not derivate containing GFP-C-term	This work

Oligonucleotide primers

F5mutI GCGGATCCCCGGTCAGCTTCTCGATCTG (BamHI)

F3mutI CGGAATTGGAGAGCAGGATGGCTGGC (EcoRI)

X5mutI CGGAATTCATGGAGGCTGGGCTTGAG (EcoRI)

X3mutI TCCCCCGGGAGATCACCTGTGCTGGCC (SmaI)

D5mutF CGGGATCCCAACGAACTCGGCATCAGC (BamHI)

I3mutF TCCCCCGGGCTGGACACGCTTGGCGAGG (SmaI)

D3MutF CGGAATTCCAACACTACATCTCCAGCAG (EcoRI)

I5mutF CGGAATTCGCCAGCCATCCTGCTCTCC (EcoRI)

I3mutF TCCCCCGGGCTGGACACGCTTGGCGAGG (SmaI)

GFP-F GGGAATTCTGATTAACTTTATAAGGAGGAAAAACAT (EcoRI)

GFP-RBamHI CGGGATCCTTTGTATAGTTCATCCATGCCAT (BamHI)

C-termF (GFP) CGGGATCCTCGCGCGCTGCAGCAAC (BamHI)

C-termR (GFP) GCCAAGCTTCAGATCAGGGTACCGGTGCC (HindIII)

FR1-C1ZC2-5' GCTCTAGAGATCCAGATCCAGATCGACGCGGC (XbaI)

FR1-C1ZC2-3' CGGGATCCCATCTACGACGCTCCGTTGTCC (BamHI)

For optimal PHA production, a preculture of the *P. putida* strains was cultivated overnight in LB medium, washed and inoculated at 0.3 OD_{600} in 0.1 N M63, a nitrogen-limited minimal medium (13.6 g of KH_2PO_4/l, 0.2 g of $(NH_4)2SO_4$/l, 0.5 mg of $FeSO_4 \cdot 7H2O$/l, adjusted to pH 7.0 with KOH) at 30°C and 250 rpm as previously described (Moldes et al., 2004). This medium was supplemented with 1 mM $MgSO_4$ and a solution of trace elements (composition 1,000× 2.78 g of $FeSO_4 \cdot 7H_2O$/l, 1.98 g of

$MnCl_2 \cdot 4H_2O$/l, 2.81 g of $CoSO_4 \cdot 7H_2O$/l, 1.47 g of $CaCl_2 \cdot 2H2O$/l, 0.17 g of $CuCl_2 \cdot 2H_2O$/l, 0.29 g of $ZnSO_4 \cdot 7H2O$/l). Sodium octanoate 15 mM was used as carbon source. Growth was monitored with a Shimadzu UV-260 spectrophotometer at 600 nm.

For analyzing: i) biofilm formation, ii) bacterial adhesion properties on PHACOS and PHO, iii) antibacterial activity of PHACOS and PHO and iv) minimal inhibitory concentration (MIC) of their fatty acid precursors, pre-culture of all bacterial strains, bacteria were transferred from a stock frozen at -80 °C with 15% of glycerol, to a screw-capped test tubes with Nutrient Agar slant culture medium (Nutrient Broth DifcoTM (ref 234000, Becton, Dickinson and Company, France) supplemented with 1.5% agar) and incubated at 37 °C for 16-24 h. Afterwards, bacteria were transferred onto fresh slant culture medium and incubate at 37 °C for 16 h-20 h.

Bacterial test inoculum for adhesion experiments and antibacterial activity testing were prepared by resuspending bacteria pre-cultured on slant medium in 2 mL of 1/500 Nutrient Broth, to serve as cell suspension according to the protocol described in ISO 22196:2007(E). Bacterial concentration was estimated via colony forming units counting (CFU) in the suspension by plating 10-fold serial dilutions in phosphate-buffered physiological saline (PBS 10mM, pH 7.2) on LB agar plates (Sambrook and Rusell, 2001). CFU were counted after 24h incubation at 37°C.

For the assays corresponding to bacterial capacity to form biofilms on polymer surfaces, cells pre-cultured on slant medium were transferred and grown with aeration in trypticase soy broth (TSB) supplemented with 0.3% glucose and 0.4% yeast extract for 20h at 37°C. Bacterial concentration was estimated spectrophotometrically at 600 nm.

For MIC determination, test inoculums were prepared by resuspending bacteria pre-cultured on slant medium in 2 mL of Muller-Hinton broth (MHB, Becton Dickinson). Bacterial concentration was estimated spectrophotometrically at 600 nm.

The bacterial strains used for *in vivo* real-time monitoring implant infection were *Staphylococcus aureus* subsp. *aureus* ATCC 12600, its two derivate luminescent strains *S. aureus* pAmiBlaz and *S. aureus* pAmiSPA2. All bacterial strains were pre-cultured in

TSA plates and incubated at 37°C for 24 h. The appropriate selection antibiotics, chloramphenicol (10 µg/mL) or kanamycin (200 µg/mL) were added when needed. Trypticase soy broth (TSB, Difco ref) was used as the growth medium to culture the bacterial pathogens.

2. Molecular biology techniques

Standard molecular biology techniques were performed as previously described (Sambrook and Russell, 2001). PCR products were purified with the High Pure plasmid isolation kit (Roche Applied Science). DNA fragments were purified with Gene-Clean Turbo (Q-BIO-gene). Genomic DNA from *P. putida* KT2442 was isolated with the Genomic Prep Cells and Tissue DNA Isolation kit (Amersham Biosciences). All cloned inserts and DNA fragments were confirmed by DNA sequencing with fluorescently labeled dideoxynucleotide terminators and AmpliTaq FS DNA polymerase (Applied Biosystems Inc.) in an ABI Prism 377 automated DNA sequencer (Applied Biosystems Inc.). Transformation of *E. coli* cells was carried out using the RbCl method (Sambrook and Rusell, 2001). All oligonucleotides used for PCR amplification are listed in Table 4.

3. Construction of different genetically manipulated *P. putida* KT2442 and *S. aureus* CECT 86 strains

3.1. Construction of PhaF null mutant and PhaI null mutant of *P. putida* KT2442

The *phaF* gene was inactivated by marker exchange as described previously using the mobilizable suicide plasmid pKNG101 (Kaniga *et al.*, 1991). The deletion of *phaF* gene was engineered with the DNA fragments DmutF and ImutF of 575 bp and 402 bp respectively, generated by PCR using the primer pairs D5mutF and D3MutF for DmutF, and I5mutF and I3mutF for ImutF. These two fragments were digested with the appropriate restriction enzymes and ligated using T4 ligase resulting in a single 977 pb

fragment carrying a deletion of the *phaF* gene which was cloned into the unique *Bam*HI and *Sma*I sites of pKNG101 to yield pKNGFdel. Plasmid pKNGFdel was used to deliver the *phaF* mutation to the host chromosome via homologous recombination. Biparental mating was performed following protocols described by de Lorenzo and Timmis (1994), using *E. coli* SM10 pir (pKNGFdel) as donor strain and *P. putida* KT2442 as recipient strain. For conjugation, 100 µl of overnight cultures of donor and recipient strains were mixed in 5 mL of 10 mM $MgSO_4$ and collected on a Millipore filter which was subsequently placed on an LB agar plate and incubated overnight at 30°C. After incubation, the cells were resuspended in 5 mL of 10 mM $MgSO_4$ and plated on M63 selective plates supplemented with 5% sucrose as described previously (Kaniga et al., 1991). Transconjugants (Suc^R, Sm^S) were isolated. The second crossover event was confirmed by PCR using primers D5MutF and I3MutF. The resultant mutant strain was denoted KT42F.

P. putida KT42I, *phaI* gene deleted strain, was constructed by disruption of *phaI* gene using plasmid pK18mobsacB (Schäfer et al., 1994). DNA manipulations and other molecular biology techniques were performed according to Stambrook and Russel (2001). The 481bp and 339bp fragments upstream and downstream *phaI* gene were PCR-amplified with F5mutI and F3mutI or X5mutI and X3mutI primers respectively. Total DNA of *P. putida* KT2442 strain was used as template. DNA fragments were purified by standard procedures using Gene Clean (BIO 101, Inc.). The resulting fragments were digested with the appropriate restriction enzymes and ligated using T4 ligase resulting in a single 820bp fragment carrying a deletion of the *phaI* gene which was cloned into the unique *BamHI* and *SmaI* sites of pK18mobsacB to yield pKI18mobsacB. Plasmid pKI18mobsacB was used to deliver the *phaI* mutation to the host chromosome via homologous recombination. Similarly, P. putida KT42C1ZC2 strain was constructed using FR1-C1ZC2-5′ and FR1-C1ZC2-3′ and FR2-C1ZC2-5′ and FR2-C1ZC2-3′ set of oligonucleotides. Triparental mating was performed following protocols described by Herrero et al. (1990), using *E.coli* DH10B (pKI18mobsacB) as donor strain and *P. putida* KT2442 as recipient strain. Successful gene disrupted strains were selected in M63 0.1N plates supplemented with 0.1% citrate, 5% sucrose and kanamycin and confirmed by PCR analysis, DNA sequencing and SDS-PAGE analysis.

The second crossover was confirmed by PCR amplification using F5mutI and X3mutI primer.

3.2. PhaF null mutant strains construction of *P. putida* KT42C1ZC2

To construct *P. putida* KT42C1ZC2F strain, the phaF gene was inactivated by marker exchange using the mobilizable suicide plasmid pKNGFdel as previously described (Galan et al., 2011). Briefly, biparental filter-mating technique was performed (de Lorenzo and Timmis, 1994) using *E. coli* SM10λpir (pKNGFdel) as donor strain and *P. putida* KT42C1ZC2 as recipient strain. Transconjugants (SucR, SmS) were isolated. The second crossover event was confirmed by PCR using primers D5MutF and I3MutF.

3.3. Complementation of *P. putida* KT42F, *P. putida* KT42I and *P. putida* KT42I-GN strains

Plasmid pPF61, harbouring the *phaF* gene from *P. putida* GPo1 under the control of the *Ptrc* promoter (Prieto *et al.*, 1999) was introduced into *P. putida* KT42F, *P. putida* KT42I and *P. putida* KT42I-GN chromosome by triparental mating. The resulting strains called KT42F-F, KT42I-F and KT42I-GNF, respectively were cultivated in PHA production medium in the presence of 5 mM (isopropyl-1-thio-β-D-galactopyranoside) IPTG as described (Prieto *et al.*, 1999).

3.4. Construction of *P. putida* strains expressing a cassette consisting in a fusion gene GFP and C- terminal domain of PhaF

The GFP::C-PhaF fusion was obtained by amplification of two DNA fragments. GFP cassette was amplified from plasmid pGreenTIR (Miller and Lindow, 1997) with GFP-F and GFP-RBamHI. After digestion with the corresponding restriction endonucleases,

the GFP cassette was cloned into pUC18Not plasmid yelding pUC18NotGFP. *phaF* C-terminal domain was PCR amplified using C-termF (GFP) and C-termR (GFP) oligonucleotides from genomic DNA of *P. putida* KT2442. Obtained PCR product was digested and cloned into pGEM-T plasmid. The fragment obtained after digestion with *Hind*III and *BamH*I was cloned into pUC18NotGFP plasmid. The resulting hybrid plasmid pUC18NotGFP-Cterm was transformed into *E.coli* strain DH10B. Construction was confirmed by sequencing using an ABI Prism 3730 DNA Sequencer. The GFP::C-PhaF fusion was cloned from pUC18NotGFP-Cterm plasmid into pCNB5 vector as *Not*I fragment. Constructed plasmid pCNB5-GFP-Cterm was introduced into the *P. putida* KT2442 and *P. putida* KT42F chromosomes by triparental mating yielding KT42-GC and KT42F-GC, respectively. Conjugates were isolated after plating on M63 0.1N selective plates supplemented with 0.2% citrate and kanamycin. Afterwards colonies were picked in LB plates and LB plates with IPTG and selected with a fluorescent magnifying lamp.

3.5. Insertion of GFP and BioF (N-terminal of PhaF protein) fusion as a monocopy into the chromosome of *P. putida* strains

To study localization of BioF *in vivo*, the mobile cassette carrrying the BioF-GFP fusions were inserted as a monocopy into the chromosome of different *P. putida* strains via mini-Tn5 transposons. A 1730-bp DNA NotI/NotI fragment containing Ptac::BioF-GFP-LYTAG was obtained after digestion from pMAB20-GFP-LYTAG plasmid kindly provided by Biomedal S.L. Plasmid pCNB5 was used as cloning vector where BioF-GFP was inserted as NotI fragment to yield pCNB5-BioF-GFP allowing to drive the expression of the fusion under the control of lacIq-Ptrc regulatory system. *E. coli* CC118λpir cells were transformed and positive clones were selected in LB plates supplemented with kanamycin. Resulting construction (pCNB5- BioF-GFP) was transferred into *P. putida* KT2442, *P. putida* KT42F, *P. putida* KT42I, *P. putida* KT42C1ZC2 and *P. putida* KT42C1ZC2F by triparental mating technique to give rise to P. putida KT42-BG, *P. putida* KT42F-BG, *P. putida* KT42I-BG, *P. putida* KT42C1ZC2-BG and *P. putida* KT42C1ZC2F-BG respectively (Figure 17A). Transconjugants were selected on

0.1N M63 plates supplemented with 0.2% citrate, kanamycin, 0.1mM IPTG (isopropyl-1-thio- -D-galactopyranoside) and confirmed by SDS-PAGE and Western Blot analysis as previously described (Moldes et al., 2004). Western blot analysis was performed with the ECL Western Blotting Detection Kit (Amersham Biosciences) according to the protocol described by the manufacturer. Rabbit polyclonal antiserum against PhaI and BioF was generated as previously described (Moldes et al., 2004). Colonies were picked to LB plate with and without IPTG. Selection of fluorescent green colonies was done from LB plate supplemented with IPTG by fluorescent magnifying lamp.

3.6. Construction of *S. aureus* luminescent strains

Bioluminescent *S. aureus* strains were generated by transforming CECT 86 strain with a modified Photorhabdus luminescens luxCDABE (lux) gene cluster using the pAmiBlaz or pAmiSPA2 plasmids. To construct the vectors, blaz (β-lactamase) with selected mutation and spa2 (protein A) promoters were inserted into promoterless-lux cloning vector, pAmilux (Mesak et al., 2009) to yield pAmiBlaz or pAmiSPA2 plasmid, respectively. Vectors were introduced into the cells by electroporation as previously described (ref). Transformants were selected on trypticase soy agar (TSA) plates containing chloramphenicol (10 µg/ mL). Successful transformation was confirmed by bioluminescent colonies screening using an IVIS Lumina bioimaging system (Xenogen).

4. Flow cytometry

Cells were harvested and washed twice with distilled water and resuspended in water to a final OD_{600} of 0.2 for staining with Nile Red. A Nile Red stock solution was made by dissolving the dye to a concentration of 1 mg/mL in dimethyl sulfoxide (DMSO). Three microliters stock solution was added to 1 mL of cell suspension. The mixture was incubated in the dark for 15 min and analyzed by Flow citometry (flow cytometer Coulter EPICS XL). *P. putida* KT42C1 minus strain (a *phaC1* mutant which produces <1% CDW PHA) (de Eugenio *et al*., 2010a) was used as negative control. A

calibration curve for the quantification of the PHA content using flow cytometry was made comparing the fluorescence intensity and PHA content analyzed by gas chromatography throughout the growth curve in *P. putida* KT2442 (data not shown). The relation between both parameters was fitted to the equation y= 30.874 Ln(x) + 38.11 with a R^2=0.9984. This equation has been used to translate the cytometry fluorescence intensity data into PHA values.

5. Transmission electron microscopy

Cells were harvested, washed twice in PBS, and fixed in 5% (w/v) glutaraldehyde in the same solution. Afterwards, cells were suspended in 2.5% (w/v) OsO_4 for 1 h, gradually dehydrated in ethanol [30, 50, 70, 90, and 100% (v/v); 30 min each] and propylene oxide (1 h), embedded in Epon 812 resin. Ultrathin sections (thickness 70 nm) were cut with a microtome using a Diatome diamond knife. The sections were picked up with 400 mesh cupper grids coated with a layer of carbon and subsequently observed in a Jeol-1230 electron microscope (JeolLtd., Akishima, Japan).

To determine the size of PHA granules from the micrographs, 50 cells of the wild type and of the mutant were selected, in which the PHA granule diameter was measured. We analyzed 100 granules of the wild type and 100 of the mutant. Only granules with sharp boundaries were selected. The number of PHA granules per cell was determined only from cells which were fully visible in the electron micrographs.

6. *In vivo* localization of the C- and N-terminal domain of PhaF by fluorescence microscopy

P. putida KT42-GC and KT42F-GC strains were cultivated overnight in LB medium. Then, cells were washed and inoculated at 0.3 OD_{600} in 0.1 N M63. Cultures were induced with 2 mM IPTG in the exponential phase of growth to induce the production of the GFP::C-PhaF fusion protein. Staining for nucleoids (Nucleoids staining) was

performed by incubation with 2 µg/mL (DAPI) for 15 min while the PHA granules were (stained) visualized after staining with 1 µg/mL Nile Red for 15 min. Then cells were fixed with 4% paraformaldehyde at room temperature for 1 h, washed tree times with PBS and visualised by confocal microscopy Laser Confocal espectral (CLSM) Leica TCS SP2-AOBS.

P. putida KT42-BG, *P. putida* KT42F-BG, *P. putida* KT42I-BG, *P. putida* KT42I-BGF, *P. putida* KT42C1ZC2-BG and *P. putida* KT42C1ZC2F-BG living cells expressing BioF-GFP fusion protein were visualized with a Zeiss Axioplan Universal epifluorescence microscope operated for incident-light fluorescence and contrasting techniques of bright field and phase contrast. Cells cultivated in LB medium or in PHA producing conditions were induced with 2 mM IPTG in the exponential phase of growth for the production of the BioF-GFP fusion protein and observed after 8h of incubation. Micrographs were recorded with digital camera Leica DFC350FX.

To examine in detail co-localization of BioF-GFP fusion protein, nucleoid and granules *P. putida* KT42I-BGF strain was cultivated overnight in LB medium. Once washed, cells were inoculated at 0.3 OD600 in 0.1 N M63. Cultures were induced with 2 mM IPTG in the exponential phase of growth for the production of the BioF-GFP fusion protein. Nucleoids staining was performed by incubation with 2 µg/mL (DAPI) for 15 min while the PHA granules were stained with 1 µg/mL Nile Red for 15 min. Afterwards, cells were fixed with 4% paraformaldehyde at room temperature for 1 h, washed tree times with PBS and visualised by confocal microscopy Laser Confocal espectral (CLSM) Leica TCS SP2-AOBS.

7. PHA quantification

Polyhydroxyalkanoate monomer composition and cellular PHA content were determined by gas chromatography-mass spectrometry (GC-MS) following previously described protocol (de Eugenio et al., 2010). Briefly, samples were subjected to methanolysis in the presence of 15% (w/v) sulfuric acid, and resulting methyl esters of monomers were analyzed by injecting 1 µl of sample into Perkin Elmer AutoSystem gas

chromatograph equipped with SPB1 Supelco capillary column (25 m x 0.25 mm inner diameter x 0.22 µm) and ionization detector. Biomass was calculated as previously described (de Eugenio et al., 2010).

An additional, quantification of the PHA content was performed by Flow citometry (flow cytometer Coulter EPICS XL). Analysis was done as described before (Galan et al., 2011). Briefly, PHA was stained adding 3 µl of Nile Red stock solution (1 mg/mL in dimethyl sulfoxide) to 1 mL of harvested and washed cells, previously diluted to OD600 of 0.2. The mixture was incubated in the dark for 15 min and analyzed. *P. putida* KT42C1 minus strain (a *phaC1* mutant which produces <1% CDW PHA) (de Eugenio et al., 2010) was used as negative control. The quantification of the PHA content using flow cytometry was made comparing the fluorescence intensity and PHA content analyzed by gas chromatography as previously described (Galan et al., 2011).

8. Protein quantification

Content of BioF-GFP fusion protein was quantified by flow cytometry, fluorometry and software package QuantityOne protein for protein quantification in SDS-PAGE protein gels.

For BioF-GFP fluorescence quantification by flow cytometry, 1 mL of cells grown in PHA producing conditions was harvested after 8h of incubation, washed twice with distilled water and resuspended in water to a final OD600 of 0.2. *P. putida* KT42C1 minus strain (a *phaC1* mutant which produces <1% CDW PHA) (de Eugenio et al., 2010) was used as negative control.

Furthermore, an additional quantification of BioF-GFP fluorescence was performed by fluorometry, allowing the comparison of fluorescence of GFP in whole cells and isolated granules carrying GFP. *P. putida* strains were cultivated in PHA producing conditions. When A600 reached 0.6 the culture was induced with 0.1 mM ITPG. After 8 h of incubation, 1 mL of cultures were harvested, washed twice with distilled water and resuspended in water to a final OD600 of 0.2 for fluorometry

analysis of whole cells. The rest of the culture was used for granule isolation. After harvesting, cells were resuspended in 15mM Tris-HCl pH 8, and disrupted by passing through a French pressure cell twice. The extracts were centrifuged 30 min at 10,000×g, and the pellet fraction was dissolved in 5 mL of 15mM Tris-HCl pH 8. Granule isolation was done by centrifugation (12,000xg for 30 min) onto 55% glycerol (Merrick and Doudoroff, 1964) of total crude extract kept at 4°C during the entire process. After extraction granules containing PHA-immobilized GFP protein were resuspended in 15mM Tris-HCl pH 8 to a final OD600 of 0.2 and analyzed by Fluorimetry (excitation/emission).

For BioF-GFP quantification by QuantityOne, isolated granules proteins were separated in 12.5% SDS-polyacrylamide gels and stained with Coomassie brilliant blue G-250 following previously described protocol (Stambrook and Russell, 2001). Protein content calculation in examined *P. putida* strains was carried out by densitometric scanning using Gel Doc XR and analyzed using Quantity One software (version 4.6 basic) (Bio-Rad, Hercules, CA) and calibrating with broad-range molecular mass markers from Bio-Rad.

9. PET disk coating with PHACOS and PHO

All medium-chain-length polyhydroxyalkanoates (mcl-PHA) applied in this study were prepared as previously reported (Escapa et al., 2011) and kindly provided by Bioplolis S.L. To determine PHA monomer composition, gas chromatography-mass spectrometry (GC-MS) and nuclear magnetic resonance (NMR) analysis were carried out as previously described (Escapa et al., 2011). The monomer content of PHACOS was 29.7% of non-functionalized monomers OH-Alk (17.5% of 3-hydroxyoctanoate (OH-C8), 10.3% of 3-hydroxydecanoate (OH-C10), and 1.9% of 3-hydroxyhexanoate (OH-C6) monomers) and 70.3% of functionalized monomers (46.4% of 3-hydroxy-6-acetylthiohexanoate (OH-6ATH) and 23.9% of 3-hydroxy-4-acetylthiobutanoate (OH-4ATB) monomers). The PHO (poly 3-hydroxyoctanoate-co-hydroxyhexanoate) consisted of 8.5% OH-C6 and 91.5% OH-C8. An optimized downstream processing was applied to eliminate endotoxins as previously described (Furrer et al., 2007). Briefly, 1 g of PHA was dissolved in 100 mL of chloroform at 40°C under intense stirring, subsequently the suspension was pressure filtrated (Vacuubrand MZ2C diaphragm vacuum pump) and the polymer was precipitated by addition of non-solvent methanol. Finally, the polymer was dried under vacuum at 40°C for 48h. The procedure was repeated two times to obtain mcl-PHA with endotoxin units (EU) as low as 20 EU/g, in compliance with endotoxin requirements of the FDA for biomedical applications. The endotoxicity was measured using a Limulus amebocyte lysate (LAL)-test (Pyrogent Plus Single Test Kit, 0.125 EU/mL, Lonza) according to the protocol described elsewhere (Furrera et al., 2007). Each analysis was carried out at least twice. Using this method, values of PHACOS and PHO endotoxicity were determined being less than 12 EU/g and 15 EU/g, respectively.

For disk fabrication, the PET disks were coated with PHACOS or PHO by solvent-casting method; polymeric materials dissolved in chloroform (2% w/v) were applied over sterile, endotoxin-free PET disks (6 mm diameter) kindly supplied by ACCIONA (Barcelona, Spain) in a dust-free atmosphere and the coatings were allowed to dry for 72 h at room temperature. The resulting PHACOS-coated disks (PHACOS disks), PHO-

coated disks (PHO disks) and control PET disks were sterilized overnight with ethylene oxide (EtO) at 40˚C.

10. Mcl-PHA microparticles preparation

The preparation of microparticles was carried out by the emulsion technique previously described (Freitas et al., 2005) and modified as follows: 1 mL water was first emulsified during the addition of 10 mL of PHA polymer solution in dioxane (1%w/v). The resulting emulsion was thereafter mixed by sonication for 1 min with a 2% PVA aqueous solution (40mL), involving the inversion of emulsion. After evaporation of ethyl acetate under reduced pressure, the microparticles were isolated by centrifugation (12 000 rpm for 20 min at 25 °C). Three washing cycles with deionized water followed by centrifugation were applied to remove the PVA. The morphology and the size of microparticles was analyzed by scanning electron microscopy (SEM) using a Philips XL 30 ESEM apparatus at an accelerating voltage of 15 keV. It was equipped with a field emission Hitachi SU800 apparatus. The samples were prepared by deposition of the corresponding microparticle suspension (0.01 mg mL1) over glass disks (13 mm diameter and 1 mm thickness), and the solvent (H2O) was evaporated at room temperature for 24 h. All the samples were coated with chrome prior to examination by SEM.

11. Biofilm formation on mcl-PHA

By means of this assay we studied the capacity of PHACOS disks to prevent bacterial biofilm formation on its surface in comparison to the other materials. *S. aureus* CECT 86 and *P. aeruginosa* CECT 4122 were used as model strains able to form biofilm on different materials. The ability of bacteria to form biofilm in vitro on PHACOS, PHO and PET disks was examined by environmental scanning electron microscopy (ESEM), crystal violet assay and CFU counting.

The same optimal conditions as previously described for pneumococcal biofilm formation (Moscoso et al., 2006) were used to induce the production of biofilms by all examined strains. Briefly, previously prepared endotoxin-free sterile PET disks or PET disks coated with PHACOS or PHO were placed in 24-flat bottom well plates (ref.353947 Falcon, Becton Dickinson) and each well was inoculated with 1 mL of 1:100 diluted in fresh TSB cultures previously grown in TSB supplemented with glucose and yeast extract. Biofilm formation on each tested disk (PHACOS, PHO or PET) was carried out in triplicate. Plates were incubated in static condition for 16h at 37°C, and bacterial growth was determined by measuring the A595 using a plate reader (microplate absorbance reader 2020; Anthos Labtec Instruments GmbH).

For ESEM examination, following the incubation samples were washed three times with PBS 10mM, pH 7.2 and fixed with 2.5% glutaraldehyde for 2h at room temperature. The dried samples were mounted on aluminum stumps and sputter-coated with gold before examination under an environmental scanning electron microscopy (ESEM) apparatus (Philips XL 30) at an accelerating voltage of 15 KeV.

Formed biofilm was quantified by crystal violet assay according to previously described protocol (Moscoso et al., 2006). Briefly, after the staining with 0.5% crystal violet and rinsing to remove non adherent bacteria, biofilm was mechanically removed from the disks, solubilized in 95% ethanol (200 µL per well) and the absorbance was determined at 595 nm using an Anthos 2020 microplate absorbance reader (Anthos Labtec Instruments).

For CFU counting of bacteria present in the biofilm, pre-incubated disks were washed with distilled water to remove non adhered bacteria. Biofilm, in this case without staining, was mechanically removed from the disk using disposable steril micropipette tip, subsequently 10-fold dilutions were made in 10mM PBS, pH 7.2 and plated on LB plates. Bacteria were enumerated after 24h incubation at 37°C.

12. Bacterial adhesion to PHACOS and PHO

The number of viable bacterial cells adhered to the surface of biopolymers was determined by fluorescence microscopy using Bacterial Viability test LIVE/DEAD BacLightTM (Invitrogen L13152). The reference strains of *S. aureus* (CECT 86) and *P. aeruginosa* (CECT 4122) were used for in vitro adherence test. The same protocol was followed as indicated for measuring the antibacterial activity on plastic surfaces according to ISO 22196:2007 (E) (see below). As test inoculum bacterial suspensions in 1/500 NB (1-2 × 108 cells/mL) were placed on PHACOS, PHO and PET disks. After the incubation, bacteria were washed out from the disks and the solution was dyed following the manufacturer's instructions (Invitrogen L13152). Samples were visualized by Zeiss Axioplan Universal epifluorescence microscope operated for incident-light fluorescence and contrasting techniques of bright field and phase contrast. Micrographs were recorded with a digital camera Leica DFC350FX.

An additional test for confirmation of bacterial cells adherence on PHACOS, PHO and PET disks was performed by ESEM. PHACOS, PHO and PET disks were incubated with bacterial suspensions in 1/500 NB (1-2 × 108 cells/mL) for 24h at 37 °C. Afterwards, disks were washed to remove unattached bacteria and samples were processed in the same way as stated for biofilm examination.

12.1. Radioactive cell labelling

For enumeration of cells attached to microparticles bacterial were radioactively labelled. Following over night precultivation in LB medium, cell were washed with PBS 15mM, pH 7.2 and inoculated in Muller Hinton Broth II to optical density A600 0.1. For radioactive labelling, previously overnight air dried C14-6-glucose 20µCi for ethanol evaporation, was added to the cell culture and incubated for 24h at 37ºC. As a control, culture with non labelled glucose was used. Following the incubation, cells were peleted and cpm of supernatant was measured. Cell concentration was determined spectrophotometricaly.

For attachment assay, 1mL of previously prepared microparticles was mixed with 108 CFU/mL and incubated 1h at 37°C with shaking. Cpm was measured before and after 1h of incubation. For enumeration of bacteria attached to the microparticles, suspension was left 10min to sediment. Cpm of unattached and attached bacteria was determined.

13. Antimicrobial activity of mcl-PHA

Antibacterial activity was determined according to ISO 22196:2007(E) Measurement of Antibacterial Activity on Plastics Surfaces, with certain modifications. The bacterial strains used in this study are listed in Table 5. PHACOS, PHO and PET disks were used as test materials. Each disk was placed into a separate sterile Petri dish with the test surface uppermost and wet filter paper beneath to maintain relative humidity not less than 90%. Test inoculums prepared in 1/500 NB (6.2-25 × 10^3 cells/cm^2) were placed onto the analyzed surfaces without cover film as stated in ISO 22196:2007(E) and incubated for 24h at 37°C. Each material was tested in triplicate. Two set of controls were used; 1) non coated PET disks for determination of bacterial viability 2) PET disks coated with PHO, to analyze the effect of non functionalized PHA on bacterial viability. The controls and the disks coated with PHACOS were analyzed according to ISO 22196:2007(E) at 0h and 24h. Following the incubation with bacterial suspension, disks were washed with 1 mL of 10mM PBS, pH 7.2. The number of colonies recovered from PET disks at 0h is the value that was later on used to determine the recovery rate of the bacteria from the disks under investigation.

Viable bacteria were enumerated by performing 10-fold serial dilutions in 10mM PBS, pH 7.2 from 1 mL bacterial solution washed out from the disks. 1mL of each dilution was placed into separate sterile Petri dishes. Afterwards, 15 mL of LB agar 38 °C was poured into each Petri dish and swirled gently to disperse the bacteria. All plating was performed in duplicate. Inverted Petri dishes were incubated at 37°C for 40h to 48h. The number of colonies in the Petri dishes was counted, considering plates that contained 30 to 300 colonies as valid. Antibacterial activity was calculated as R

value according to the equation stated in ISO 22196:2007(E). R value of "0" means that the logarithm of number of viable cells in the sample disk after 24h is the same to that of control disk after 24h, whereas R=1 means 10-fold less viable cells recovered from sample disk after 24h when compared to that of control disk.

An additional test was performed to determine the activity of PHACOS against higher cell density conditions up to 1×10^{10} cells/cm^2. Bacterial viability was determined on PHACOS and PHO disks according to ISO 22196:2007(E) following the protocol stated before. Each disk was inoculated with correspondent S. aureus (CECT 86) suspension in 1/500 NB, starting with suspensions of 1×10^4 cells/cm^2 to 1×10^{10} cells/cm^2. Following the incubation, disks were washed with 1 mL of 10mM PBS, pH 7.2. 10-fold serial dilutions were made and plated on LB plates. Viable bacteria were enumerated after 24h incubation on 37 °C.

Table 5. Bacterial strains used for antibacterial activity assay

Bacteria	Strains
Staphylococcus aureus subsp*. aureus*	CECT 86
Mycobacterium smegmatis mc2	CECT 3020
Escherichia coli	CECT 516
Pseudomonas aeruginosa PAO1	CECT 4122
Staphylococcus epidermidis	CECT 232
Bacillus subtilis subsp. *subtilis*	ATCC 6051
Streptococcus dysgalactiae subsp. equisimilis	CECT 926
Streptococcus pyogenes	CECT 59T
Staphylococcus aureus 61115	MRSA 201232560
Staphylococcus aureus 61286	MRSA 201237858
Staphylococcus aureus 61314	MRSA 201238814/12

14. Determination of Minimal inhibitory concentration (MIC)

The minimal inhibitory concentration (MIC) of polymer precursors 6-acetythiohexanoic acid (545554, Sigma-Aldrich), octanoic acid (C5038, Sigma-Aldrich) and hexanoic acid (P9767, Sigma-Aldrich) was calculated by microdilution assay according to CLSI (Clinical and Laboratory Standards Institute) standard procedure. Moreover, to determine the antibacterial activity of PHACOS hidrolizate, two reaction mix containing 3.4 mg/ml of e PHACOS latex in 0.2 M Tris-HCl (pH 8), and a control containing 3.0 mg/ml of PHO latex in 0.2 M Tris-HCl (pH 8) were separately subjected to enzimatic hydrolysis with mcl-PHA extracellular depolymerase PhaZGK13, from *Pseudomonas fluorescens* GK13 (0.2 mg per assay). Following 1h incubation at 37°C, supernatants of each reaction mix were centrifuged and filtrated (filter de 0.2 µm). The degradation products were identificated and quantificated by HPLC mass spectrometry (HPLC-MS). It was determined that PHACOS hydrolizate was composed of 63% of trimer (tree monomeros of 3OH-acetyltiohexanoate fused) and 30% of trimeros containing mix of 3-hydroxioctanoic and 3-hydroxy-acetyltiohexanoic monomeros. The rest (7%) was a mix of all monomers and dimers. The PHO hydrolizate contained 66% of dimer (two 3-hydroxioctanoic monomers fused) and 26% of trimer (tree 3-hydroxioctanoico monomers fused) and the rest was a mix of all 3-hydroxioctanoic and 3-hydroxihexanoic monomers and dimers.

Stock solution of each compound was prepared in 10mM PBS, pH 7.2 with an initial concentration of 60 mM. Afterwards, serial dilutions were made in Muller-Hinton broth (MHB, Becton Dickinson) to determine MIC values. Briefly, the sterile 96-well round bottom clear polystyrene plates (Cultek S.L.U., Spain) were prepared by dispensing 100 µL of appropriate dilution of tested compound in culture broth per well. The *S. aureus* (CECT 86) inoculum in MHB was added to each well, providing a final concentration of 5 x 10^5 CFU/ml. A positive control (containing inoculum without tested compound) and negative control (containing tested compound without inoculum) were included in each microplate. The minimum inhibitory concentration (MIC) was defined as the lowest concentration of tested substance that inhibited visible growth of test bacteria.

15. *In vitro* biocompatibility

15.1. Cell cultures

The effect of toxicity of the analyzed systems was evaluated using two type of cells, mouse monocyte macrophages RAW 264.7 (ECACC, Sigma P11) and mouse fibroblasts BALB 3T3 (ATCC, CCL-163, P12), while anti-inflammatory activity and effect on cell proliferation was monitored on RAW 264.7. The cells were cultured in Dulbecco´s modified Eagle´s medium (DMEM) enriched with HEPES for BALB 3T3 cells and 110 mg/L of sodium pyruvate for RAW 264.7 cells and supplemented with 10% FBS, 100 units/mL penicillin, 100 µg/mL streptomycin and 200 mM L-glutamine (complete medium). A humidified atmosphere at 37 °C with 5% CO2 and 95% of air was used for maintenance of cell culture.

15.2. MTT assay

The *in vitro* effect of products possibly liberated from polymers, while being in contact with culture media, on cellular viability was assessed by the 3-(4,5-Dimethylthiazol-2-yl)-2,5-diphenyltetrazolium bromide) MTT assay (Mosmann et al., 1983). Previously prepared PHO, PHACOS and control PET disks were immersed in 5 mL of FBS-free DMEM each and placed on a roller mixer at 37 °C. The medium was removed at different time points (1, 2 and 7 days) and replaced with fresh medium. All the extracts were obtained under sterile conditions. RAW 264.7 cells were seeded at a density of 2 x 105 cells/mL in complete medium, while BALB 3T3 cells at a density of 1 x 105 cells/mL, plated in a sterile 96-well culture plate and incubated to confluence. Medium was replaced with the corresponding extract and incubated at 37 °C in humidified air with 5% CO2 for 24h. After incubation cell viability was determined by adding MTT (0.5 mg/mL in PBS pH 7.2) and incubated for 4h at 37 °C. Excess medium

and MTT was removed and DMSO was added to each well in order to achieve solubilization of formazan crystal formed in viable cells. The absorbance was measured at 570 nm (test wavelength) and 630 nm (reference wavelength) using a microplate reader (Biotek SYNERGY-HT). The cell viability (CV) was calculated from equation:

CV (%)=100 x (ODS – ODB)/ODC

where ODS, ODB and ODC are the optical density of formazan production for the sample, blank (DMEM without without cells) and control respectively.

15.3. Griess assay

The inflammatory activity of polymers was investigated using nitric oxide inhibitory assay performed according to the method of Wang et al. Briefly, RAW 264.7 cells were seeded in 96-well plates at a density of 2 x 10^5 cells/mL and incubated at 37 °C for 24h. After incubation corresponding extracts were added. To the control wells 1 mg/mL of lipopolysaccharide (LPS) was added and the cells were incubated for 24 h. The nitrite concentration was determined applying Griess reaction (Schmidt and Kelm, 1996). Aliquots of 100 µl of the supernatant from RAW 264.7 cells were reacted with 100 µl of Griess reagent (1:1 mixture of 0.1% N-(1-naphthyl) ethylenediamine in water and 1% sulphanilamide in 5% phosphoric acid) in a 96 well plate. The absorbance was recorded using a Biotek SYNERGY-HT reader at 548 nm. The nitrite concentration was calculated from a calibration curve previously obtained using known $NaNO_2$ concentrations. Data were expressed as percentage of NO production.

15.4. Cell proliferation assay

Alamar Blue assay (AB) was performed to follow cell adhesion and proliferation. Mouse fibroblasts BALB 3T3 were seeded at a density of 8 x 10^4 cell/mL over the disks placed in 24-well culture. After 24h incubation, 1 mL of Alamar Blue dye (10% Alamar Blue solution in phenol red free DMEM medium) was added to each specimen and incubated for 4h. Then, 100µL of culture medium from each test sample was

transferred to a 96-well plate, and the absorbance was measured at 530 nm emission/590 excitation on a Biotek SYNERGY-HT spectrometer. The disks were washed with 10mM PBS, pH 7.2 twice to remove rest of the reagent, and 1 mL of culture medium was added in order to monitor the cell growth over the time. This step was repeated at defined time points (5 and 10 days). Adhesion and proliferation of cells was also followed by direct analysis of the seeded disks by environmental scanning electron microscopy (ESEM).

15.5. Cell adhesion and cell growth

For determination of cell adhesion and growth, PHO, PHACOS and control PET disks were placed in a 24-well tissue-culture plate. BALB 3T3 cell suspension was added at a density of 8 x 10^4 cells/mL per well in 1 mL of respective culture medium and allowed to attach at 37 °C. Cell morphology and growth was monitored by scanning electron microscopy (SEM). For examination under ESEM microscope samples were collected at different time points (1, 2 and 7 days), washed with 10mM PBS, pH 7.2 to remove unattached cells and immobilized with 2.5% glutaraldehyde in distilled water for 1h at room temperature. The dried samples were mounted on aluminum stumps and sputter-coated with gold before examination under an environmental scanning electron microscopy (ESEM) apparatus (Philips XL 30) at an accelerating voltage of 15 KeV.

16. *In vivo* biocompatibility

16.1. Preparation of hydro-indocyanine green (H-ICG)

Hydro-indocyanine green (H-ICG) was synthesized from ICG (Acros Organics) by reduction with sodium borohydride as described previously (Kundu et al., 2009). Briefly, 2 mg of dye was dissolved in 4 mL of methanol and reduced with 2-3 mg of

sodium borohydride (Aldrich). Solvent was removed by stirring reaction mix for 5 min under reduced pressure. The dye was nitrogen capped and stored overnight at -20 °C. For bioimaging, the resulting solid was dissolved in sterile water to final concentration of 1 mg/mL and further filtered to remove solid precipitates.

16.2. Implant preparation for *in vivo* antimicrobial assay

Biomaterial disks were incubated for 30 min at 37 °C with *S. aureus* suspension in 1/500 NB (1×10^4 cells/cm^2) under static conditions. After incubation disks were placed in sterile containers.

16.3. Disk implantation and ROS bioimaging

National Institutes of Health guidelines for the care and use of laboratory animals (NIH Publication #85-23 Rev. 1985) were observed. All surgical procedures were approved by the Institutional Animal Care and Use Committee at the Georgia Institute of Technology. Sterile, endotoxin-free disks (6 mm diameter) were implanted subcutaneously in the back of 6-8 weeks old male BALB/c mice (Jackson Laboratories) anesthetized by isofluorane. A single 1-cm incision was made on the dorsum proximal to the spine, and a subcutaneous pocket laterally spanning the dorsum was created. Sterile disks (two per subject on either side of the spine) were implanted, and the incision was closed using sterile wound clips. Mice undergoing the same surgical procedure but receiving no biomaterial implants were used as sham controls to account for surgery-associated trauma/inflammation. The same procedure was followed for implants incubated with bacteria.

For bioimaging, 30 µL of hydro-indocyanine green (H-ICG) at a concentration of 1 mg/mL in sterile water was injected near the vicinity of the implant. Thirty minutes after dye injection, the animal was anesthetized and the whole body of the animal was scanned in an IVIS Lumina® bioimaging system (Xenogen). Biofluorescence was integrated using Living Image®software Version 3.1 (Xenogen). ROS bioimaging was

performed 30 min after dye injections immediately following surgery/implantation and 1, 4, 7 and 14 days post-surgery/implantation.

16.4. Implant analysis

Mice were sacrificed at specific time points (7 and 14 days post-implantation) and the disks were carefully explanted with the surrounding tissue intact to avoid disrupting the cell-material interface. For immunohistochemical staining, explants were embedded in optimal cutting temperature compound (Tissue-Tek) and cryosectioned at 10 µm. Fresh-frozen cryostat sections were incubated in 100 mM hydro- Cy5 (H-Cy5) for 45 min at 37 °C to stain for intracellular ROS. Following incubations in H-Cy5, sections were fixed with 4% paraformaldehyde and were stained with primary rat monoclonal antibodies (Abcam) against the macrophage marker (CD68) or neutrophil marker (NIMP-R14). AlexaFluor 488-conjugated goat anti-mouse specific antibody (Invitrogen) was used as a secondary antibody. The sections were mounted with antifade mounting media containing 4´,6-diamidino-2-phenylindole (DAPI, Vector Labs) and imaged under a Nikon C1 imaging system. Five-six fields per sample were acquired and ImageJ software was used to count the fluorescent-labeled cells. For CFU counting, each explant was placed in glass tube containing 1 mL of 10mM PBS, pH7.2 and sonicated for 10min in ultrasonic bath (REFF) to remove adhered bacteria. Afterwards, two more sonicating cycles were applied (5min and 30sec) interspersed with 30sec vortex treatment. Bacterial solution was plated on LB agar plates and CFU were counted after 24h incubation at 37°C.

17. Gravimetry assay

The kinetics of weight loss of polymers was studied by immersing disks (6 mm diameter and 1 mm thickness) in 10mM PBS, pH 7.2 at 37 °C. The weight of the damped disks was monitored after different intervals of immersion time (1, 7, 14, 30 and 60 days). Disks were dried and weight on balance (Sartorius). The percent of

weight loss was calculated from the initial dry mass of the disks and the mass of the damped disks after certain immersion time.

18. Implant preparation for *in vitro* and *in vivo* assays with *S. aureus* luminescent strains

Both parental strains and their bioluminescent derivatives were tested in vitro and in vivo. Bacterial strains were cultivated overnight in TSB with aeration at 37 °C. The cultures were diluted with fresh TSB to reach absorbance A595 0.1 and incubated for 3-4h to A595 0.7. Afterwards, bacterial test inoculum for were prepared in 2mL of 1/500 Nutrient Broth DifcoTM (ref 234000, Becton, Dickinson and Company, France), to serve as cell suspension. Bacterial concentration was estimated spectrophotometrically at 595nm using (spectrophot ref).

Bacterial suspensions (1×10^4 to 1×10^{10} cells/cm^2) were placed on previously prepared sterile endotoxin-free PHO and PET disks. Set of disks was prepared for bioluminescence screening, and the other for CFU counting. Each tested concentration was examined in triplicate.

To correlate luminescence signal intensity and colony forming units counts (CFU), each disk was placed into a separate sterile Petri dish with a wet filter paper beneath to maintain relative humidity not less than 90% and incubated for 24h at 37 °C under static conditions. Two set of controls were used; 1) non coated PET disks for determination of bacterial viability 2) PET disks coated with PHO, to analyze the effect of non functionalized PHA on bacterial viability. Both set of controls were incubated for 1h at 37 °C under static conditions.

For *in vivo* assay, following 30min incubation under static conditions at 37 °C disks were placed in sterile containers.

19. *In vitro* assay with *S. aureus* luminescent strains

Bacteria incubated on PHO and PET disks were scanned in an IVIS Lumina® bioimaging system (Xenogen). Bioluminiscence was integrated using Living Image® software Version 3.1 (Xenogen). Luminiscence after 1h of incubation was compared to that after 24h of incubation. For estimating bacterial concentration via colony forming units counting (CFU), disks were washed with phosphate-buffered physiological saline (PBS 10mM, pH 7.2), 10-fold serial dilutions of suspension were made and plated on TSA plates (ref). CFU were counted after 24h incubation at 37°C. Number of recovered bacteria after 1h of incubation and 24h of incubation were compared.

20. *In vivo* real time monitoring of bacterial infection

For the measurement of bioluminescence of subcutaneously implanted disks precolonized with bioluminescent *S. aureus* strains, mice were anesthetized with isofluorane and imaged with a CCD camera (IVIS Lumina® bioimaging system, Xenogen) directly following implantation and 1, 4, 7 days post implantation. Total counts from the metabolically active S. aureus were collected during a 2-min exposure using the IVIS Imaging System and Living Image software (Xenogen Corporation). Bioluminescent images were displayed using a pseudocolor scale (blue representing the least-intense light and red representing the most-intense light) that was overlaid on a gray-scale image to generate a two-dimensional picture of the distribution of bioluminescent bacteria in the animal. To account for the background luminescence, one uninfected mouse was imaged along with the infected animals. The total counts from a region were quantified using the Living Image software package (Xenogen Corporation), and the data are presented as total counts contained within each region.

21. Disk implantation and ROS bioimaging

Previously prepared sterile, endotoxin-free disks (6 mm diameter) were implanted subcutaneously following IACUC-approved procedures in 6-8 weeks old male BALB/c mice (Jackson Laboratories) anesthetized by isofluorane. A single 1-cm incision was made on the dorsum proximal to the spine, and a subcutaneous pocket laterally spanning the dorsum was created. Sterile disks (two per subject on either side of the spine) were implanted, and the incision was closed using sterile wound clips. Mice undergoing the same surgical procedure but receiving no biomaterial implants were used as sham controls to account for surgery-associated trauma/inflammation. The same procedure was followed for implants incubated with bacteria.

For bioimaging, 30 µl of hydro-indocyanine green (H-ICG) at a concentration of 1 mg/mL in sterile water was injected near the vicinity of the implant. Thirty minutes after dye injection, the animal was anesthetized and the whole body of the animal was scanned in an IVIS Lumina® bioimaging system (Xenogen). Biofluorescence was integrated using Living Image®software Version 3.1 (Xenogen). ROS bioimaging was performed 30 min after dye injections 7 days post-surgery/implantation.

IV. RESULTS

Herein we describe two different strategies for polymer functionalization to obtain added value PHA for industrial and biomedical applications. The first strategy consists in *in vivo* bacterial production of tailor-made functionalized nano-beads where proteins attached to the natural PHA granule have been engineered to display fusion proteins of interest. The second strategy relays on the functionalization of polymer itself using metabolic engineering approach to design bacterial strains able to produce new non-natural polyesters carrying functionalized groups at the side chain. In the previous work, a strain of *Pseudomonas putida* able to accumulate poly-acetylthio-hydroxyalkanoate (PHACOS) was constructed (Escapa et al., 2011). This functional group at the side chain of PHACOS confers new biological properties to the biomaterial. Thus, we analyzed novel properties of PHACOS both *in vitro* and *in vivo*.

1. Bacterial production of tailor made functionalized nano-beads

PHA granules represent a useful tool for recombinant protein immobilization due to their unique structure (Figure 3). Using the advantage of the presence of natural proteins (GAPs) on the granule surface we designed functionalized PHA nano-beads. Phasins are one of the most abundant proteins attached to the PHA granule. Therefore, they were chose as tags for anchoring recombinant proteins to bacterial PHA granules. Moreover, we investigated their physiological function trying to describe the key factors involved in the *in vivo* immobilization of proteins to PHA granules. To that end, *P. putida* phasin PhaF was used as a peptide tag to anchor the protein to bacterial PHA granules. This system provides a useful tool for *in vivo* immobilization of active proteins to a biodegradable support for protein delivery to environments, diagnosis, antigen delivery and many others.

2. The role of PhaF in the PHA machinery

In the previous work of our group phasins have been used for protein immobilization, however their physiological role in mcl-PHA machinery is not completely understood. To improve existing model and maximize recombinant protein yield we investigate phasin involvement in cell physiological processes. Therefore, by swapping different phasin domains we intent to optimize the *in vivo* attachment of proteins to mcl-PHA granules and achieve the most favorable conditions for recombinant protein immobilization.

2.1. PhaF affects heterogeneity of the cell population concerning the PHA production

Previous results from our laboratory showed that the total PHA content of a PhaF mutant strain of *P. putida* GPo1 was reduced considerably in comparison to that of wild type strain, when the PHA content was studied in cell dividing continuous culture (Prieto *et al.*, 1999). Based on this observation, we focus our interest in studying the PHA production not only at stationary phase but throughout the growth curve to analyze PhaF dependent variation in terms of PHA content in all fermentation stages. With this aim, the *phaF* gene of the prototype PHA producer strain *P. putida* KT2442 was deleted by using a suicide vector (see Experimental Procedures section). The PHA production abilities of the resulting strain *P. putida* KT42F was compared to that of the wild type bacterium when cultured in optimal PHA production conditions. To monitor the PHA content at every stage of the growth curve, a fast and accurate method for analysis of PHA content by flow cytometry was adapted for *Pseudomonas* strains. Fluorescence intensity of Nile red stained granules obtained by flow cytometry was correlated with data of PHA content analyzed by gas chromatography. Relation between those parameters was further on used to translate the cytometry fluorescence intensity data into PHA values.

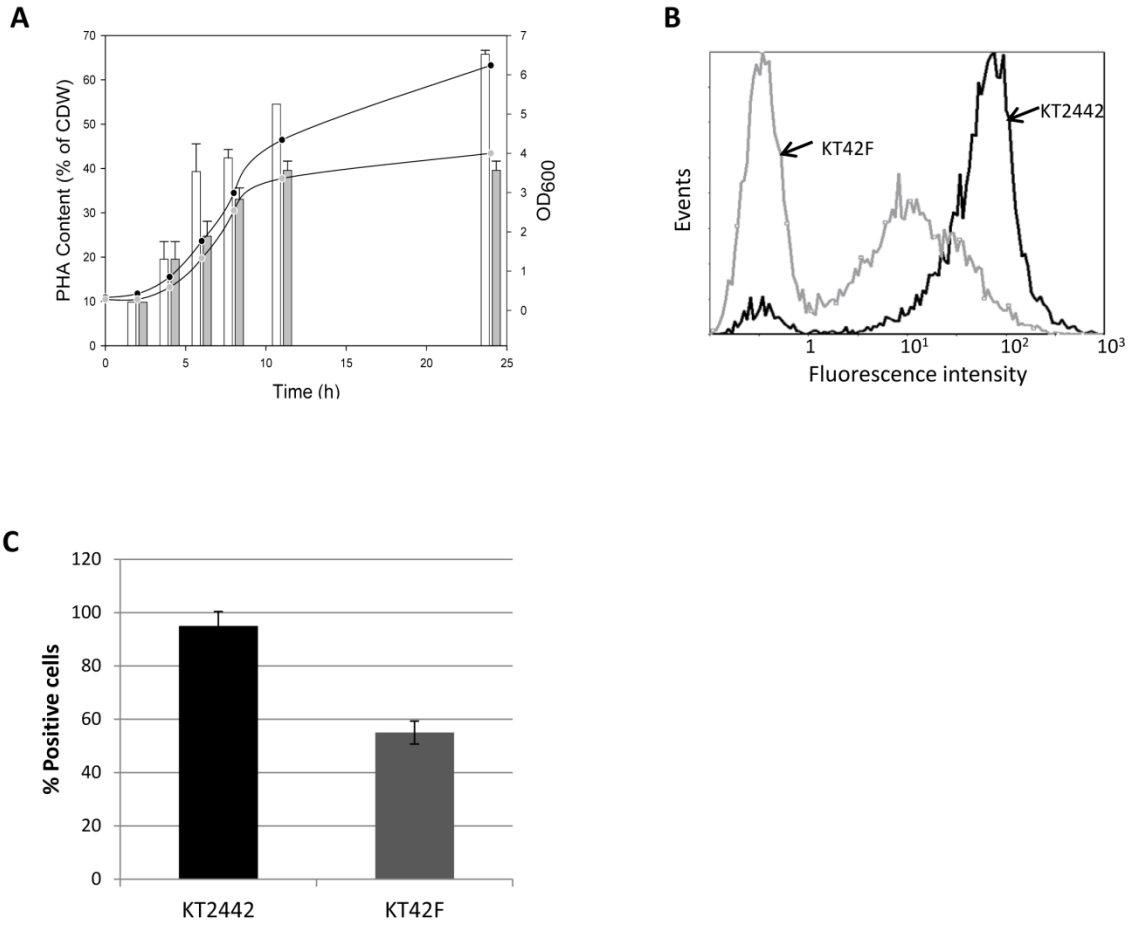

Figure 11. Study of cell population heterogeneity in terms of PHA production by flow cytometer. A, Quantification of PHA content (bars) and OD600 (circles) of *P. putida* KT2442 (black bars and black circles) and KT42F (gray bars and gray circles) strains throughout the growth curve; B, Example of a flow cytometer histogram of the *P. putida* KT2442 (black plot) and the *P. putida* KT42F (grey plot) strains grown in PHA production medium during 7 h (see Experimental Procedures for details); C, Percentage of PHA positive cells KT2442 (black column) and KT42F (gray column).

Cells from *P. putida* KT2442 and its *phaF* disrupted mutant strain KT42F were harvested from the culture at different growth times. Figure 11A shows that at the early exponential phase of growth (2 h and 4 h), wild type and mutant strains showed similar PHA content, around 10% and 20% of cell dry weight (CDW), respectively. After 6 h of growth the total PHA content detected in the wild type strain KT2442 was slightly higher than that of the mutant strain KT42F. This difference increased over the

growth curve, being maximal (1.5-fold) after 24 h of growing (Figure 11A). This result demonstrates that PhaF is not essential for the synthesis of PHA in *P. putida* KT2442 but contributes to optimize the yield of PHA synthesis and accumulation.

Besides, these flow cytometry analyses allowed us to relate the total PHA content of the cell population *versus* the PHA content of individual cells (heterogeneity of the population). Figure 11B shows an example of a histogram of KT42F and wild type cells after 7 h of growing. A major overlay corresponding to positive fluorescent cells was detected in the wild type cells (Figure 11B), demonstrating a homogeneous population regarding the PHA granules content. Interestingly, two main overlays showing different fluorescence intensities (Figure 11B), were detected in the KT42F sample. In this case, only 55% of cell population displayed positive PHA content while the rest of the cells were negative, suggesting that they did not contain PHA granules (Figure 11C). These results demonstrated the presence of at least two different cell populations in terms of PHA content in the KT42F cultures suggesting a role of PhaF in PHA granules partition during cell division.

2.2. Impact of PhaF mutation on granule location and segregation during cell division

To monitor the presence of the PHA granules during cell division at early growth phase and the influence of the presence or absence of PhaF protein on the PHA content, samples from wild type and KT42F mutant strains were taken at different growth times for TEM analysis (Figure 12 and 13).

Interestingly, cells at time zero, that means LB grown cells used to inoculate the cultures contain a few and small granules of PHA which constitute less than 1% of the CDW (Figure 12 and 13). In perfect correlation with the PHA content (Figure 11A), the size and number of the PHA granules in the wild type cells increased progressively during the growth curve being maximal at 24 h of growing (Figure 14). Most of the cells contained 5-6 granules of about 500 nm of diameter (Figure 14). The number and average size of the granules in the KT42F mutant decrease when compared to those of

the wild type strain (Figure 14). These results confirmed those obtained by flow cytometry, which showed a remarkable heterogeneity on the total population in the KT42F culture in terms of PHA content and the presence of PHA empty cells when PhaF protein is not produced.

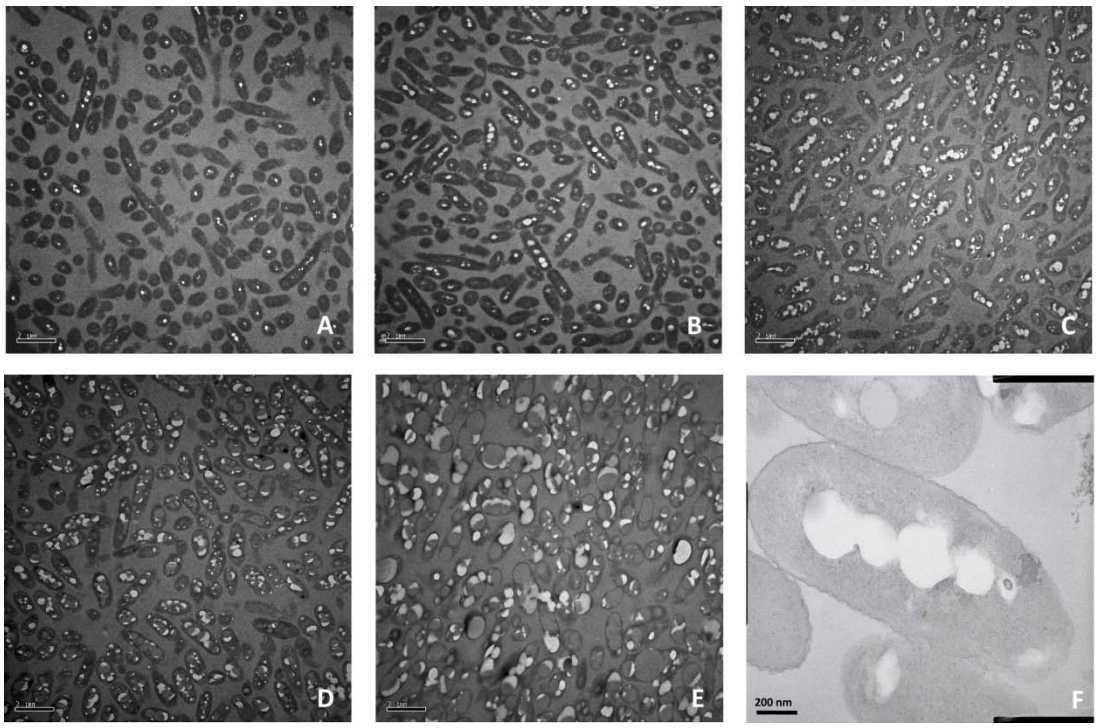

Figure 12. TEM images of *P. putida KT2442 growth curve in PHA production medium.* A-E, Samples were taken 0, 2, 4, 6 and 24 h after the inoculum (Panels A, B, C, D and E, respectively) and processed as described in Experimental Procedures; F, Detail of the granule distribution of a single cell from a 4 h culture in PHA production medium.

TEM studies also provided additional information about granule distribution in the cell, and we observed that after 2 h and 4 h of growing, granules were detected in the wild type at the center of the cross section of the majority of the cells, *i.e.*, located running lengthwise the cell, forming a characteristic needle array (Figure 12B, 12C and 12F). This distribution was less evident when the accumulation of PHA was close to the 50% CDW after 6 h of growing (Figure 12D and 12E). In contrast, the granules in the KT42F mutant strain were agglomerated in one of the cell poles (Figure 13B, 13C and 13F) at the early growth stages (2 h and 4 h).

In agreement with the results observed by flow cytometry (Figure 11), the PHA content of the mutant was similar to that of the wild type strain at the earliest stages of growth (Figure 13B, 13C and 13F).

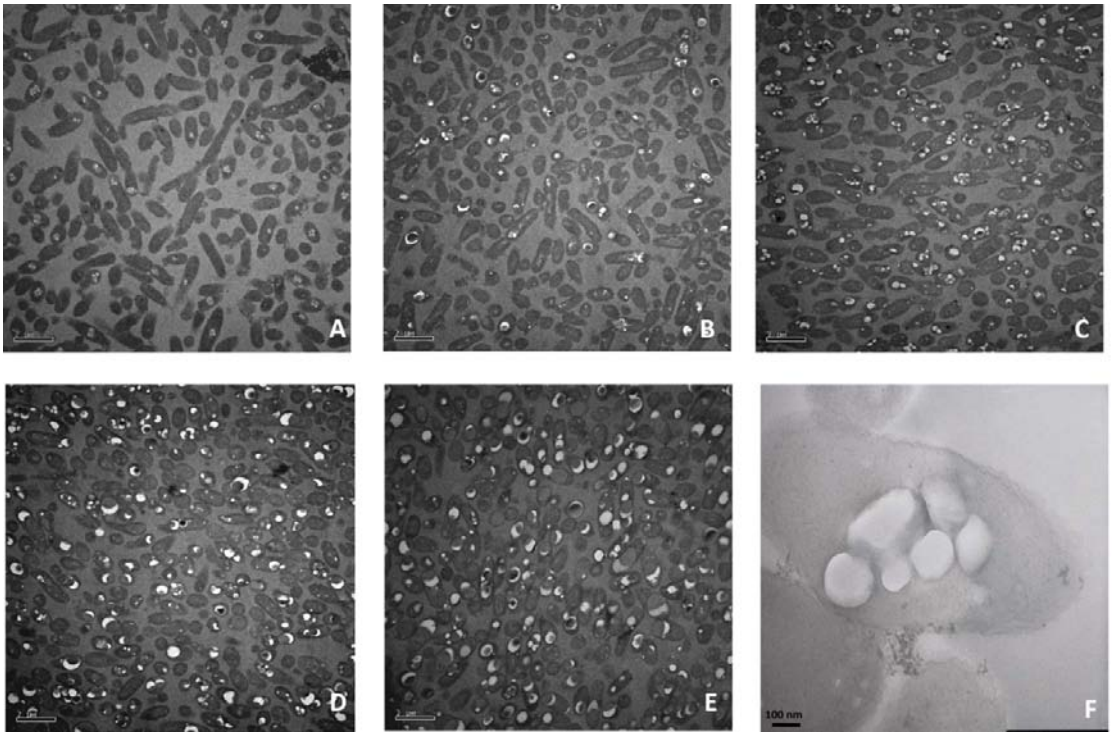

Figure 13. TEM images of *P. putida* KT42F growth curve in PHA production medium. A-E, Samples were taken 0, 2, 4, 6 and 24 h after the inoculum (Panels A, B, C, D and E, respectively) and processed as described in Experimental Procedures; F, Detail of the granule distribution of a single cell from a 4 h culture in PHA production medium.

Moreover, at 24 h of growing 34% of mutant cells did not contain PHA granules generating two markedly different cell populations in the culture, *i.e.*, with and without PHA (Figure 11B and 13E). While wild type strain distributed the previously formed PHA granules among the daughter cells keeping the needle array structure, the PHA granules in the PhaF mutant strain remained agglomerated in one of the daughter cells (Figure 15). It is worth noting that granules did not coalesce in a single big granule, as reported for other microorganism lacking phasins (Wieczorek *et al*., 1995), very likely due to the presence of the other phasin PhaI (see below).

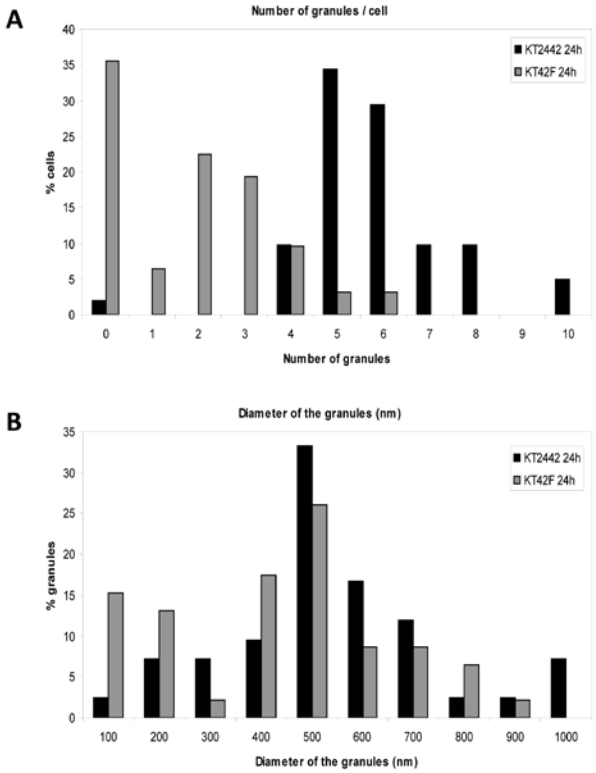

Figure 14. Determination of granule size and number in KT2442 and KT42F strains of *P. putida*. A-B, The granule number (A) and granule size distributions (B) in KT2442 (black bars) and KT42F (gray bars) were determined by TEM images analysis.

On the other hand, *P. putida* KT42F cells were complemented by *in trans* production of PhaF from *P. putida* GPo1 giving rise to *P. putida* KT42F-F strain (see Experimental Procedures for details) (Figure 15). These results demonstrated that the presence of PhaF ensures the segregation of the PHA granules during the cell division. In addition, these results explain the reduction of the total PHA content at 24 h in the mutant strain (Figure 11) by a dilution effect due to the presence of PHA empty cells.

Figure 15. Analysis of the *P. putida* KT42F complementation and PHA segregation by TEM. A-C, Samples were taken after 4 h growth in PHA production medium. Detail of the PHA granule distribution of KT2442 (A), KT42F (B) and the complemented strain KT42F-F (C); D-F, Segregation of PHA granules during cell division in KT2442 (D), KT42F (E) and KT42F-F (F).

2.3. DNA binding abilities of PhaF protein

The involvement of PhaF in the *pha* transcriptional regulatory system was first demonstrated in *P. putida* GPo1 (Prieto *et al.*, 1999). Disruption of the *phaF* gene led in this strain to an increased expression rate of *phaC1* gene, suggesting that PhaF acted as a negative regulator of the *pha* cluster in this strain. This function was ascribed to its C-terminal half due to the similarity observed to histone-like proteins, but there was no evidence pointing to direct binding of PhaF to the *pha* promoter regions so far. It was demonstrated that the binding of PhaF protein to DNA is not specific, *i.e.,* it is independent of the recognition of a specific operator DNA sequence. Moreover, it was shown by spectroscopical techniques that PhaF binds DNA *in vitro* through its C-terminal domain in a non-specific manner (Galan et al., 2011, Maestro et al., 2013).

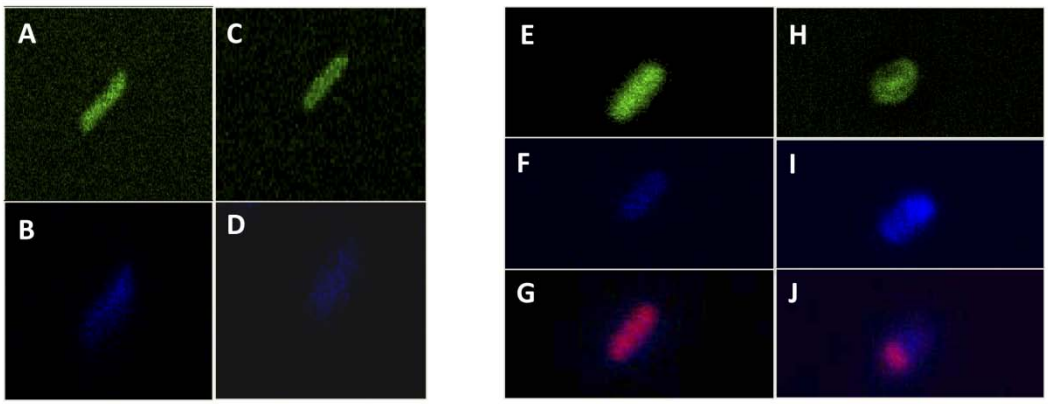

Figure 16. *In vivo* localization of GFP::C-PhaF fusion protein in KT42-GC (A,B,E-G) and KT42F-GC (C,D,H-J) *P. putida* strains by confocal microscopy. A, localization of GFP::C-PhaF fusion protein (in green) in KT42-GC strain cultured in LB medium (non PHA producing conditions); B, localization of nucleoid(in blue) in KT42-GC strain cultured in LB medium; C, localization of GFP::C-PhaF fusion protein (in green) in KT42F-GC strain cultured in LB medium; D, localization of nucleoid(in blue) in KT42F-GC strain cultured in LB medium; Localization of GFP::C-PhaF fusion protein (in green) E, nucleoid(in blue) F and PHA granules (in red) G in KT42-GC strain cultured in PHA producing conditions; Localization of GFP::C-PhaF fusion protein (in green) H, nucleoid(in blue) I and PHA granules (in red) J in KT42F-GC strain cultured in PHA producing conditions.

To confirm these findings *in vivo*, we have constructed a fusion protein between the reporter green fluorescent protein (GFP) and the DNA binding domain of the protein PhaF (C-PhaF). This GFP::C-PhaF fusion protein was introduced into the *P. putida* KT2442 and *P. putida* KT42F chromosomes giving rise to KT42-GC and KT42F-GC, respectively. The strains KT42-GC and KT42F-GC producing GFP::C-PhaF fusion protein, have been used to analyse the *in vivo* localization of the GFP::C-PhaF fusion protein by confocal microscopy (Figure 16). By staining the cells with two different dyes, we have analysed localization of i) the PHA granules (Nile Red-stained), ii) the nucleoid (DAPI-stained) and iii) the protein GFP::C-PhaF. Our results confirm the co-localization of the fusion protein GFP::C-PhaF and nucleoid in wild type and PhaF minus cells, independently of the presence or absence of the PHA granules. Furthermore, PHA granules produced in the wild type cells, which contain native PhaF protein, co-localised with the nucleoid and GFP reporter. However, PHA granules

produced in the KT42F mutant strain localised independently of the nucleoid and GFP reporter system. These results provide support to the role of PhaF as nucleoid-binding protein and its role in the intracellular localization of the PHA granule.

3. The function of PhaI in the PHA metabolism

As it was previously mentioned in Introduction section, *P. putida* KT2442 has two phasins, PhaF and PhaI. Those phasins belong to the same operon (Figure 4) and share considerable sequence similarity (Prieto et al., 1999). Since we spotted the key role of PhaF, we analyzed the physiological role of other *P. putida* phasin protein PhaI. The effect of its absence and possible coordinated work with PhaF was tested.

3.1. The outcome of PhaI phasin deficiency considering PHA granule accumulation/formation

Previously we showed that lack of PhaF phasin, involved in PHA granules localization and balanced distribution during cell division induce considerable reduction of total PHA content due to the defect in granule segregation, and consequently, population heterogeneity. Those findings demonstrated a new role for phasins within the PHA apparatus that could be critical for cell survival under stress conditions. Based on this observation, we focus our interest in studying the influence of phasins on PHA accumulation, comparing the PHA production abilities of different phasin mutant strains to that of the wild type bacterium. With this aim, *P. putida* KT2442 strain was genetically manipulated to generate disruption mutations of the respective phasin genes designing *P. putida* KT42F that lacks PhaF phasin, *P. putida* KT42I-F that lacks PhaI phasin and *P. putida* KT42I that lacks both PhaF and PhaI phasins (Figure 17A). By western blot analysis we demonstrate that wild type and phaF mutant strain produce PhaI, while strains KT42I-F and KT42I do not produce PhaI (Figure 17B). Furthermore, we show that wild type strain produce higher quantity (7.5

fold) of PhaF when compared to KT42I-F strain, whereas KT42F and KT42I do not produce PhaF, last due very likely to a polar mutation in the operon *phaIF* (Figure 17B).

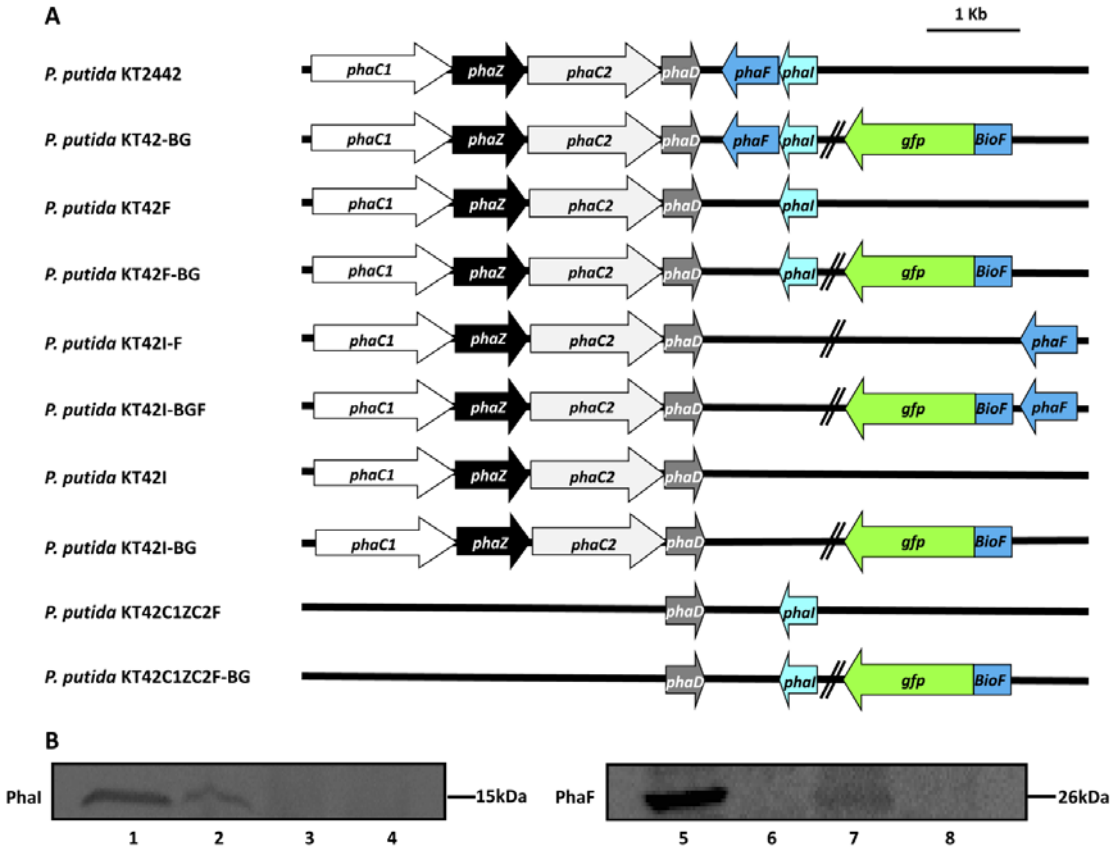

Figure 17. Comparative representation of *pha* gene cluster organization of different *P. putida* strains and Western blot analysis. A, Scheme of constructed *P. putida* KT2442 mutant strains. Arrows indicate different genes involved in PHA metabolism, their relative size and transcriptional direction. *P. putida* KT2442 *pha* cluster is composed of *phaC1* (white) and *phaC2* (light grey) genes that encode two synthases, *phaZ* gene (black) that encodes an intracellular depolymerase, *phaD* gene (dark grey) that encodes a transcripitonal regulator and *phaF* (dark blue) and *phaI* (cyan) genes that code for phasins. Different mutant strains were constructed KT42F, KT42I-F, KT42I, KT42C1ZC2F lacking *phaF*, *phaI,* both *phaF* and *phaI* and *phaC1*, *phaZ, phaC2*, *phaF* respectively. *bioF* was fused with *gfp* (bi-colour arrow, blue and green) and randomly (marked with two parallel lines) inserted in the chromosome of each strain, wild type and mutant strains on *pha* cluster giving rise to KT42-BG, KT42F-BG, KT42I-BGF, KT42I-BG and KT42C1ZC2F-BG; B, Western blot analysis of phasin expression in different *P. putida* strains applying antibody against PhaI (left) and BioF tag (right). Lines 1, 5: KT2442; lines 2, 6: KT42F; lines 3, 7: KT42I-F; lines 4, 8: KT42I.

For PHA content, analysis by GC-MS cells were cultured in optimal PHA production conditions and harvested after 24h of growth. Wild type strain showed PHA content of 63% of cell dry weight (CDW), while mutant strain lacking phasin PhaF, PhaI and both phasins produced less amount of PHA, 33%, 21% and 7% respectively (Table 6). These results demonstrate that when P. putida strain lacks both phasins, PHA production dramatically decreases, suggesting that PhaF and PhaI phasins work in harmony and are essential for the optimal PHA synthesis and accumulation.

Table 6. Quantification of PHA content by GC-MS and protein quantification by QuantityOne analysis

P. putida strain	PHA %	Biomass (g/l)	Protein mg/g biomass	Protein mg/l culture	Protein mg/g PHA
KT2442	63.27±1.42	1.40±0.11	_	_	_
KT42F	33.36±1.19	0.65±0.18	_	_	_
KT42I-F	20.75±1.35	0.62±0.22	_	_	_
KT42I	7.44±0.39	0.58±0.17	_	_	_
KT42-BG	53.51±3.22	1.14±0.10	1.46±0.36	1.49±0.37	2.92±0.53
KT42F-BG	33.85±1.88	0.80±0.06	4.06±0.66	3.53±0.57	11.38±0.65
KT42I-BG	19.62±1.02	0.69±0.07	4.16±0.35	2.62±0.47	20.17±0.73
KT42I-BGF	42.10±1.28	1.00±0.23	9.73±0.42	10.31±0.49	22.42±0.85

3.2. BioF tag or its fusion derivatives can replace PhaI role in P. putida in terms of PHA production

Since PhaI and N-terminal domain of PhaF (BioF) show high structural similarity and their 3D models predict a possible interaction between proteins through the oligomerization linker (Maestro et al., 2013), we investigated the possibility of PhaI functional replacement by BioF. To monitor the influence of BioF on PHA content,

BioF-GFP was stably integrated into the chromosome of *P. putida* phasin mutant strains. *P. putida* KT2442-BG, KT42F-BG, KT42I-BGF and KT42I-BG cells (Table 4; Figure 17A) were cultured in optimal PHA producing conditions for 24h and their PHA content was analyzed by GC-MS. Interestingly, *P. putida* KT42I-BGF and KT42I-BG showed an increase in PHA content being, 42% and 20% of CDW respectively, when compared to their correspondent strains that did not contain BioF-GFP (Table 6). However, we did not observe significant difference in PHA accumulation in KT42F-BG strain when compared to KT42F strain, showing PHA content of 34% and 33% of CDW respectively. These results were confirmed by flow cytometry analysis, where fluorescence of nile red stained PHA granules was recorded for the determination of PHA cell content. In perfect correlation with GC-MS results, no significant difference was observed between KT2442 and KT42-BG. Similarly, the result obtained for PhaF phasin mutant (KT42F) and KT42F-BG strain showed no difference between these two strains in PHA content (data not shown). However, PhaI mutant harboring BioF::GFP fusion protein recovered PHA production to the level of PhaF mutant and KT42I-BGF strain showed PHA content similar to that of wild type. Taking into account the results presented above we definitively conclude that BioF tag or its fusion derivatives can replace the role of PhaI phasin in *P. putida* strain in terms of PHA content.

3.3. The effect of PhaI absence on population homogeneity

Since, a deletion of the PhaF phasin resulted in a defect in granule segregation and population heterogeneity in terms of PHA granules content (see section 2.2.), we interrogated the required imposition of phasin domains to reconstruct a uniform granule distribution and optimal PHA production.

By flow cytometry analyses, we were able not only to determine the PHA content but to relate this parameter to the cell population, this is, the PHA content of individual cells (heterogeneity of the population). Figure 18A and C show a major overlay corresponding to positive fluorescent cells in the wild type cells indicating a homogeneous population regarding the PHA granules content. Two main overlays showing different fluorescence intensities were detected in the KT42I, KT42I-BG and

KT42F samples (Figure 18A). In the case of KT42I, KT42I-BG and KT42F strains, only 24%, 51% and 45% of cell population displayed positive PHA content while the rest of the cells were negative, suggesting that they did not contain PHA granules (Figure 18A). These results indicate the presence of at least two different cell populations in terms of PHA content, confirming the role of C-terminal of PhaF in granule distribution. Interestingly, strain KT42I-BGF did not show population heterogeneity (80% positive cells) as shown in Figure 18B and C, suggesting that PhaI phasin can be replaced by BioF domain, and that the presence of PhaF at low dosage (Figure 17B) is sufficient to control granules segregation during cell division.

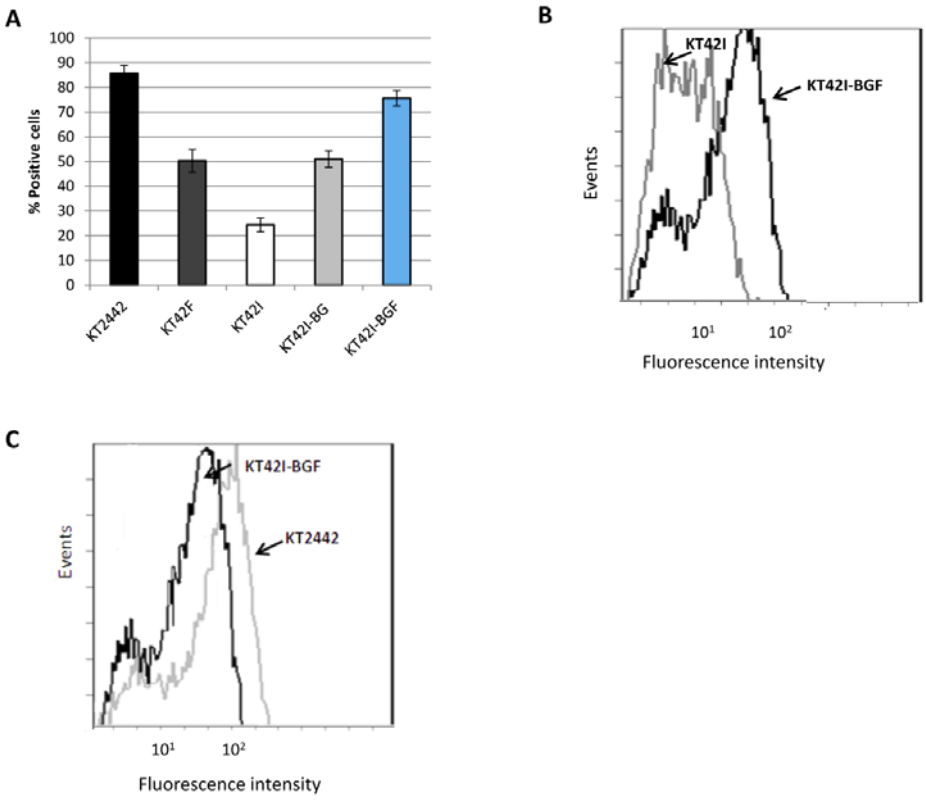

Figure 18. Study of cell population heterogeneity in terms of PHA production by flow cytometer. A, Percentage of PHA positive cells KT2442 (black bar), KT42F (dark grey bar), KT42I white bar, KT42I-BG light grey bar and KT42I-BGF (blue bar); B, Example of a flow cytometer histogram of the *P. putida* KT42I and *P. putida* KT42I-BGF strains grown in PHA producing conditions; C, Example of a flow cytometer histogram of the *P. putida* KT2442 and *P. putida* KT42I-BGF strains grown in PHA producing conditions.

Flow cytometry assay confirmed that lack of wild type phasins affects PHA production and influence granule segregation, and that BioF can replace those roles of PhaI. To analyze in vivo granule segregation and BioF fusion localization, we monitored the reporter, green fluorescent protein (GFP) fused to BioF (see Materials and methods section). The strains KT42-BG, KT42F-BG, KT42I-BGF, KT42I-BG (Table 6; Figure 17A) producing BioF-GFP have been used to analyse the *in vivo* localization of the BioF-GFP fusion protein by epifluorescent microscopy. These experiments were performed as well with the strain KT42C1ZC2F-BG, unable to accumulate PHA since it lacks both synthase genes, *phaC1* and *phaC2*. As reported for the wild type strain (see section 2.2.; Figure 15), KT42-BG strain contained more than one granule located running lengthwise the cell, forming a characteristic needle array and during cell division equally distributed between daughter cells. PhaF and double PhaF and PhaI phasins mutant strains expressing BioF-GFP fusion (KT42F-BG, KT42I-BG) contained usually one or agglomerated pool of granules in one of the cell poles (Figure 19B,C).

However, PhaI phasin mutant strain complemented with *phaF* and expressing *biof::gfp* fusion (KT42I-BGF) showed similar phenotype to that of wild type strain in terms of granule segregation and number (Figure 19D,H). Additionally, diverse functions of BioF and the C-terminal module of PhaF were confirmed by comparative in vivo monitoring of GFP-BioF and GFP::C-PhaF (Figure 19); BioF-GFP fusion protein co-localize with PHA granules in wild type and phasin minus in PHA producing conditions, whereas the PhaF C-terminal domain interacts with nucleoid independently on the strain and growth conditions (Figure 19G). By monitoring BioF-GFP fusion protein in KT42C1ZC2F-BG strain, not capable of producing PHA, we investigated the localization of BioF module in the absence of PHA granules (Figure 19E,F). In fact, in the absence of PHA granules, BioF domains interact, likely through leucine-zipper motif, forming small cytoplasmatic inclusions that are accumulated mainly in the vicinity of the membrane at the cell poles.

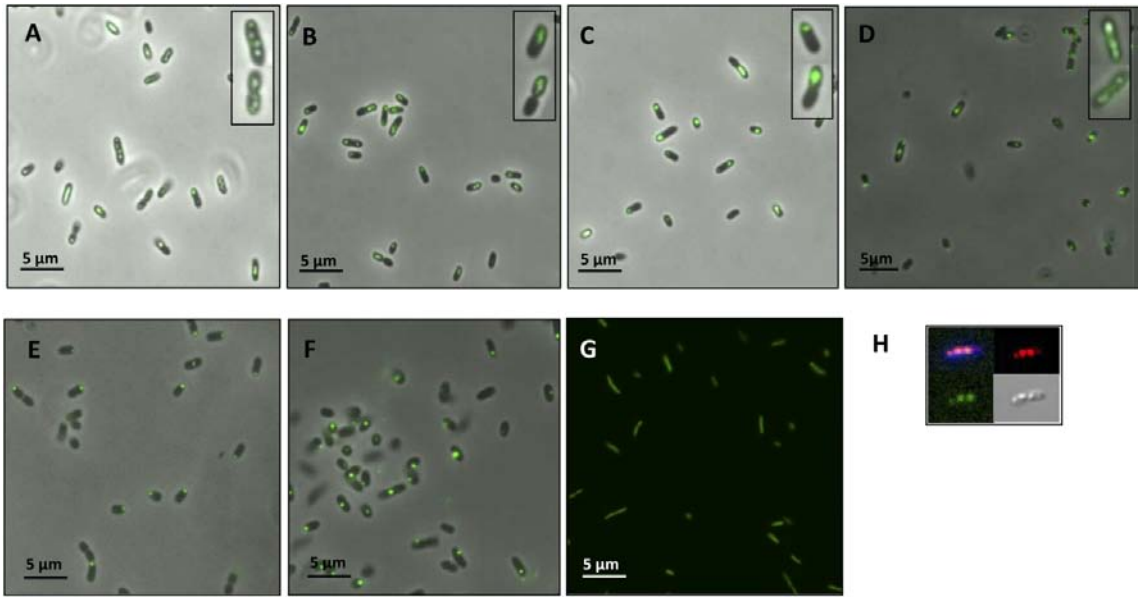

Figure 19. *In vivo* localization of BioF::GFP (A-F; H) and GFP::C-PhaF (G) fusion protein in *P. putida*. Epifluorescence analysis of A, KT42-BG; B, KT42F-BG; C, KT42I-BG; D, KT42I-BGF and E, KT42C1ZC2F-BG in PHA producing condition; F, Shows KT42C1ZC2F-BG strain cultured in LB medium (non PHA producing conditions); G, Shows *in vivo* localization of GFP::C-PhaF fusion protein in KT42I-GC in PHA producing conditions; H, Represents detailed confocal microscopy analysis of BioF::GFP protein localization within KT42I-BGF cells demonstrating granules (in red), nucleoid (in blue) and BioF::GFP protein (in green).

To analyse in detail the recovery of wild type phenotype of KT42I-BGF strain and the localization of the granules, the cells were stained with two different dyes and visualized by confocal microscopy (Figure 19H). With this aim, we monitored in vivo localization of i) the PHA granules (Nile Red-stained), ii) the nucleoid (DAPI-stained) and iii) the protein GFP::BioF. Obtained results confirm the co-localization of the fusion protein BioF-GFP and PHA granules in KT42I-BGF cells. Furthermore, we confirm that the presence of PhaF ensures the segregation of the PHA granules during the cell division. Moreover, when whole protein PhaF is expressed together with BioF tag the strain recovers wild type phenotype accumulating more than one granule and showing granule distribution similar to that of wild type strain.

3.4. The influence of phasins on BioF protein recruitment on the surface of PHA granule

Based on the results presented above and to optimize the best BioF fusion protein yield achievement, we focused our interest in encountering most favourable host for the BioF system concerning expression or not of the natural *phaF* and *phaI* phasins. To establish the optimal conditions for *in vivo* immobilization of BioF fusion proteins, we monitored the biomass and PHA production, as well as the concentration of fusion protein attached to the granules in the absence or the presence of phasins in the *P. putida* strains.

The results obtained according to the SDS-PAGE analysis suggested that the amount of BioF-GFP protein is higher in phasin mutant strains (Figure 20). Additionally, in all tested conditions BioF-GFP fusion protein was mainly associated with the granules (Figure 19 and 21). To quantify the difference in fusion protein content in the presence and the absence of phasins, Gel Doc Quantity One analysis were conducted on the base of SDS-PAGE acrylamide gels. Relative content of BioF-GFP fusion protein in phasin mutant strains was 4-folds higher than the concentration of fusion protein accumulated by wild type strain. The best immobilized protein yield was obtained when PhaF phasin and BioF tag were expressed together, giving BioF-GFP concentration of 9.73 mg per gram of biomass in the strain *P. putida* KT42I-BGF. Furthermore, BioF-GFP concentration obtained in wild type strain was 6.6-fold lower when compared to KT42I-BGF strain as shown in Table 6.

The influence of different pattern of phasin expression on BioF-GFP concentration was monitored by flow cytometry. In perfect correlation with the results obtained by Quantity One the lowest BioF-GFP concentration was observed in KT42-BG strain. KT42F-BG and KT42I-BG showed similar levels of BioF-GFP protein, that were about 4-fold higher when compared to that of KT42-BG strain. The best protein yield was also obtained in KT42I-BGF strain (Figure 22).

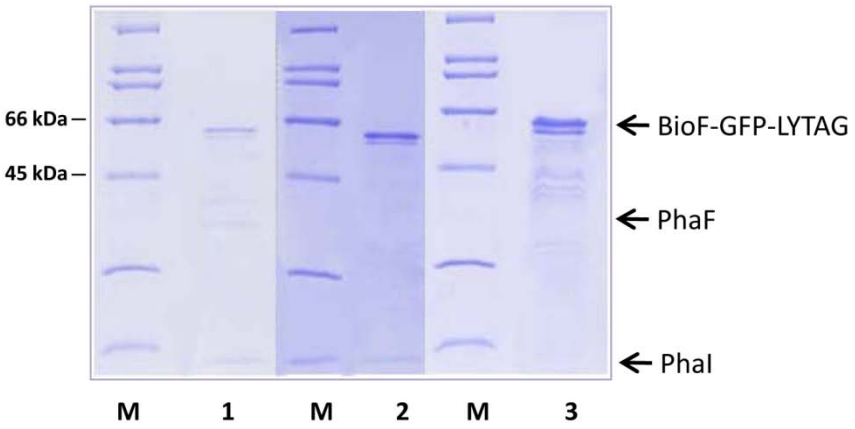

Figure 20. Comparative SDS-PAGE analysis of BioF::GFP fusion protein production and granule association depending on phasin presence/absence in *P. putida* strains. Line 1, *P. putida* KT42-BG granules; Line 2, *P. putida* KT42F-BG granules; Line 3, *P. putida* KT42I-BG granules; M, Molecular weight markers (BioRad, Prestained SDS-PAGE Broad Range Standard). BioF::GFP fusion protein, PhaF and PhaI are marked with the arrows.

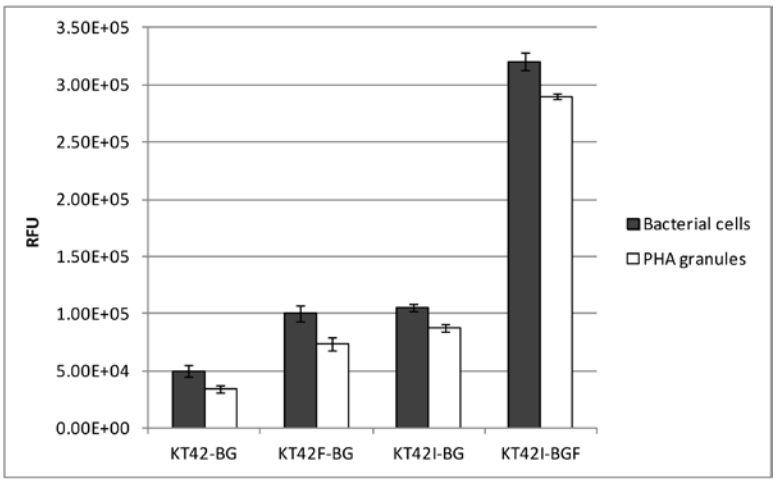

Figure 21. Fluorymetry comparative analysis of green fluorescence level of *P. putida* cells and PHA granules. From left to right KT42-BG, KT42F-BG, KT42I-BG and KT42I-BGF cells harbouring BioF::GFP fusion protein (grey bars) and isolated PHA granules (white bars) of correspondent strains carrying BioF::GFP fusion anchored to the granule surface. RFU (relative fluorescence unit).

To compare the quantity of BioF-GFP in the cells with the quantity of BioF-GFP immobilised to the granules fluorometry analysis were performed. According to obtained results, similar concentration of fusion protein was found in the cells and in the isolated granules. Those results are in perfect correlation with the data obtained by SDS-PAGE analysis that showed that majority of the BioF-GFP protein was immobilised on the surface of PHA granules (Figure 20). In addition, fluorometry results confirm the results of flow cytometry for BioF-GFP quantification in different *P. putida* strains.

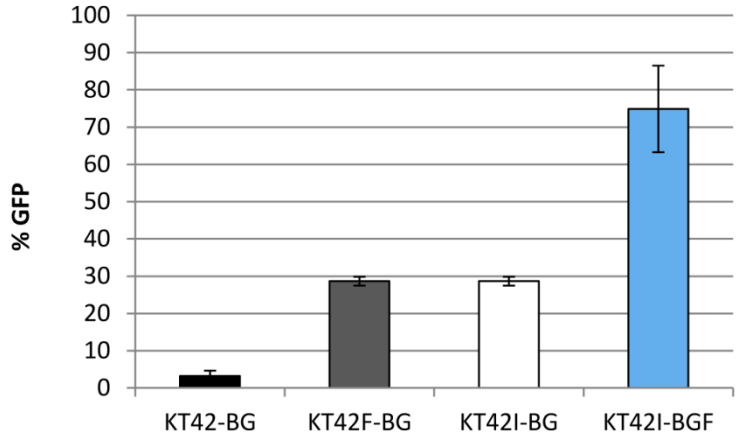

Figure 22. Relative quantification of fusion protein production in *P. putida* cells by flow cytometry. KT42-BG (black bar), KT42F-BG (grey bar), KT42I-BG (white bar) and KT42I-BGF (blue bar).

4. Mcl-PHA side chain functionalization

Many examples of mcl-PHA side chain functionalization have been reported, however there is no published data on thioester group incorporation in side chain of mcl-PHA. Previously, in our laboratory we established the optimal conditions for PHACOS production. Herein we investigate PHACOS antibacterial activity, as well as its advantages in terms of bacterial adhesion and biocompatibility over non functionalized PHO-*co*-HHx for biomedical application.

4.1. PHACOS prevents *Staphylococcus aureus* biofilm formation

Previous results showed that the quality of bacterial biofilm on mcl-PHA, varies depending on both bacterial strain and material purity that supports biofilm formation (Mauclaire et al., 2010). Based on this observation, we focused our interest in studying the ability of *S. aureus* and *P. aeruginosa* (Table 5) to form biofilm on PHACOS and PHO surfaces. Biofilm formation was examined by environmental scanning electron microscopy (ESEM), crystal violet assay and CFU counting.

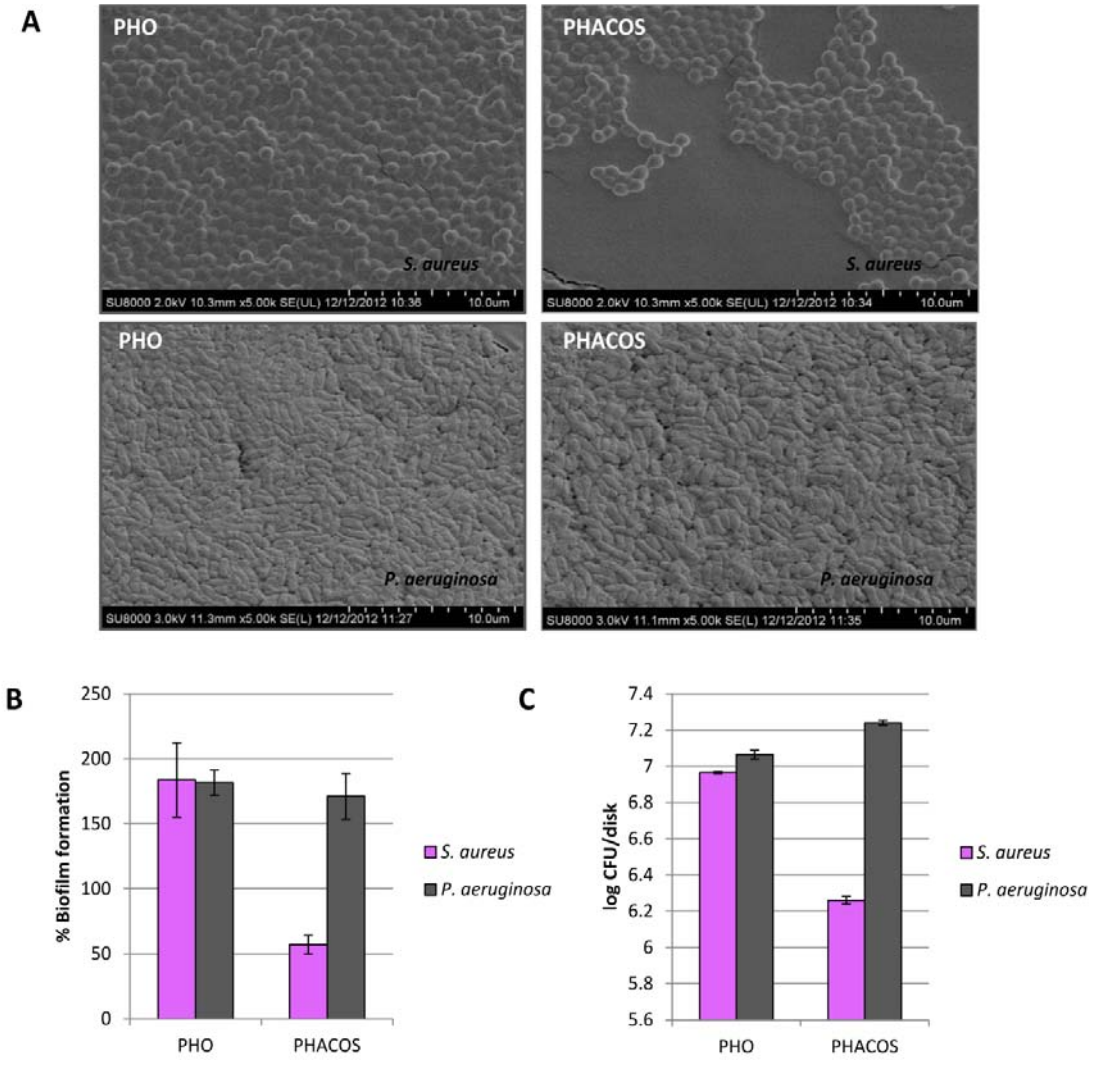

Figure23. Study of PHACOS and PHO disks capacity to inhibit bacterial biofilm formation. A, Environmental Scanning Electron Microscopy (ESEM) of *S. aureus* and *P. aeruginosa*; B, Crystal violet staining assay to quantify formed biofilm where the value of capacity of biofim

formation on PET disks is considered 100%; C Colony Forming Units CFU counting of deatached cells that were forming biofilm.

ESEM observation suggested less biofilm formed by *S. aureus* than *P. aeruginosa* on PHACOS, while the biofilms formed on PHO were similar. However, adhered cells were always observed in both polymers (Figure 23A). The differences between biofilm formation by *S. aureus* and *P. aeruginosa* on PHACOS, were quantified by crystal violet assay and CFU counting. *S. aureus* formed (3-fold) less biofilm than *P. aeruginosa* on PHACOS, whereas the biofilm formed on PHO was similar for both strains (Figure 23B). Moreover CFU counting confirmed these results, showing that the *S. aureus* biofilm on PHACOS was composed of 1 log less cells than that of *P. aeruginosa* (Figure 23C).

4.2. *S. aureus* adheres equally to PHACOS and PHO

The initial bacterial cell attachment to mcl-PHA was monitored to determine its possible influence on biofilm formation. Mcl-PHA microparticles were prepared by water-in-oil-in-water emulsion/solvent evaporation technique and used to evaluate *S. aureus* and *P. aeruginosa* surface adhesion. Commercially available polystyrene 5µm particles were used as positive control. Cells were radioactively labelled and the number of adhered bacteria was analyzed by cpm monitoring of labelled bacterial cells attached to microparticles. To radioactively label the cells, bacteria were cultured in MHBII medium supplemented with C14-6 glucose. The adhesion assay was performed by incubating the suspension of microparticles and bacterial cells. Advantages of this approach are the automation of the method that allows recording an immense number of interactions and the possibility to simultaneously record effects on both surface adhering and planktonic bacteria. Obtained results suggested lower adhesion of *S. aureus* when compared to *P. aeruginosa* to PHO microparticles. 4.1% of assayed *S. aureus* cells were attached to PHO microparticles, while in case of *P. aeruginosa* 13% of assayed cells were attached to particle surface, demonstrating 3-fold higher adhesion of *P. aeruginosa*. To monitor the stability of microparticles, we analyzed their

size and surface morphology by ESEM. Obtained results demonstrated PHO particle aggregation and subsequently size increment (Figure 24). Therefore, to confirm results obtained for bacterial adhesion and discard the possibility of particle aggregation influence on bacterial cell adhesion we used different approach.

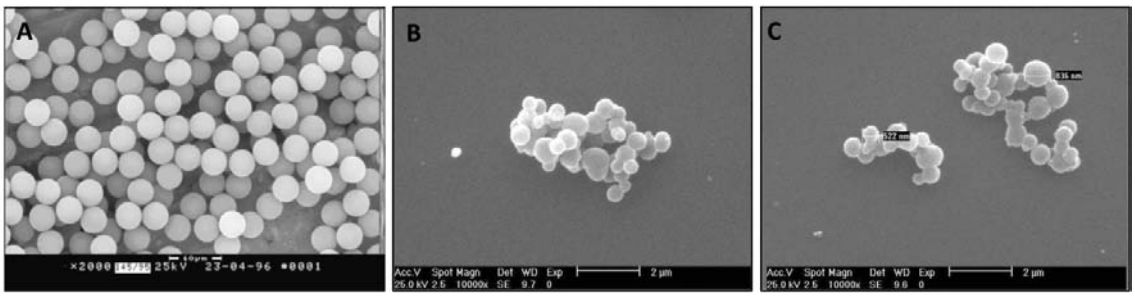

Figure 24. Microparticles stability examination by ESEM. A, Polystyrene microparticles; B, PHB microparticles; C, PHO microparticles.

Table 7. Monitoring of bacterial adhesion to microparicles

Bacterial strain	% of attached cells to PHO microparticles	% of attached cells to polystyrene microparticles
Pseudomonas aeruginosa	13	1.6
Staphylococcus epidermidis	4.2	3.1
Salmonella typhimurium	3.6	35.7
Staphylococcus aureus	4.1	32.6

We monitored bacterial adhesion to mcl-PHA films by ESEM. To that end, PET (6mm) disks were coated with PHO and PHACOS by solvent-casting method. In these experiments cells were previously suspended in a 1/500 NB medium and deposited on the PHACOS and PHO surfaces during 24 h. The lack of nutrients in the diluted suspension avoided biofilm formation but allowed us to test the adhesion step in the biofilm formation. The number of *S. aureus* cells was lower on both surfaces (PHO and

PHACOS) when compared with the number of *P. aeruginosa* cells. However, there was no difference in adhesion of *S. aureus* to PHO and PHACOS (Figure 25A,B).

We next examined whether PHACOS impacted bacterial viability cell. To do so, adhered cells onto PHACOS and PHO were removed by washing out with saline solutions and tested by LIVE/DEAD BacLightTM kit (Figure 25C-D). Interestingly, the number of viable *S. aureus* cells incubated on PHACOS was much lower (20%) in comparison to those on PHO (83%). As shown in Figure 25C, most of *S. aureus* cells were not viable (red stained) after the contact with PHACOS, whereas bacteria were mostly viable (green stained) on PHO (Figure 25D). These results indicated a possible PHACOS antimicrobial activity against *S. aureus*.

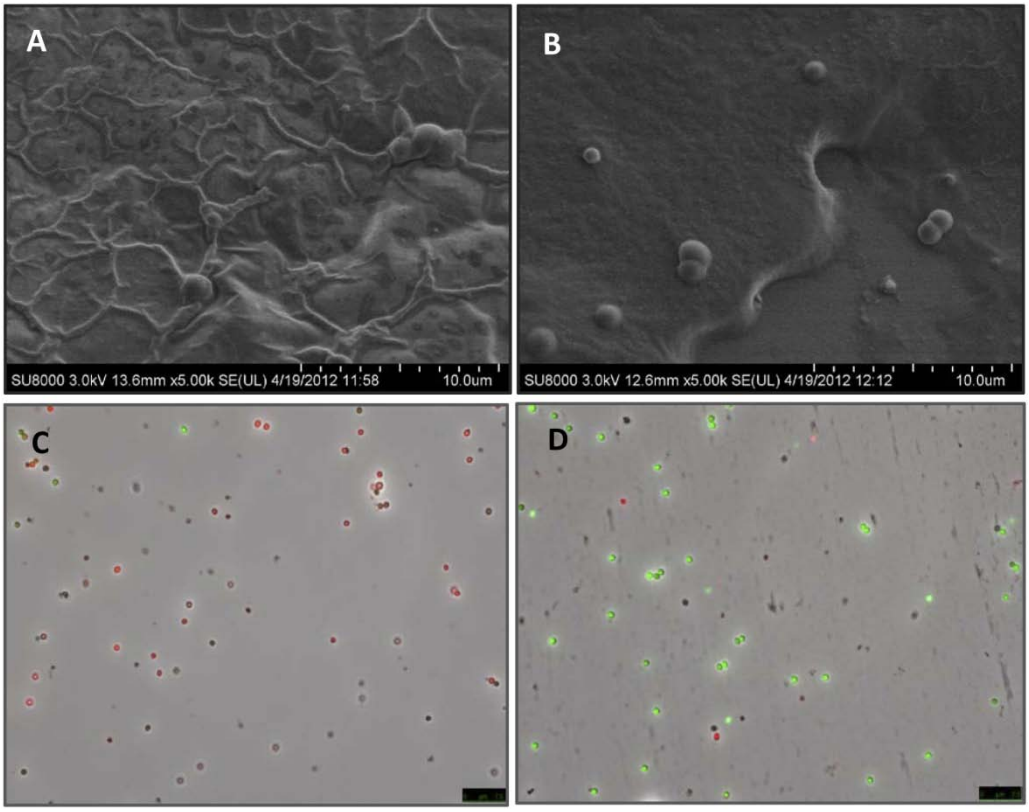

Figure 25. Measurement of antiadherent (A, B) and antibacterial activity (C, D) of PHACOS and PHO surfaces against *S.aureus*. A,B Environmental Scanning Electron Microscopy (ESEM) of PHACOS (A) and PHO (B); C,D Fluorescent Microscopy using Bacterial Viability test (LIVE/DEAD *Bac*Light^{TM}, Invitrogen) of *S. aureus* that was in contact with PHACOS (C) and PHO (D).

4.3. PHACOS shows antibacterial activity against methicillin-resistant (MRSA) *S. aureus* strains

We further analyzed the antibacterial activity of PHACOS by precisely measuring of antibacterial activity on the material surface. In these assays we compared the viability of ten Gram-positive and two Gram-negative pathogen strains (Table 5) after contacting to PHACOS surface (see Material and methods section for details). Susceptibility to PHACOS was found in *S. aureus*, while it was not detected among Gram-negative bacteria. Moreover, antimicrobial activity of PHACOS against *S. aureus* was higher than the one of other Gram-positive pathogens, showing R value of 1.03 (Figure 26) concluding that PHACOS shows significant antimicrobial activity (one order of magnitude) exclusively in the case of *S. aureus* type strain and MRSA strains (less than 10% bacterial cell survival).

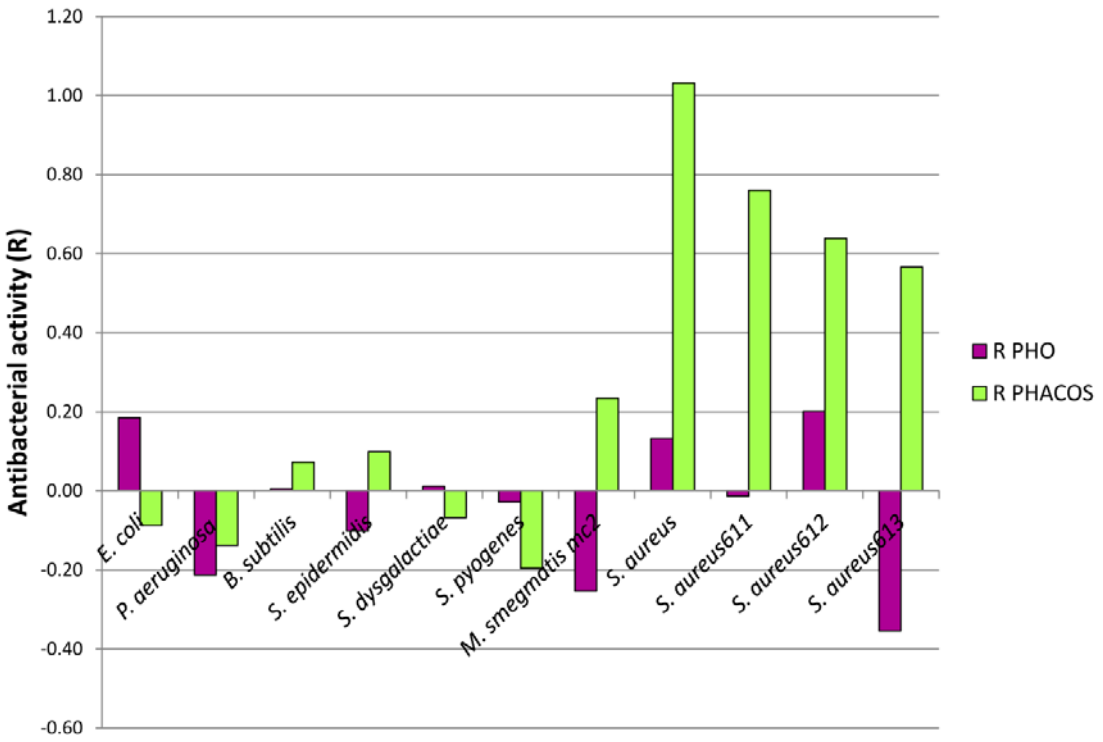

Figure 26. Measurement of antibacterial activity of polymer (PHACOS and PHO) surfaces according to ISO 22196:2007 (E) standard protocol, where R=1 means 10-fold less viable cells recovered from sample disk after 24h when compared to that of control disk .

To calculate the maximal PHACOS antimicrobial activity in terms of cell/cm^2, we analyzed the antibacterial effectiveness of PHACOS in the presence of a range of bacterial concentration (10^4 to 10^{10} cells/cm^2). It was observed that PHACOS is not effective against high bacterial concentration, when inoculums exceed 10^6 cells/cm^2. This result could suggest the PHACOS mode of action where all cells have to be in direct contact with the polymer.

4.4. Antimicrobial activity of PHACOS lies on thioester group

In order to check whether antimicrobial effect is due to the presence of thioester groups in the side chain of PHACOS, antimicrobial activity of some fatty acids with close structures to PHACOS monomers (octanoic, hexanoic and 6-acetylthiohexanoic acids) was studied against *S. aureus* (CECT 86). Values of MIC for 6-acetylthiohexanoic acid were 15-fold higher than that of hexanoic (40µM and 0.7mM respectively). These results clearly demonstrate inhibitory effect of thioester group on *S. aureus* growth. Moreover, *S. aureus* showed higher tolerance to octanoic acid (MIC 3mM) in comparison with hexanoic acid.

Furthermore, we tested minimal inhibitory concentration of suspension containing hydroxycarboxylic acid dimers (7%) and trimers (63%). Obtained results show the same MIC for dimmers/trimers as for 6-acetylthiohexanoic acid.

4.5. Examination of possible toxic effect of mcl-PHA on mammalian cells

Mammalian cell viability and metabolic function was measured by MTT assay. This test is dependent on the intact activity of a mitochondrial enzyme, succinate dehydrogenase, which may be impaired after exposure of cells to toxic species. MTT results showed the absence of mitochondrial damage in any of the tested surfaces. Cellular viability (CV) of macrophages in presence of extracts from all tested polymers was around 100%, indicating the absence of cytotoxic effect (Figure 27A,B). Figure 27C

shows CV values of fibroblasts for PHO and PHACOS extracts. All tested polymers present cytocompatibility levels equivalent to the PET control.

Nitric oxide (NO) inhibitory assay was applied to measure the inflammatory activity of tested polymers. NO is a mediator and regulator in many pathological reactions, especially in acute inflammatory responses (Wang et al., 2008). Pro-inflammatory agents, such as LPS, can significantly increase NO production in macrophages through activation of inducible nitric oxide synthase (iNOS) (Kojima et al., 2000). LPS-stimulated RAW 264.7 cells were used as a reference to evaluate the NO production of extracts coming from the polymeric samples. Figure 28A shows no inflammatory effects produced by the extracts of PHO and PHACOS. The extracts of PHO and PHACOS induced production of less than 10mM NO, being lower concentration when compared to that of negative control.

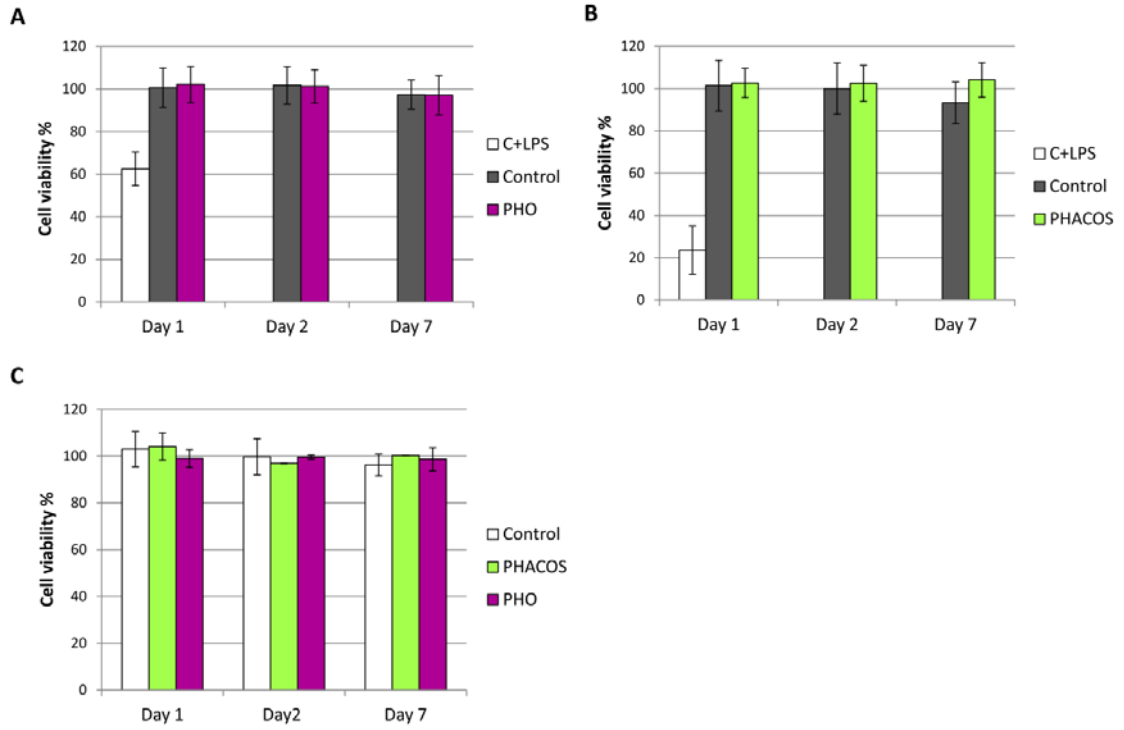

Figure 27. *In vitro* determination of PHACOS and PHO cytotoxicity by MTT assay. A,B Viability test performed on mouse monocyte macrophages RAW 264.7 where for negative control extracts incubated with PET disks were used and as a positive control cells were treated with LPS to monitor the decrease in cell viability; C- MTT assay on mouse fibroblasts BALB 3T3 where as a control extracts incubated with PET disks.

Alamar Blue assay was performed to monitor cell adhesion and proliferation. AB is a redox indicator that changes colour with the chemical reduction of the culture medium, occurring as the result of cells growth and proliferation. This reagent can be withdrawn and replaced with fresh medium, for monitoring cell proliferation. It is soluble, stable in culture media and nontoxic for cells (Nakayama et al., 1997). Results of the assay demonstrate similar cell metabolic activity between PHACOS and control (Figure 28B). However, lower metabolic activity was observed on PHO compared to PHACOS and control. Consequently, lower adhesion rate and proliferation were observed. Figure 28B demonstrates twofold higher adhesion of cells on PHACOS then on PHO during first 10 days. This behaviour can be explained based on the higher roughness of PHACOS. It is known that the cell behaviour depends on surface roughness and surface free energy (Wise et al., 1998).

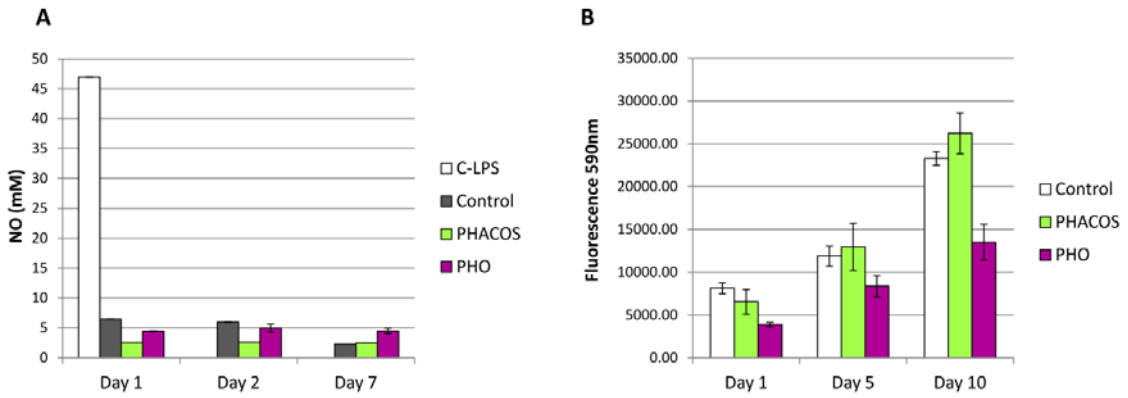

Figure 28. Determination of PHACOS and PHO *in vitro* immunocompatibility by Griess (A) and Alamar blue assays (B). A, Griess test for determination of PHACOS and PHO inflammatory effect on mouse monocyte macrophages RAW 264.7 as a measurement of NO production in cells treated with lipopolysacharide-positive control (white bars), extracts incubated with PET-negative control (grey bars), extracts incubated with PHACOS (green bars) and extracts incubated with PHO (purple bars); B, Alamar blue assay for determination of mouse fibroblasts BALB 3T3 *in vitro* proliferation on PHACOS (green bars) and PHO surfaces (purple bars), where white bars represent PET control.

ESEM studies provided additional information about fibroblasts adhesion, morphology and growth when being in direct contact with materials. Obtained results show adequate adhesion and expansion of cells during 7 days (Figure 29). On PHACOS less quantity of adhered cells was observed when compared to control. Fibroblasts showed normal growth and no evidences of morphological changes. In contrast, poor cell adhesion was observed on PHO surfaces during first two days. However, after 7 days growth process was recovered as well as cell morphology, being similar to that of control surface.

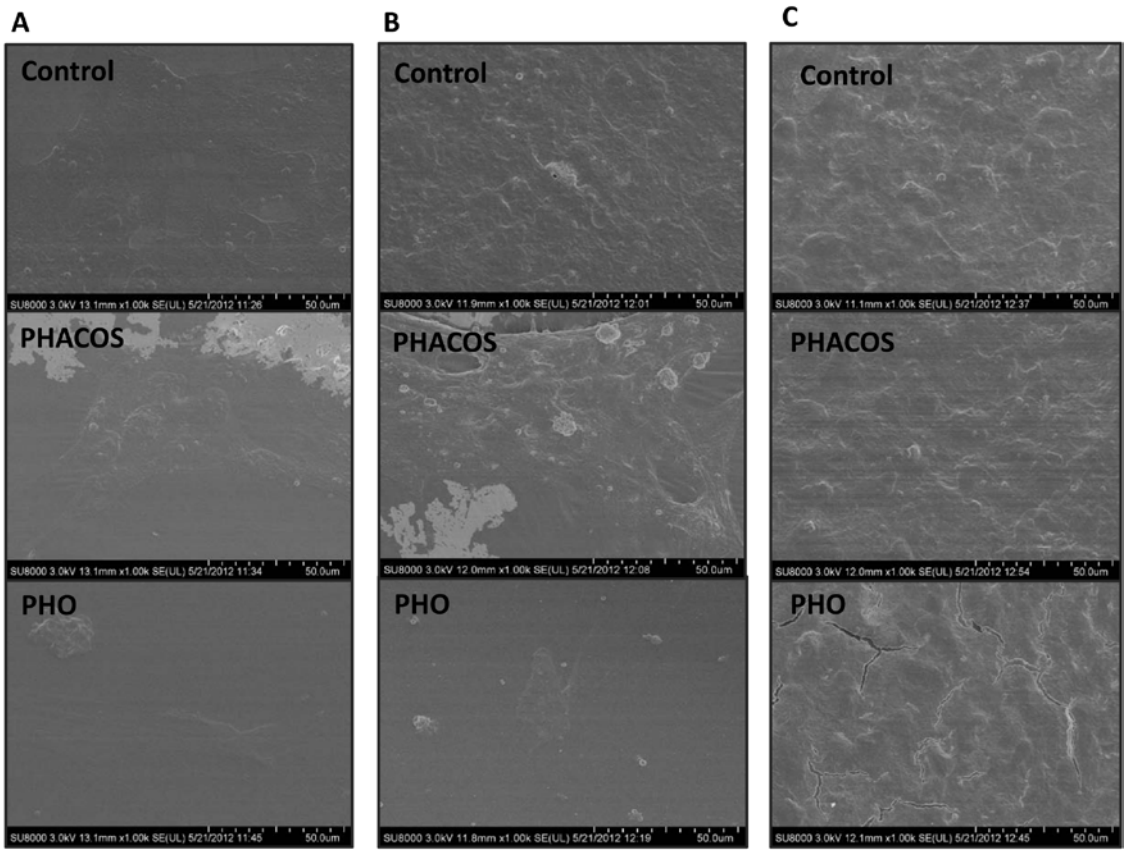

Figure 29. Environmental Scanning Electron Microscopy study of mice fibroblasts BALB 3T3 morphology and *in vitro* adhesion to PHACOS and PHO. A, Cell adhesion after 1 day incubation on PET, PHACOS and PHO disk (from top to bottom); B, Cell adhesion after 2 days incubation on PET, PHACOS and PHO disk (from top to bottom); C, Cell adhesion after 7 days incubation on PET, PHACOS and PHO disk (from top to bottom).

4.6. Inflammatory responses of mammalian cells to mcl-PHAs

The use of hydro-indocyanine green (H-ICG) to measure reactive oxygen species (ROS) associated with implant-associated inflammation has recently established (Selvam et al., 2011). The H-ICG was synthesized from commercially available ICG dye via a one-step reduction with sodium borohydride. This dye possess excellent stability to auto-oxidation, tunable emission wavelengths, and importantly, high selectivity and specificity as well as nanomolar sensitivity to ROS. In addition, it is small a molecule that can diffuse from the injection site or vascular bed into the tissue and cells directly associated with the implanted device. These attributes render H-ICG ideal probe for detecting implant-associated inflammation. Of note, ICG is a FDA-approved fluorophore that has found wide use as a noninvasive imaging agent. PET is used in many biomedical devices including sutures, vascular grafts, sewing cuffs for heart valves, and components for percutaneous access devices. Therefore, sterile, endotoxin-free disks (6 mm diameter) PET disks and PET disks coated with PHO and PHACOS were implanted subcutaneously in the back of 6-8 weeks old male BALB/c mice (Jackson Laboratories) anesthetized by isofluorane. A single 1-cm incision was made on the dorsum proximal to the spine, and a subcutaneous pocket laterally spanning the dorsum was created. Sterile disks (two per subject on either side of the spine) were implanted, and the incision was closed using sterile wound clips. Mice undergoing the same surgical procedure but receiving no biomaterial implants were used as sham controls to account for surgery-associated trauma/inflammation.

To monitor extracellular ROS associated with inflammatory responses to implanted biomaterials a single local injection of H-ICG dye was applied near the vicinity of the surgery site/implant of anesthetized mice. After 30 min animals were imaged via an IVIS fluorescence imaging system. Mice undergoing the same surgical procedure, but receiving no PET implants were used as sham controls to account for surgery-associated trauma/inflammation. Mice receiving biomaterial implants exhibited increases in fluorescence signal over time (Figure 30,31). Importantly, no significant differences in fluorescence signal were observed among sterile PHACOS, PHO and PET implant groups or the sham control during 14 days.

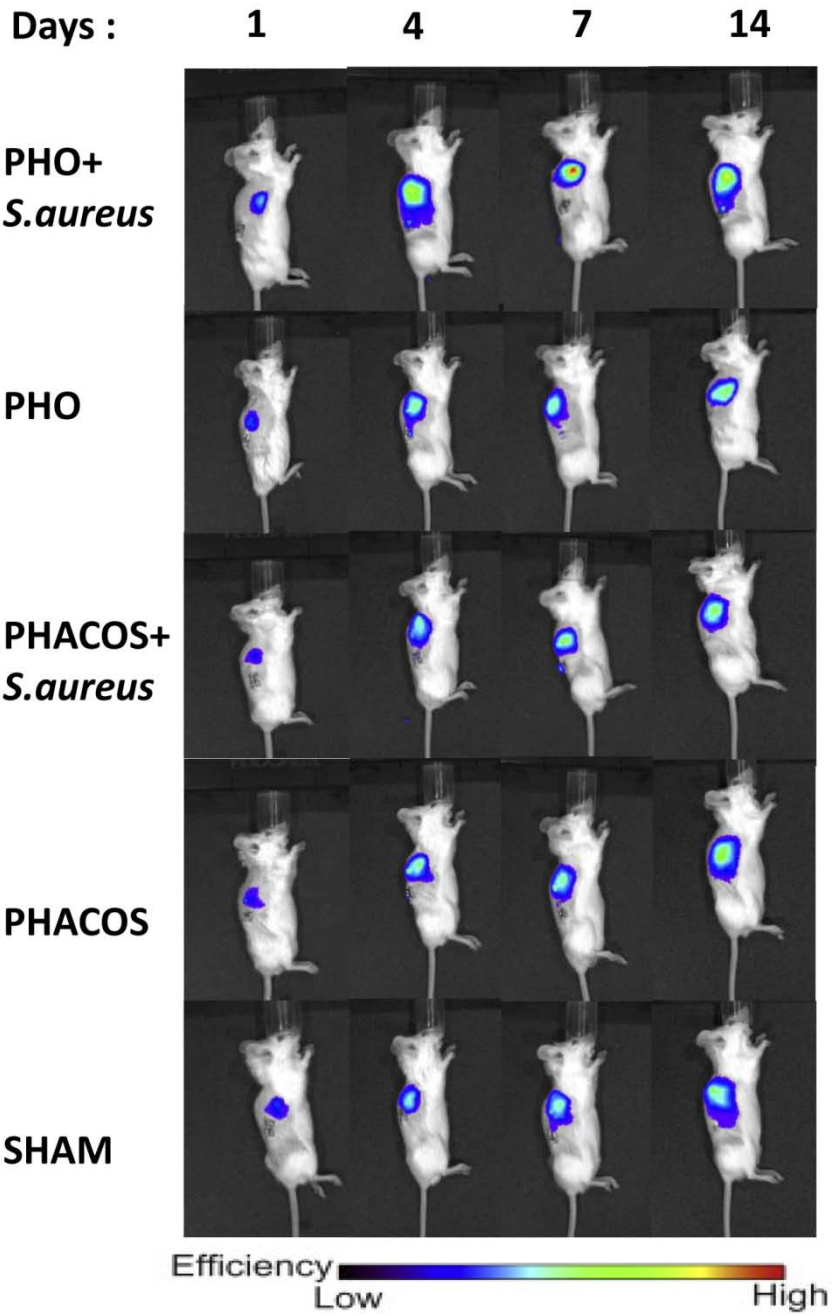

Figure 30. *In vivo* biocompatibility ROS imaging of PHACOS and PHO implant associated inflammation after subcutaneous administration of H-ICG. Bioimaging data of animal scanned in an IVIS® imaging system.

4.7. *In vivo* study of PHACOS antibacterial properties against *S. aureus*

We next examined whether PHACOS exhibits antimicrobial properties *in vivo*. With that aim, six animal groups were monitored: i) control group (shaved mice, no surgical procedure), ii) sham group (mice undergoing surgical procedure, but not receiving implant), iii) mice receiving sterile PHO disk, iv) mice receiving sterile PHACOS implant, v) mice receiving PHO implant precolonized with *S.aureus* and vi) mice receiving PHACOS implant precolonized with *S. aureus*. After a short incubation with *S. aureus*, biomaterial disks (PHACOS and PHO) were implanted subcutaneously as previously described for sterile implants. Implant associated inflammation was monitored for 14 days.

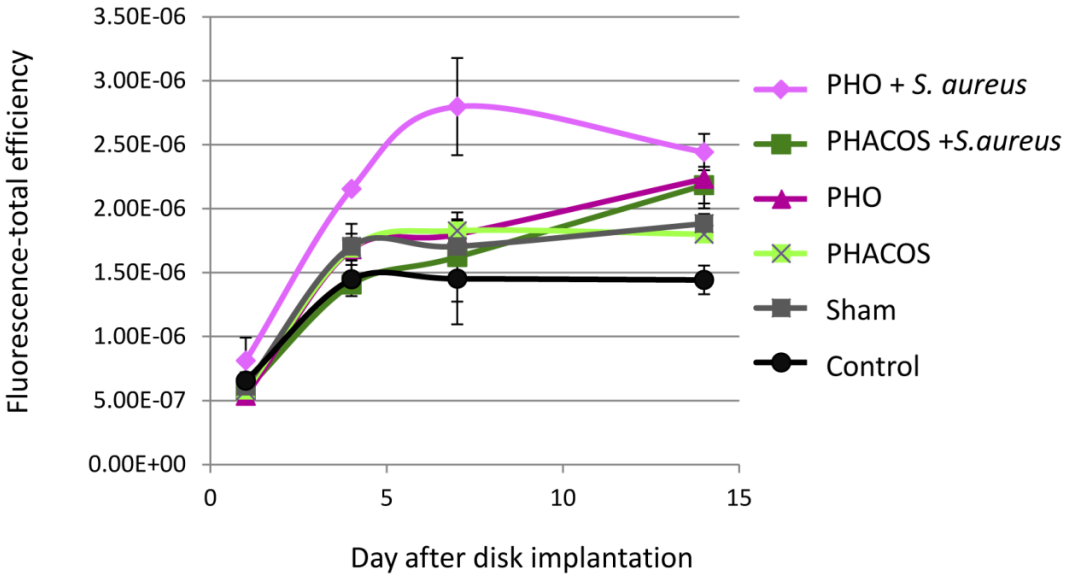

Figure 31. *In vivo* biocompatibility ROS imaging of PHACOS and PHO implant associated inflamation after subcutaneous administration of H-ICG. Quantification of ROS fluorescence data from mice with PHACOS and PHO implants incubated with *S. aureus* and sterile PHACOS and PHO implants.

Significantly higher fluorescent signal was observed for PHO disks incubated with bacteria compared to sterile PHO disks (Figure 30,31). These increased levels reflect the increased inflammatory response associated with the infected implant. Remarkably, PHACOS disks incubated with bacteria exhibited significantly lower ROS

signal compared to bacteria-incubated PHO, and the ROS levels for bacteria-incubated PHACOS were not different from the levels for sterile PHACOS implants. Taken together, these results demonstrate that PHACOS effectively controls biomaterial-associated infections in an *in vivo* model of device-related infection.

Following imaging, mice were sacrificed and the disks were retrieved along with implant-associated tissues intact to avoid disrupting the cellematerial interface. Explants were embedded in optimal cutting temperature compound (Tissue-Tek), freezed and cryosectioned at 10µm. For immunohistochemical staining, fresh-frozen cryostat sections were incubated in hydroCy5 (H-Cy5) to stain for intracellular ROS. After fixation, by immunohistochemistry, we analyzed macrophage (CD68+) and neutrophil (NIMP-R14+) recruitment to the implant (Figure 32).

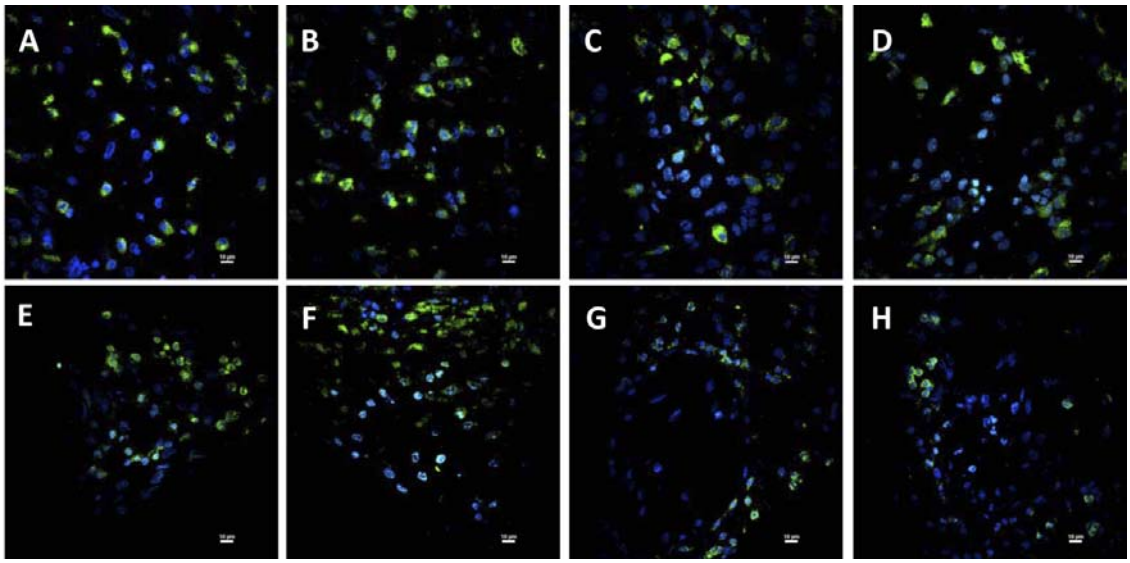

Figure 32. Immunohistochemical staining for macrophages (A-D) and neutrophils (E-H) in implant-associated inflammation. A-D, Representative co-localization images of macrophages (CD68+,green) and nuclei (DAPI ,40,6-diamidino-2-phenylindole, blue) in 14-day sterile PHO (A), *S. aureus* precolonized PHO (B), sterile PHACOS (C), *S. aureus* precolonized PHACOS implants (D); E-H, neutrophils (NIMP-R14+, green) with DAPI in 14-day sterile PHO (E), *S. aureus* precolonized PHO (F), sterile PHACOS (G), *S. aureus* precolonized PHACOS implants (H).

In addition, we co-stained for ROS activity using hydro-Cy5 (H-Cy5) as previously described (Lin et al., 2009). We observed an influx of inflammatory cells (76% of all cells; 33% macrophages, 43% neutrophils) to the vicinity of the PHO implant and PHACOS implant (62% of all cells; 29% macrophages, 33% neutrophils) at day 14 of implantation (Figure 33). Moreover, when the implants were precolonized with *S. aureus* influx of inflammatory cells was higher (82% of all cells; 38% macrophages, 44% neutrophils) in the vicinity of the PHO implant and (69% of all cells; 31% macrophages, 37% neutrophils) PHACOS implant. It is worth noting that there was statistically significant difference between macrophage recruitment to sterile and *S. aureus* precolonized PHO implant. However, there was no statistically significant difference in macrophage recruitment between *S. aureus* precolonized PHACOS and sterile PHACOS and PHO implants. Moreover, obtained results show significant difference in neutrophil recruitment to PHO and PHACOS sterile implants, as well as between *S. aureus* precolonized PHO and PHACOS implants. Importantly, co-staining analysis for inflammatory cell markers and ROS activity demonstrated that neutrophils and macrophages are primarily responsible for the ROS activity associated with the implant (Figure 33). Neutrophils are mainly responsible for ROS activity, when the implants are precolonized with *S. aureus*.

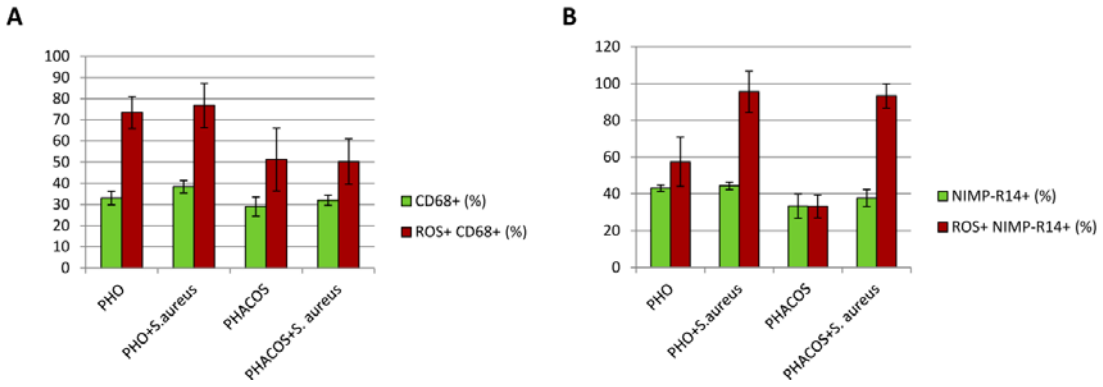

Figure 33. Immunohistochemical staining for macrophages and neutrophils in implant-associated inflammation. A, Quantification of CD68+ and ROS+ cells that stained positive for CD68+; B, Quantification of NIMP-R14 (±s.e.m.) and ROS+ cells that stained positive for NIMP-R14+ cells (±s.e.m.).

4.8. *In vitro* degradation of mcl-PHAs

To monitor *in vitro* degradation of PHO and PHACOS, polymers were analyzed by gravimetry assay. *In vitro* degradation was monitored during 1 month incubation of polymers in PBS. According to the obtained results no significant weight change was observed (Table 8). Consequently, applying this method we could not detect any sign of polymer degradation.

Table 8. *In vitro* PHACOS and PHO degradation monitoring

Incubation period	PHO (mg)	PHACOS (mg)
6 h	0.0281	0.0388
24 h	0.0281	0.0383
7 days	0.0283	0.0395
15 days	0.0281	0.0391
32 days	0.028	0.0385

5. Real-time non invasive in vivo monitoring of mcl-PHA implant associated infection

On time detection and appropriate treatment of implant associated infection is of great importance, taking into account that each year from 150 million implanted intravascular devices in the United States (Mermel, et al. 2009), 250,000 result in bloodstream infections (O'Grady, et al., 2011). *S. aureus* is one of the most common pathogens associated with these cases. Herein we describe a strategy for noninvasive real-time monitoring of bacterial mcl-PHA implant infection using bioluminescent *S. aureus* strains. Furthermore, we develop a new method for detecting early stages of bacterial infection and quantification of pathogen number correlating infection and induced inflammatory response. To that end, the sensitivity of imaging probes, H-ICG

was tested in correlation with increasing bacterial cell concentration and subsequently higher inflammation response.

5.1. Correlation between bioluminescence measurement and viable bacteria counting over different growth stage

To assess the feasibility of using bioluminescence as a quantitative indicator of bacterial number, *in vitro* studies were performed to compare bioluminescence to the number of viable cells on PHO and PET disks. During exponential phase of growth (1h of incubation), the luminescence output was proportional to the bacterial biomass, as determined by the number and bioluminescence of cells. Bioluminescence was found to closely correlate with viable-cell count, yielding correlation coefficients of 2.06 for *S. aureus* pAmiSPA2 (Figure 34). However, once the cultures reached stationary phase (24h of incubation), the bioluminescence no longer correlated with the number of cells. While the number of bacteria was constant the bioluminescence signal drastically decreased, indicating that as metabolic activity of the population decrease, monitoring bioluminescence of cells no longer reflects the bacterial counts. Nevertheless, as it was previously demonstrated that reduced expression of bioluminescence can be restored by replacement of the culture medium with fresh medium together with removal of planktonic cells (Kadurugamuwa et al., 2003), we investigated the relationship between bioluminescence expression and CFU in mice model *in vivo*.

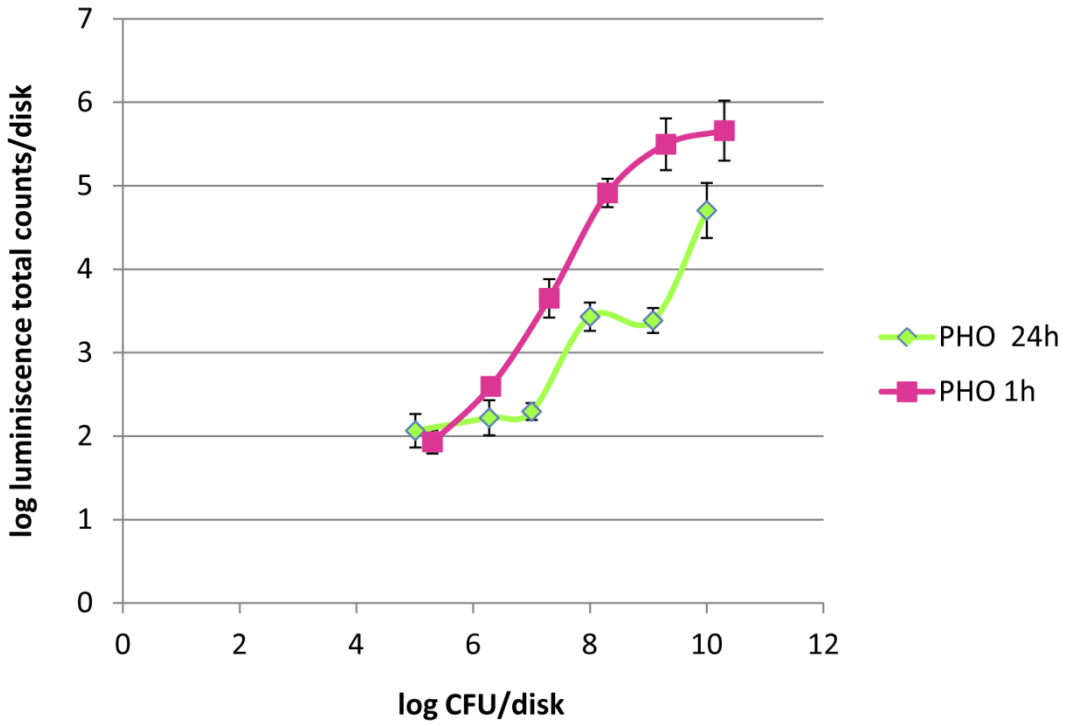

Figure 34. *In vitro* assay correlating *S. aureus* bioluminiscence and CFU counts during different growth stages. In pink demonstrated correlation between luminiscence and bacterial number after 1h incubation of *S.aureus* on PHO, while in green represented the correlation between luminiscence and bacterial number after 24h incubation of *S.aureus* on PHO.

5.2. *In vivo* detection of bioluminescent S. aureus strains PHO implant colonization

We next analyzed *in vivo* bioluminescence in mice model, for that, disks were precolonized with bioluminescent *S. aureus* pAmiSPA2 and *S. aureus* pAmiBlaz and implanted in the back of the mice. 7-day implant-based infection was real-time monitored. Moreover, we investigated if stable infection could be achieved and subsequently bacterial bioluminescence might be monitored. Both strains produced a bioluminescent signal in mice when the disks were precolonized with high bacterial inoculums (10^9 - 10^{10} CFU/disk). The total bioluminescent counts from the infected sites were quantified using Living Image software. Following implantation of

precolonized disks, the bioluminescence measurements decreased over 4 days post-implantation, whereas by day 7, bioluminescence could not be detected (Figure 35).

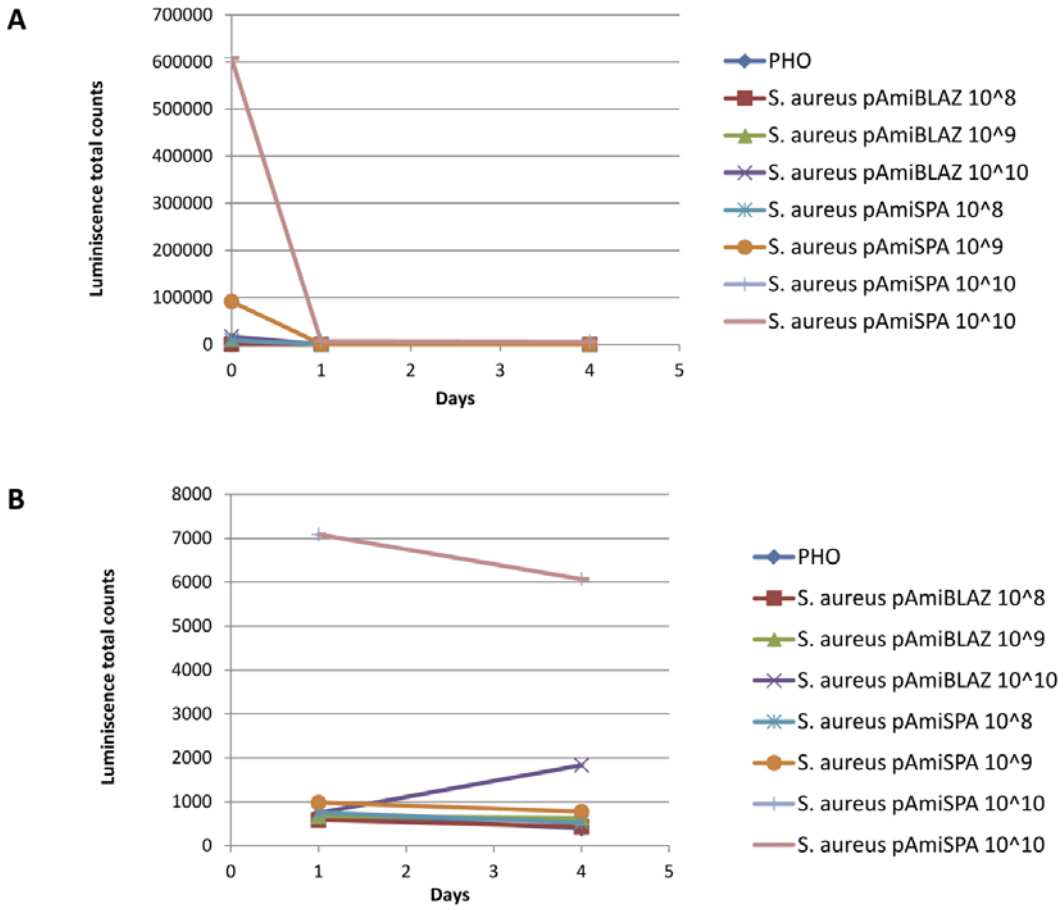

Figure 35. Non invasive monitoring of bacterial infection in mouse animal model using luminiscent *S.aureus* strains. Monitoring of luminiscent signal of *S.aureus* in PHO implants precolonized with different CFU counts.

5.3. Precise monitoring of biomaterial-associated inflammation by fluorescence imaging

Applying H-ICG, NIRF ROS sensor we monitored differences in inflammation levels associated with disks precolonized with different bacterial inoculums. Moreover, we examined the correlation between inflammation and density of *S. aureus* pAmiSPA2 and *S. aureus* pAmiBlaz inoculum used to precolonize disks 7 days post implantation. We observed the link between fluorescent signal and density of bacterial inoculums. It

is worth noting that the greater bacterial inoculum was used to precolonize implant the higher fluorescent signal was obtained, induced inflammation was higher (Figure 36). Therefore, we conclude that H-ICG sensor posses enough sensitivity to detect difference in inflammation induced by different bacterial inoculums.

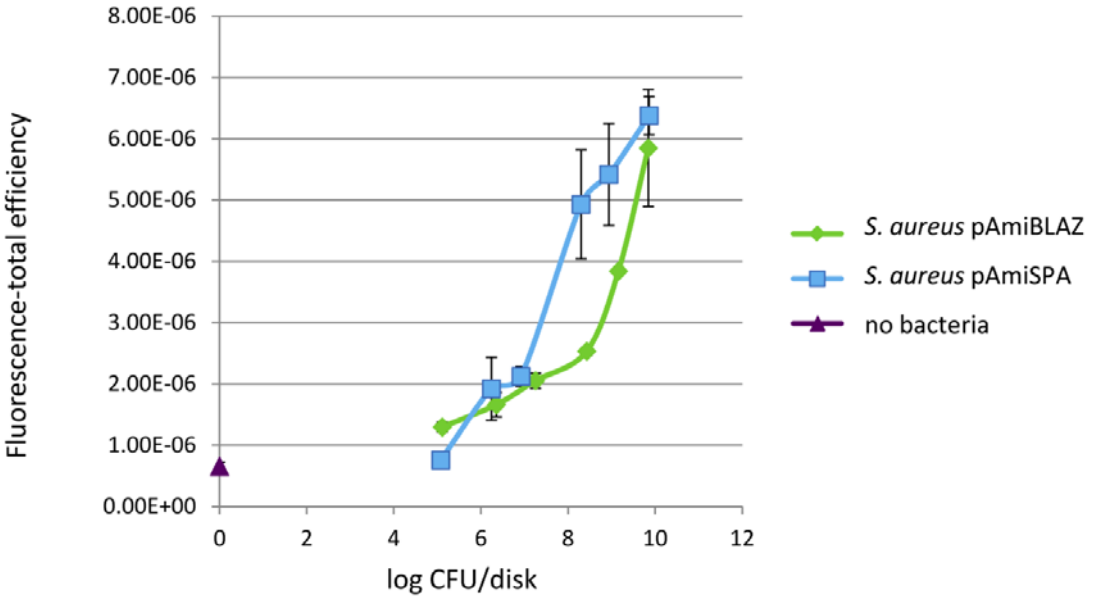

Figure 36. *In vivo* ROS imaging of implant associated inflammation using H-ICG NIFR sensor. Green line demonstrates inflammation provoked by PHO implant precolonized with different CFU of *S.aureus* pAmiBLAZ 7 day postimplantation, blue line line demonstrates inflammation provoked by PHO implant precolonized with different CFU of *S.aureus* pAmiSPA 7 day postimplantation, while in purple demonstrated inflammation provoked by steril PHO implant 7 day postimplantation.

Following imaging, mice were sacrificed and the disks were retrieved along with implant-associated tissues. The number of CFU recovered from disks was counted following the 7-day imaging. We observed that independent on the starting density of bacterial inoculums mice were able to eliminate 10^3 CFU (Figure 37). Therefore, we conclude that stable infection was not achieved using this model. However, we demonstrated that *S. aureus* strains are able to form biofilm *in vitro* on both surfaces, PET and PHO (see above).

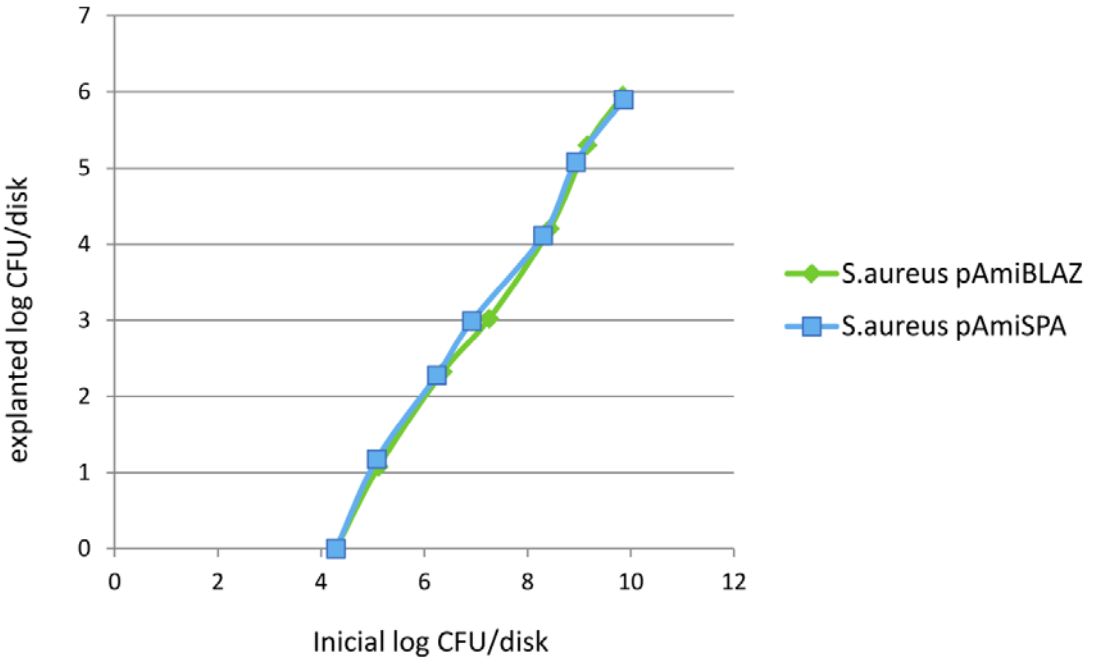

Figure 37. Infection stability analysis. Comparison of inicial CFU and CFU after PHO disk explantation. Green line represents *S. aureus* pAmiBLAZ strain, while blue line demonstrates *S.aureus* pAmiSPA.

By means of immunohistochemistry, we analyzed macrophage (CD68) and neutrophil (NIMP-R14) recruitment to the implant at day 7 post implantation (Figure 38). It was observed that as bacterial inoculums used to precolonize PHO implants was higher, the influx of inflammatory cells was higher being 76% for sterile implant and growing exponentially to 100% for implant precolonized with 10^7CFU/disk (Figure 38). Moreover, the number of both macrophages and neutrophils was increasing in the vincinity of PHO implant with the increasing number of cells used to precolonize implants.

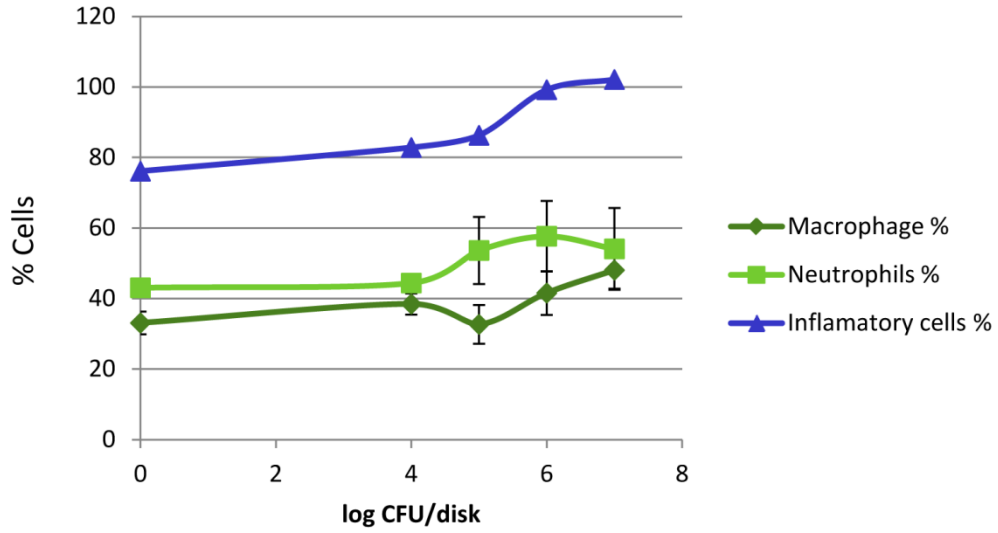

Figure 38. Immunohistochemical staining for macrophages and neutrophils in implant-associated inflammation. Quantification of CD68+, NIMP-R14 (±s.e.m.) and total number of inflammatory cells stained with DAPI.

Furthermore, it was observed that as the number of bacteria used to precolonize increase, the implant surrounding tissue shows more signs of necrosis, being completely destroyed when inoculums of 10^{10} CFU/disk was used to precoplonize implant. In addition, antibodies against *S. aureus* were used to analyze the formed

biofilm in the vincinity of implants (Figure 39).

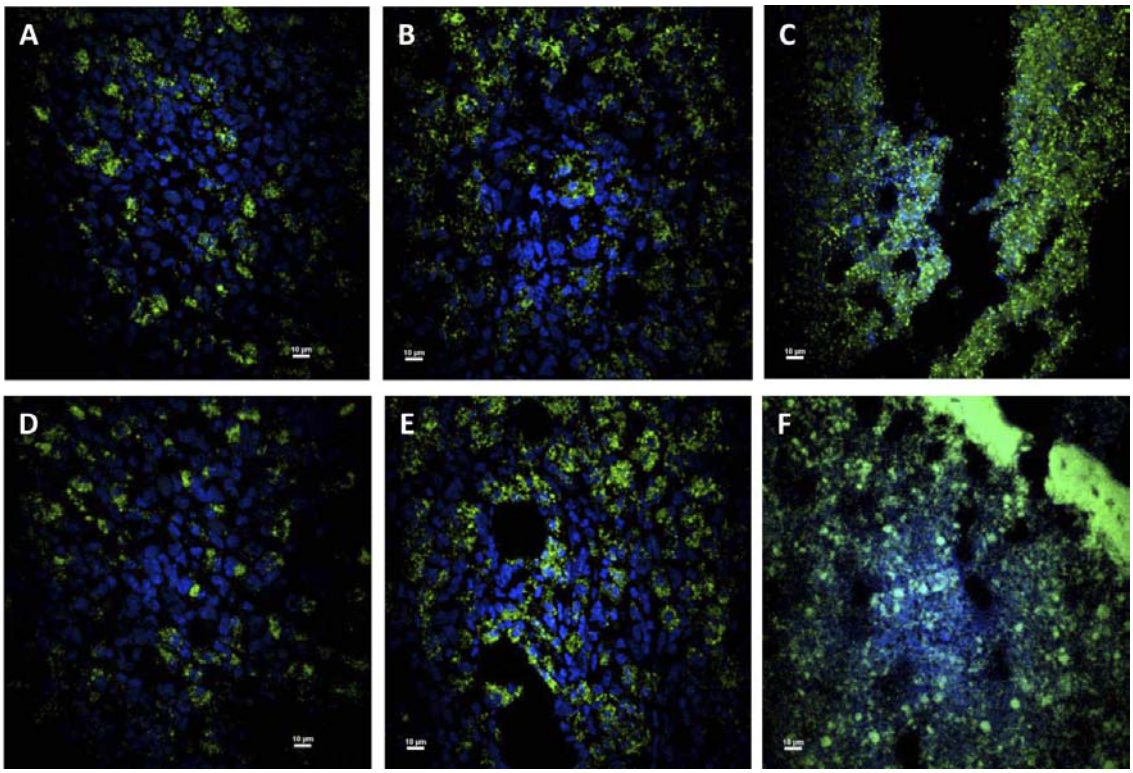

Figure 39. Immunohistochemical staining for *S. aureus* pAmiBLAZ (A-C) and *S. aureus* pAmiSPA (D-E) in PHO implant associated infection. A,D 10^8 CFU/implant; B,E 10^9 CFU/implant; C,F 10^{10} CFU/implant.

V. Discussion

Microbial polyesters play an important role in the development of second and third generation biomaterials, especially for biomedical applications. Various modification techniques were developed to improve their properties. Herein, we describe different strategies focused on designing new PHAs by introducing specific modifications that confer novel properties to the polymer (Figure 40).

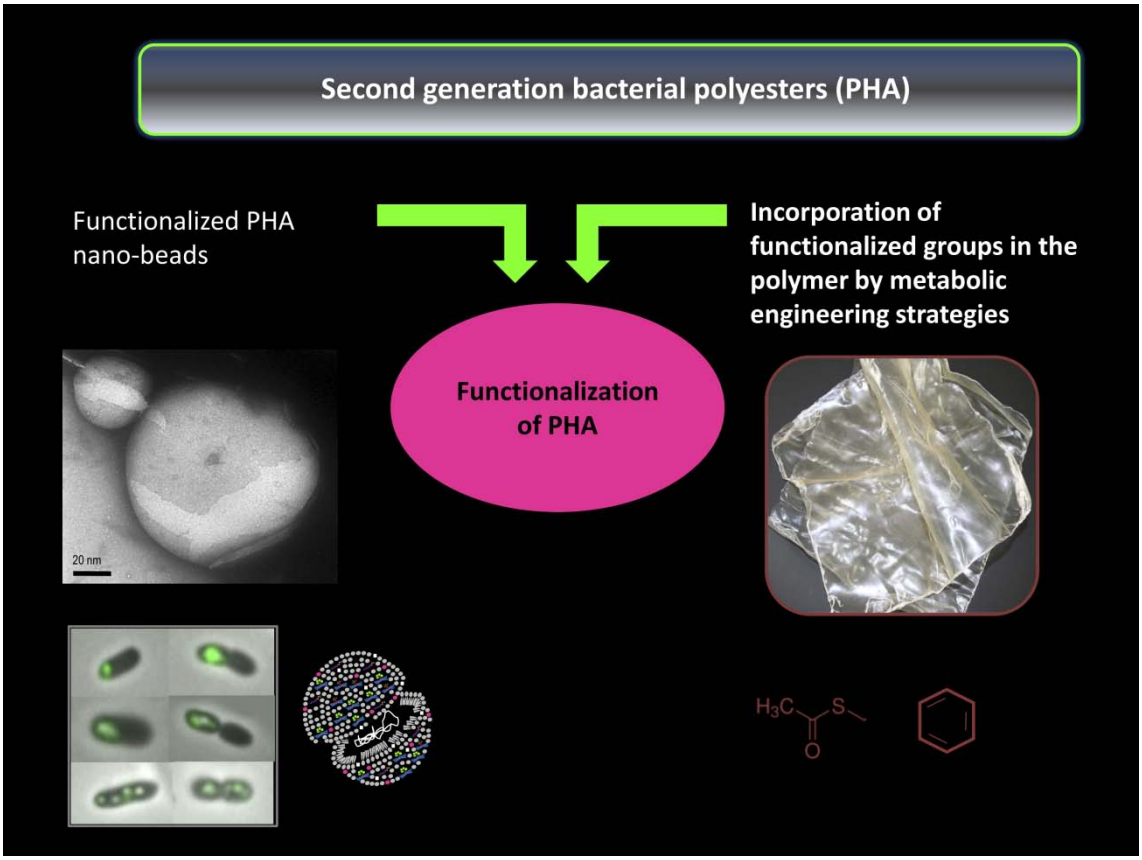

Figure 39. Strategies for added value PHA production. Two different strategies were applied, functionalizing of PHA nano-beads and metabolic engineering.

1. Nucleoid-associated PhaF phasin drives intracellular location and segregation of polyhydroxyalkanoate granules in *Pseudomonas putida* KT2442

One of the applied approaches consists in *in vivo* bacterial production of tailor-made functionalized nano-beads where proteins attached to the natural PHA granule have been engineered to display fusion proteins of interest (Figure 40). To refine the system, we try to resolve the puzzle of how functionally diverse, or even multifunctional set of phasins, should be combined to generate an optimal yield of *in vivo* protein immobilization onto granule surface in a coherent cell phenotype of *P. putida* KT2442. The modules of *P. putida* phasin proteins were proved to perform different functions supported by their peculiar structure distributed in separate domains (Figure 5).

Nevertheless, the role of phasins in granules formation is still unrevealed (Rehm, 2006). Two models of polyhydroxybutyrate (PHB) granule formation have been described in bacteria, the micelle model and the budding model, both accounting for the stabilized location of the synthase and phasin on the surface of the granule (revised in Grage *et al*., 2009). In the micelle model, a self-assembly process is initiated resulting in the formation of insoluble cytoplasmic inclusions with a phospholipid monolayer which contains covalently attached polyester synthases at the surface. In the budding model, the hydrophobic synthase binds to the inner face of the plasma membrane and buds from this membrane, leading to a granule surface covered with a lipid monolayer and phasins. However, TEM studies of granule formation and degradation in *Cupriavidus necator* H16 (formerly *Ralstonia eutropha* H16) revealed dark-stained elements ringed by small granules at early stages of PHB production. These structures named “mediation elements” were located near the center of cells or along a longitudinal strip in the center of the cells (Tian *et al*., 2005). These results were at odds with the micelle and membrane budding models, but led to an alternative model for granule formation, in which granule are localized and the new “mediation elements” function as scaffolds for the granule initiation sites. The fate of

granules during cell division, that is, whether they are equally distributed between daughter cells, is not known (Tian *et al*., 2005).

We have explored the physiological role of the histone-like PhaF phasin and PhaI phasin from the prototype microorganism *P. putida* KT2442. One of the peculiarities of PhaF phasin is its modular organization in a PHA granule binding domain (located at the N-terminus) and an AKP rich domain (located at the C-terminus). In fact, we had previously demonstrated the abilities of PhaF from *P. putida* GPo1 for binding to PHA granule (phasin-like activity), and as transcriptional regulator, suggesting a putative DNA binding activity (Prieto *et al.,* 1999; Moldes *et al.,* 2004). This C-terminal domain from the PhaF protein with a DNA-binding function histone-like is unique among phasins. In this sense, the identified phasins from *C. necator* H16 (PhaP1, PhaP2, PhaP3 and PhaP4) display an alanine-rich C-terminal region showing a very high isoelectric point (Neumann *et al.*, 2008). Nevertheless, further investigations are needed to exclude that this positive charge might participate in the interaction with the mediation elements or the latter might be simply the nucleoid of the cell.

This work demonstrates that PhaF plays a crucial role in granule localization and distribution, since the lack of this protein unbalance granule segregation during cell division (Figure 13). Similar system of localization of organelles as needle array inside prokaryotic cells has been observed for the intracellular organelles magnetosomes from *Magnetospirilum gryphiswaldense* (Komeili *et al.*, 2006). They are assembled into a regular chain in order to achieve the maximum magnetic moment, against the physical tendency of magnetosome agglomeration. In this system, the protein responsible for this alignment is MamJ which has a high content of acidic amino acids and a repeated domain structure, which appears to interact with a linear cytoskeleton-like structure composed by MamK (actin-like protein) that directs the assembly and localization of the prokaryotic organelles (Scheffel *et al.*, 2006). *P. putida* KT2442 (Nelson *et al.*, 2002) posses members of all cytoskeletal systems described in bacteria (revised in Gitai *et al.*, 2005 and Gerdes *et al*., 2010) like the tubulin homologous FtsZ (annotated as PP1342 in the chromosome); ParAB (PP_0001-2) and MinCDE (PP_1732-34) systems, where ParA and MinD are similar variant P loop ATPases that form cytoskeletal-like filaments on DNA and membranes, respectively, to solve different

problems (DNA segregation and septum placement) by analogous molecular mechanisms; Actin homologue MreB (PP_0934), similar to the actin-like protein MamK, which forms a helix essential for maintenance of cell shape, and it has been recently hypothesized to act as a scaffold for transporting proteins to different locations throughout the bacterial cell (Kimberly *et al.*, 2010). Our work demonstrated PhaF as central player in the machine to control PHA granule segregation and localization in the cell. Moreover, whether or not *P. putida* KT2442 cytoeskeletal proteins facilitate the needle array structure by direct or indirect interaction with PhaF, is still an open question and at this point, the precise mechanisms by which PHA granules are positioned by PhaF remains elusive. Since PhaF shows a unique ability for binding at least two ligands, the PHA granules and the nucleoid, our work provides support to consider that the PhaF function localizing and segregating the PHA granules implies new mechanisms different to that of described for magnetosomes (MamK/MamJ) or DNA segregation in bacteria (ParA-like mechanism). Taking into account the unspecific DNA binding abilities of the C-terminal part of PhaF (Galan et al, 2011), we cannot discard that the bacterial chromosome could play a role as granule carrier during the division process. In this sense, previous studies have determined the cellular position of different chromosomal sites demonstrating that they were positioned along the long axis of the cell in a linearly ordered fashion from the origin to the terminus (Teleman *et al.*, 1998; Niki *et al.*, 2000; Viollier *et al.*, 2004).

The unspecific PhaF-DNA interaction validates the classification of this phasin as histone-like protein and raises further questions about the physiological roles of PhaF in *P. putida*. Eukaryotic H1 histones are also called linker histones because they are chromatin-associated proteins that bind to the exterior of nucleosomes and dramatically stabilize the highly condensed states of chromatin fibers (Zlatanova *et al.*, 2000). In eukaryotic organisms, there is evidence that linker histones are also involved in transcriptional regulation by determining the accessibility of the nucleosomal DNA to the transcriptional machinery (Zlatanova *et al.*, 2000). Furthermore, it has been demonstrated that histones of the H1 family provide the DNA compactation required by the changing physiological needs of the cell during the different stages of cell cycle (Kasinsky *et al.*, 2001).

Examples of bi-functional proteins containing the AKP rich domain are found in eukaryotic organisms, such as the ribosomal proteins L22 and L23a of *Drosophila melanogaster* (Koyama *et al.*, 1999), and in the prokaryotic organisms like AlgP from *Pseudomonas aeruginosa* (Deretic and Konyecsni, 1990) and the putative DnaK suppressor from *Stenotrophomonas* sp. It is also worth to mention the cases of the traslation factor IF-2 from Actinobacteria which contains an AKP rich region in its N-terminal domain that is involved in translation initiation and binds to the ribosome by interacting with the initiator tRNA (Caserta *et al.*, 2006). Also, the Hc1 and Hc2 proteins from *Chlamydia trachomatis* play a role in the chromosome condensation regulating the stage specific differentiation during the life cycle (Kaul *et al.*, 1996) and BpH1 and BpH2 proteins from *Bordetella pertussis,* that are known to condense the DNA and protect it from digestion with DNaseI *in vitro* could be involved in transcriptional regulation (Goyard, 1996).

2. Swapping of phasin modules to optimize the *in vivo* immobilization of proteins to medium-chain-length polyhydroxyalkanoate granules in *Pseudomonas putida*

PhaF N- and C-terminal domains are linked via leucine zipper motif, also present in phasin PhaI. The leucine zipper motif is hypothesized to be a protein-protein interface. Moreover, it has been suggested that many of the biological properties of phasin proteins are dependent on multimerization via this coiled-coil region which provides a highly specific, physiologically relevant protein-protein interaction (Maestro et al., 2013).

The function of PhaI phasin, and the possibility of its substitution by PhaF phasin or BioF tag has been investigated in this study. We illustrate the utility of the PhaF/PhaI structure redundancy, being autonomous modular units working in harmony. Both C- and N-terminal phasin modules are revealed to be essential for the optimal PHA biosynthesis and accumulation in *P. putida* KT2442. When one of the modules is missing, PHA production decreases. Moreover, when strain lacks both

phasins, the PHA production falls to 7% of CDW, suggesting their cooperative work. However, BioF tag or its fusion derivatives can replace PhaI role in *P. putida* in terms of PHA production. However, the phenotype of the phasin mutant strains lacking of C-terminal domain of PhaF differs to that of wild type strain in terms of granule distribution, showing population heterogeneity. PhaF N- and C-terminal domains were tracked *in vivo* via monitoring their fusions with GFP reporter. As expected, GFP::C-PhaF co-localized with nucleoid, independently of the host strain and the presence or absence of the PHA granules, whereas N-terminal co-localized with PHA granules in all analyzed *P. putida* strains. Moreover, in the absence of PHA granules, BioF forms intracellular inclusions, mainly at the cell poles (Figure 19E,F), that could be explained by the existence of the short leucine zipper involved in protein oligomerization, as predicted in the structural, three-dimensional model. The phenotype of wild type strain is recovered in KT42I-BGF strain, which produces BioF::GFP fusion and PhaF at low dosage (Figure 17B, 18B, 19D), definitively demonstrating the essential role of C-terminal domain of PhaF protein in granule segregation and the swappable character of PhaI and BioF PHA binding modules.

It was previously demonstrated that phasins binding prevents unspecific attachment of other proteins not related to the PHA metabolism to the granules surface, and limits the space for anchoring of recombinant proteins (Neumann et al., 2008). We confirm that the absence of natural PhaI phasin favours the binding of the fusion protein to the granule surface. In the absence of wild type phasins, higher number of molecules of recombinant tagged proteins was anchored to the granules surface (Table 6). This could be explained by the lack of space on the surface of wild type PHA granules coated with PhaI/PhaF N-terminal phasin modules. In fact, the protein immobilization per gram of PHA in both strains KT42I-BG and KT42I-BGF were, similarly, more than 6 folds higher than that of the wild type strain. However, PHA production in KT42I-BG strain (19.6%) is two-fold lower when compared to the one obtained in KT42I-BGF (42.1%). Moreover, the low dosage of PhaF protein produced in the strain KT42I-BGF ensures granule distribution among cell population, yielding a total production of 10 mg of PHA immobilized protein per liter of culture and 9.73 mg of protein per gram of CDW. This protein concentration has been reported till now

only when *E. coli* was used as host strain for recombinant protein production anchored to PHB granules. In this sense, we have also identified the key phasin factors for optimal PHA production in *P. putida*. We have addressed the minimal necessary amount of complete phasin proteins to achieve adequate PHA production and subsequently higher yield of immobilized recombinant protein. In wild type *Bacillus megaterium*, GAPs represent close to 2% of the total mass of a standard granule,[35] what is in perfect agreement with the maximum BioF fusion concentration reported in this work 2.2 % of recombinant protein per PHA content.

Tagged proteins were co-produced with PHB granules in the *E. coli* cells. Multiple phasins (2-3 repeats) were used and successful purification of several proteins (maltose binding protein (MBP), β-galactosidase (LacZ), chloramphenicol acetyltransferase (CAT), and (NusA) with yields of 3.17-7.96 mg of protein/g CDW was reported (Banki et al., 2005). Thought *E. coli* can produce high PHB content (Chen, 2009) and consequently, high recombinant protein yield, advantages of using *P. putida* as host strain should not be overlooked (Poblete-Castro et al., 2012). The growing understanding of model mcl-PHA producer strains such as *P. puitda* KT2440 gained from System Biology studies ("omics" data, genome scale metabolic models etc.) (Poblete-Castro et al., 2012a; Poblete-Castro et al., 2012b; Poblete-Castro et al., 2013; Follonier et al.2013, Nogales et al., 2008) and powerful genetic tools based on Synthetic Biology (Silva-Queiroz et al, 2009; Silva-Rocha et al., 2013) support bottom-up approaches to design specialized *P. putida* strains to generate added value bioproducts such as active mcl-PHA based nano-beads. Its great value as autolytic specialized strain for mcl-PHA production has been also demonstrated (Martinez et al., 2011). Due to its broad metabolic versatility and genetic plasticity that allow use of variety of renewable carbon sources for PHA production, *P. putida* is one of the most prominent candidates to be used for protein production. Our work provides new findings related to phasin physiological function that will enable important insights into targeting the critical factors for improvement of existing models. Moreover, this work defines the needs for designing *in vitro* immobilization system to mcl-PHA where PhaI or BioF would be the only request tag for anchoring the recombinant protein to mcl-PHA nano-beads.

3. PHACOS, a functionalized bacterial polyester with bactericidal activity against methicillin-resistant *Staphylococcus aureus* (MRSA)

The second approach that was applied for polymer functionalization to obtain added value PHAs is based on the use of metabolic engineering to design bacterial strains able to produce new non-natural polyesters carrying functionalized groups at the side chain (Figure 39).

Today's polymeric and biodegradable systems used in medicine are mainly based on poly(lactic acid) (PLA), poly(glycolic acid) (PGA) and on their copolymers (Gomes and Reis, 2004). One of the prime current candidates with potential applications in the medical field is the group of naturally produced bacterial polyesters, PHAs, representing a large class of biodegradable and biocompatible biopolymer (Chen and Wu, 2005). However, for packaging materials, tissue engineering, and other specific applications, the physical and mechanical properties of microbial polyesters need to be diversified and improved (Steinbuchel and Valentin, 1995; Hazer et al., 2012).

In spite all existing application where polymers found their function a state of the art requirement due to increased level of emerging antibiotic-resistant bacteria 'superbugs' is creating a new possible function of polymers as antimicrobial surfaces. In addition, the effectiveness of antibiotics is decreasing and the development of new antibiotics to replace those that become ineffective is slower. Moreover, current actions to prevent antimicrobial resistance are not sufficient. Therefore, antimicrobial polymers are a class of biocides that has become increasingly important as an alternative to existing biocides and in some cases even antibiotics (Siedenbiedel and Tiller, 2012). Antimicrobial surfaces that prevent growth of biofilms are considered as an effective strategy to inhibit the spread of microbial infections (Siedenbiedel and Tiller, 2012). Such surfaces either repel microbes, so they cannot attach to the surface, or kill microbes in the vicinity (Siedenbiedel and Tiller, 2012). Antimicrobial polymers have been known since 1965, when Cornell and Dunraruma described polymers and copolymers prepared from 2-methacryloxytroponones that kill bacteria. In the past decade the number of FDA-approved disinfecting polymers has significantly increased,

which indicates the need for alternatives to antibiotics and environmentally critical disinfectants (Siedenbiedel and Tiller, 2012).

Bacterial infections are a major cause of morbidity and mortality in the hospital and community, and many infections can be attributed to species of the genus Staphylococcus (Kiedrowski and Horswill, 2011). While this group is best known for the acute pathogenic properties of *Staphylococcus aureus* (DeLeo and Chambers, 2009), the ability of these bacterial pathogens to cause chronic infections and persist on medical implants or host tissues is an area that has increasingly drawn attention as a significant healthcare problem (Darouiche, 2004). In fact, the ability of *S. aureus* to establish biofilms has been linked to the persistence of these chronic infections (Kiedrowski and Horswill, 2011). Methicillin-resistant *Staphylococcus aureus* (MRSA), also called multidrug-resistant *Staphylococcus aureus*, is referred to any strain of *S. aureus* that has developed resistance to beta-lactam antibiotics, which include the penicillins (methicillin, dicloxacillin,nafcillin, oxacillin, etc.) and the cephalosporins (Grundmann et al., 2006). MRSA is especially troublesome in hospitals, prisons, schools, and nursing homes, where patients with open wounds, invasive devices, and weakened immune systems are at greater risk of infection than the general public (Klein et al., 2009).

Tremendous efforts have been given to developing compounds that not only show high efficacy, but also those that are less susceptible to resistance development in the bacteria. The high incidence and rapid emergence of resistance to antibiotics in various Gram-positive cocci makes Gram-positive pathogens a major health hazard. *S. aureus* is Gram-positive bacteria and common human pathogens that most commonly colonize the anterior nares. The rest of the respiratory tract, open wounds, intravenous catheters, and the urinary tract are also potential sites for infection. *S. aureus* causes a diversity of diseases ranging from minor skin and soft tissue infections to life-threatening systemic infections, including endocarditis and sepsis (Raygada and Levine, 2009). It has been estimated that biofilms are associated with 65% of nosocomial infections (Mah and O'Toole, 2001). In addition, it was reported that during 1999–2006 the percentage of *S. aureus* infections resistant to methicillin increased >90%, or≈10% a year, in outpatients admitted to US hospitals (Klein et al.,

2009). The development of newer, stronger antibiotics which can overcome these acquired resistances is still a scientific challenge because a new mode of antimicrobial action is likely required. Antimicrobial polymers have emerged as a promising candidate for further development as an antimicrobial agent with decreased potential for resistance development (Kuroda and Caputo, 2013).

Recently in our laboratory we produced PHACOS, a new second generation polymer containing thioester groups in the side chain (Figure 8). This functionalized bacterial polyester was obtained applying 6-ATH as precursor and decanoic acid as co-substrate in a co-feeding strategy for *Pseudomonas putida* strains (Escapa et al., 2011). We have explored the possibilities of this second generation polymer application as biomedical device. One of the peculiarities of this naturally produced bacterial polyester is the presence of thioester groups in the side chain of the polymer. In fact, we show that those thioester groups play a crucial role in polymer activity against *S. aureus* clinical isolates. In this sense, we demonstrate the unique property of this *P. putida* polymer to have activity against other bacterial strains. Nevertheless, further modification of this second generation polymer for fine tuning of its activity and specific applications could be easily achieved as it is carrying functionalized side chains. In addition, we observed the certain inhibition of *S.aureus* biofilm development on PHACOS.

Biofilm formation on biomaterials can generally be divided into two main stages: bacterial adhesion, which depends on surface properties of both substrates and cells, and increase of biofilm mass which depends on initial attachment and specific growth rate of attached cells. It was demonstrated that the biofilm formation on PHAs, varied depending on both bacterial strain and material quality that supported biofilm formation. *E. coli* attaches better to mcl-PHA coatings than *S. aureus* (Mauclaire et al., 2010). Impurity elimination in the biopolyester coating drastically limits the biofilm formation (Mauclaire et al., 2010). Significant correlation was observed between bacterial attachment and roughness for *S. aureus*, a bacterium which is known to be sensitive to surface irregularities (Harris and Richards, 2006). Even though, PHACOS shows higher roughness than PHO no increase in attachment of *S. aureus* cells was observed. What is more, *S. aureus* biofilm formation was decreased on PHACOS when

compared to PHO. Interestingly, investigating the previously mentioned phenomenon we discovered the antimicrobial properties of PHACOS.

The potential of pathogenic biofilm development on mcl-PHAs was evaluated, nevertheless antibacterial activity of PHAs not modified or mixed with other compounds for that purpose, was not reported (Mauclaire et al., 2010). Furthermore, it was not observed that PHAs posses antiadherent properties against bacteria. However, it is known that R3HAs, monomers derivated from PHAs, show antibacterial activity. Antibacterial activity of *R*-3-hydroxy-n-phenylalkanoic acid against *Listeria monocytogenes* was reported (Sandoval et al., 2005). Moreover, data provided by Ruth et al. demonstrates antibacterial activity of aliphatic (*R*)-3-hydroxycarboxylic acids against not only Listeria species, but the other bacterial strains such as *S. aureus* (Ruth et al., 2007). Even though, the antibacterial efficiency of previously mentioned compounds is low showing very high MICs values (Minimal Inhibitory Concentration), 1-5 mM.

Many commonly used antimicrobial agents active against planktonic pathogens have minimal or no effect against biofilm-embedded pathogens (Agarwal et al., 2005; Giacometti et al., 2005). Interfering with the biofilm may liberate device-colonising organisms and therefore increase the efficacy of antimicrobial agents. Thus, there is a pressing need to explore novel approaches that utilize compounds with a dual ability to disrupt the biofilm and to eliminate pathogens.

Novel approaches for the development of antimicrobial polymers are an important area of research and many reports have been published referring to the synthesis of macromolecules that are inherently antimicrobial (biocidal polymers). These are usually positively charged macromolecules that interact with microbial cells that generally carry a negative net charge at the surface due to their membrane proteins, teichoic acids of Gram-positive bacteria, and negatively charged phospholipids at the outer membrane of Gram-negative bacteria (Siedenbiedel and Tiller, 2012). Cationic polymers have been the main focus (Waschinski and Tiller, 2005) including those containing ammonium (Kenawy et al., 2002), phosphonium salts (Popa et al., 2003), pyridinium salts (Tashiro, 2001; Worley and Sun, 1996), polyguanidines

and polybiguanidines (Albert et al., 2003), polylysine (Hancock and Chapple, 1999), polyacrylates (Kenawy et al., 1998), polystyrenes (Gelman et al., 2004) and polyoxazolines (Waschinski et al., 1998). Antimicrobial peptides also represent a large group of natural compounds with a broad spectrum of antimicrobial activity (Zasloff, 2002). Other class of antimicrobial polymer known as polymeric biocides, that consist of bioactive repeating units, i.e., the polymers are just multiple interconnected biocides, which act similarly to the monomers. Often, the polymerization of biocidal monomers does not lead to active antimicrobial polymers, either, because the polymers are water-insoluble or the biocidal functions do not reach their target. Last but not least are biocide-releasing polymers, which in turn do not act through the actual polymeric part, instead the latter function as carriers for biocides that are somehow transferred to the attacked microbial cells. Such polymers are usually the most active systems, because they can release their biocides close to the cell in high local concentrations (Siedenbiedel and Tiller, 2012). These subjects have attracted the attention of many researchers, and significant improvement in understanding of their essential physiochemical properties and mode of action has been made, conversely there are still a number of antibacterial polymers whose exact working principles are unknown.

Following our major finding, the antibacterial activity of PHACOS, we have focused on investigating the possible ways of its action. This work demonstrates that PHACOS acts as contact active surface and therefore could be considered as biocidal polymer. However, taking into account the antibacterial activity of PHACOS derived monomers we cannot discard the possibility that it is polymeric biocide, as the polymerization of active monomeric units leads to antimicrobial polymer. Moreover, one of the peculiarities of the mode of action of this polymer is the antibacterial activity of its precursor and monomers. Moreover, we demonstrated low level of *in vitro* degradation of the polymer. In this sense, it is possible that the releasing of monomers gives PHACOS antimicrobial properties. If that is the mode of action of PHACOS, it could be classified as biocide-releasing polymers. However, as the degradation rate of PHACOS is very low, we consider that the concentration of released monomers is too low to be the main way of polymer functioning. Nevertheless, it could certainly

contribute to its antibacterial activity. Other property that needs further investigations is the specificity of PHACOS antimicrobial effect against *S. aureus*.

Several antibacterial polymers are known to be selective against *S. aureus* over other strains, although there is no report on polymers with selective activity to bacteria other than *S. aureus*. Cationic polymers including polynorbornenes (Lienkamp et al., 2008), oligolysins (Epand et al., 2009), and chitosan (Raafat et al., 2008) all showed selective activity against *S. aureus* over *E. coli*. Although the chemical structures of these polymers are quite different from each other, the cationic functionality appears to be in common, which may be the key determinant in the activity against *S. aureus*. Recently, Gibney et al. demonstrated that commercially available unmodified polyethyleneimines (PEIs) with branched structures (MW = 500–12,000) also are antimicrobial with selective activity against *S. aureus* over *E. coli* (Gibney et al., 2012).

Even thought, there are examples of polymers selective activity against *S.aureus*, the precise mechanisms by which PHACOS decrease biofilm formation and kills the cell is still an open question at this point. N-acetylcysteine NAC, an antioxidant with disruptive properties for disulfide bonds, has been shown not only to reduce adhesion but also to detach bacterial cells adhered to surfaces and to inhibit bacterial growth *in vitro* (Olofsson et al., 2003; Perez-Giraldo et al., 1997). NAC inhibits *S.aureus* growth at concentration of 2.5 mg/mL and has bactericidal properties at concentration of 5 mg/mL (Hernandez et al, 2009). The similarity between NAC and PHACOS lies on -SH group. Although PHACOS does not contain free -SH group there is a possibility that its functionalized thioesther side chain breaks and give rise to free -SH group. The recent review of Timofeeva et al. thoroughly discusses the influence of relevant parameters, such as molecular weight, type and degree of alkylation, and distribution of charge on the bactericidal action of antimicrobial polymers (Timofeeva and Kleshcheva, 2011). Therefore, there are many factors that should be investigated to determine the mode of action of PHACOS. Although, there is no published data on mcl-PHA antimicrobial activity, their monomers, medium- and long-chain fatty acids (containing 8 to 18 carbons) have been shown to be bactericidal to many different Gram-negative and Gram-positive bacteria (Bergsson et al. 1998, 1999, 2001, 2002).

The bioactivity of different doses of the short-chain, medium-chain and long-chain fatty acids against gram-positive oral bacteria *Streptococcus mutans*, *S. gordonii* and *S. sanguis* were studied (Huang et al., 2011). It was demonstrated that short-chain fatty acids C2-C5 exhibit minimal antimicrobial activity for this range of bacteria (estimated by the inhibitory concentration at 80%, IC80), while among the medium chain fatty acids, the IC80 decreased with increasing size of the fatty acid. IC80 values for octanoic acid were in a range of 2.5mM-<0.1mM, whereas IC80 values for hexanoic acid were 2.5-0.6mM, both depending on a tested strain (Huang et al. 2011). Similarly, in our study we confirm MIC values of octanoic acid and hexanoic acid for *S. aureus*, 3mM and 0.75mM respectively. While 6-acetylthiohexanoic acid, showed much lower MIC value (40µM), being more effective against *S. aureus*.

The effect of fatty acids and monoglycerids on Gram-positive cocci was investigated (Bergsson et al., 2001). It was reported that 10mM caprylic acid, myristic acid, oleic acid, monocaprylin, monolaurin, monomyristin, monopalmitolein and monoolein caused only a minor inactivation of *S. aureus*, while lauric and palmitoleic acid showed an intermediate effect, reducing the viability count by 1.0 to 2.8 log10 CFU. However, monocaprin and capric acid reduced the infectivity titres of *S. aureus* by 5.0 to 7.1 log10 CFU, showing the highest activities (Bergsson et al., 2001). Bactericidal activity of monocaprin, capric, lauric and palmitoleic acids are reported for streptococci and staphylococci, and therefore may be useful for protection against or treatment of infections caused by Gram-positive cocci where rapid killing of the bacteria is desirable (Bergsson et al., 2001). Caprylic acid at concentration of 15mM was bactericidal for *Dermatophilus congolensis* (Valipe et al., 2011) and at concentration of 35mM for *E. coli* O157:H7 (Annamalai et al., 2004).

The specificity in the activities of fatty acids and monoglycerides against various bacteria is notable. The difference between the activity profiles of lipids for streptococci and *S. aureus* could possibly be explained by differences in cross-linkage of peptidoglycan polymers in the cell wall of the bacteria. Also, the peptidoglycan of *S. aureus* is interspersed with molecules of ribitol-teichoic acid, which is relatively specific for this bacterium (Sherris, 1990). A further study of the reason for the difference in activity profiles of lipids against various bacteria would be of interest.

In spite the existence of many examples of different polymers higher activity of against *S. aureus* precise mechanism is still unrevealed. To compare antimicrobial activity of hydroxycarboxylic acids with compounds known to have antimicrobial properties such as quaternary ammonium salts we used dual functional biologically active acrylic system that bears quaternary ammonium salts ionically linked to non steroidal anti-inflammatory drugs (NSAID). Antimicrobial activity of the dual functional monomers and polymers was analyzed comparatively with those of the corresponding halide precursors against several Gram-negative and Gram-positive bacteria. Ketoprofen derivatives were tested due to their higher hydrophilic character. In general, the NSAID counterion had little effect on the antimicrobial activity of the monomeric specie, giving MIC and MBC values similar to those of the halide counterion. The antimicrobial effect of the monomeric compounds strongly depended of the substitute group of the ammonium cation as reported for 3-alkoxymethyl-1-methylimidazolium salts (Pernak et al., 2003). The hexadecyl ammonium derivatives (HK, HI^-) showed the lowest MIC and MBC values for all tested strains, as published in other works (Caillier et al., 2009; Lu et al., 2007), while the benzyl derivatives (BK, BBr^-) showed the highest values (>4.0 x 10^{-2} mM). Naphthyl derivatives (NK, NBr^-) presented intermediate values. In general, MIC values coincided with MBC values for each compound excepting the hexadecyl derivatives monomers for *P. aeruginosa*, which showed MBC values higher than MIC ones. Obtained MBC values of the monomers BBr^- and HI^- are in perfect correlation with the data previously reported for the HI^- acrylate (MIC of 275 µM) against *S. aureus* (Lu et al., 2007; Callier et al., 2009). For the polymers poly-BBr^- and poly-BK, the incorporation of the ketoprofenate anion improved the bactericidal activity compared with that of the bromide anion. This effect was observed in all bacterial strains being more evident for the Gram-positive strains, in which MIC and MBC values of poly-BK were one order of magnitude lower. Both polymers showed much higher antibacterial activities than their corresponding monomers, e.g. MIC = 1.6 x 10^{-4} mM for poly-BK. This result could be explained by a different mechanism of action of polymers vs monomers. Moreover, polymerization might increase the density of positively charged coil in the polymer, which in turn could enhance the ability to be absorbed onto the negatively charged bacterial surface (Kenawy et al., 2002). Subsequently, this would improve the first step of cationic

biocides mode of action (Hugo and Longworth, 1966). In addition, the binding to the cytoplasmatic membrane would be enhanced due to the high density of negatively charged species like acidic phospholipids and membrane proteins (Ikeda et al., 1984). In general, all of the compounds, monomers and polymers, presented lower MIC values against *S. epidermidis* and *S. aureus*, suggesting that the structure of the Gram-positive cell wall is more sensitive to their mode of action (Costerton and Cheng, 1975).

4. Real-time monitoring of bacterial infection *in vivo*: Development of bioluminescent *Staplylococcal* foreign-body mouse infection model

Apart from the development of biomaterials with desirable antimicrobial properties, it is of great importance for infections to be diagnosed and treated on time. However, conventional methodologies for monitoring gram-positive pathogens *in vivo* are cumbersome and include biological assessment regimens. In addition, diagnosis of those infections with marginal laboratory and radiography evidence is difficult (Zimmerli et al., 2004) and there is compiling need for new sensitive diagnostic techniques development. Two thirds of implant infections are caused by staphylococci (O'Grady et al., 2011). As a general guideline, device removal is recommended for *S. aureus* infections due to the virulent nature of this pathogen (Darouiche, 2004). One of the reasons catheter and implant infections occur frequently is due to poor vascularization at implantation sites (Zimmerli et al., 2004). The inability of the innate and adaptive defense mechanisms to reach implantation sites makes it difficult for the host to fight off infection. In regions devoid of circulation, staphylococci are free to grow, spread, and form a resistant biofilm structure.

When implanted the device is immediately coated with host matrix proteins (Francois et al., 1998; Francois et al., 2000) (Figure 10). *S. aureus* possesses numerous cell wall-bound surface proteins that contain binding domains for these matrix proteins (Foster and Hook, 1998), and such surface proteins are referred to as microbial surface components recognizing adhesive matrix components (MSCRAMMs).

An underappreciated explanation for the infection of implants with staphylococci is the low inoculums required to establish infection. Moreover, some infections, such as post-arthroplasty related, are associated with nonspecific signs, which subsequently cause the development of chronic infections with catastrophic complications (Del Pozo and Patel, 2009).

Moreover, implant surface chemistry is known to be an important factor that contributes to bacterial adhesion and biofilm development. Higher rates of infection associated with stainless steel then to titanium were reported (Harris and Richards, 2006), possibly due to better association of soft tissue with titanium surfaces. Biomaterials play an important role in the disease treatment and health care improvement (Langer and Tirrell, 2004).

Herein we describe the use of bioluminescent noninvasive imaging strategy for detection and real-time monitoring of PHO implant bacterial infection *in vivo*. Bacterial adhesion and biofilm formation on mcl-PHAs have been studied before; however this is the first example of *in vivo* monitoring. Using genetically engineered bioluminescent *S. aureus* strains we were able to noninvasively monitor PHO implant-related infection throughout the study. However, we observed that when the implant is precolonized with low number of cells bioluminescent signal could not be detected. Furthermore, when bacteria go out from exponential phase and enter stationary phase of growth, bioluminescence decay indicating a decrease in growth. The same behavior was observed by Kadurugamuwa et al., explaining that limitation of oxygen and/or substrate could be possible cause since the reduced expression of bioluminescence within the biofilm could be restored by replacement of the culture medium with fresh medium every 12 h (Kadurugamuwa et al., 2003).

As infection could not be monitored *in vivo* in long-term study due to the bioluminescence signal decrease we investigated whether fluorescent H-ICG could be applied for noninvasive monitoring of implant-associated infection. By measuring the inflammation, the correlation between inflammation intensity and bacterial number used to precolonize the implant was observed. The higher starting bacterial inoculums are applied, the higher inflammation was detected. Applying H-ICG-based fluorescence

imaging of ROS, we were able to precisely detect the infection even when bioluminescence could not be detected. Moreover, statistically important differences in inflammatory response between sterile PHO and control group were not detected. In perfect correlation with previously reported data, we demonstrate *in vivo* biocompatibility of PHO implants and good tissue integration.

A high biocompatibility is essential for the acceptance of an incorporated object by humans and mammals. Several factors determine whether an object is biocompatible: shape, surface porosity chemistry of the material, and the environment (tissue) where it is incorporated (Zinn et al., 2001). PHA has the potential to become an important compound for medical applications. Tests have shown that PHB is biocompatible, which is not surprising when considering the fact that R-3-hydroxybutyric acid is a normal constituent of blood at concentrations between 0.3 and 1.3 mM (Wiggam et al., 1997) and is also found in the cell envelope of eukaryotes (Reusch, 2000). A successful application of PHAs as implants has been demonstrated as well as their biodegradability, biocompatibility and thermoprocessibility (Chen and Wu, 2005). Application of PHO was mainly focused on heart valves fabrication regarding its mechanical and thermophisical properties. Sodian et al. constructed PHO heart valve scaffolds using stereolithographic models and tested in a pulsatile bioreactor. Leaflets opened and closed synchronously under subphysiological and supraphysiological flow conditions. Futrhermore, to improve constructed PHO trileaflet heart valve, scaffold were seeded with vascular cells harvested from ovine carotid arteries and expanded *in vitro*. Results of this study showed that tissue-engineered heart valve scaffolds fabricated from PHO can be used for implantation in the pulmonary position with an appropriate function for 120 days in lambs (Sodian et al., 2000). The biomedical application of PHO and other mcl-PHAs has been reported before (Hazer et. al., 2012), however this is the first example of *in vivo* monitorin of bacterial adhesion and infection development on mcl-PHA implant.

From an industrial standpoint PHAs are biopolyesters attracting extensive interest as technical grade polymers due to their singular set of properties: (i) substitution potential for industrial thermoplastics such as polypropylene, polyethylene, polyvinylchloride and polyethylene terephtalate, (ii) biodegradability both in aerobic

and anaerobic conditions, including water environments, (iii) bio-based, renewable origin, (iv) biocompatibility with cells and tissues and (vi) structural diversity (Van der Walle, 2001; Chen 2009). This last characteristic is critical to define potential applications since the specific chemical monomer composition and molecular structure will determine the biological, thermal and mechanical properties of the resulting polymer.

VI. Conclusions

1. A new and unexpected role of *P. putida* KT2442 PhaF phasin involved in the balanced distribution of the PHA reserve granules between daughter cells during cell division has been described. The particular composition of PhaF C-terminal domain mimics histon-like proteins, and confers the protein an unspecific DNA binding capacity.
2. We demonstrated a new role for phasins within the PHA apparatus that could be critical for cell survival under stress conditions.
3. The key factors involved in *in vivo* immobilization of recombinant proteins onto PHA granules using the previously designed BioF system were determined.
4. We illustrated the swappable characteristic of PhaI and BioF PHA binding modules.
5. The optimal conditions that allow the highest recombinant protein immobilized *in vivo* onto PHA granules yield were achieved. A particular combination of phasin modules synthesis leads to optimal PHA production and granule distribution among cells have been defined.
6. We described a new and unexpected property of PHACOS, second generation biopolymer, showing antibacterial activity specifically against *S. aureus* clinical isolates including MRSA and decreasing *S. aureus* biofilm formation.
7. Antibacterial activity of PHACOS has been ascribed to the functionalized side chains containing thioester groups. These findings led arguments to possible mode of action of PHACOS as contact active surface and opens new questions about the still unknown antibacterial mechanism linked to this biomaterial.
8. We showed the possibility of PHACOS application as implant demonstrating its biocompatibility and antimicrobial properties *in vivo*.
9. A noninvasive method for *in vivo* real-time monitoring of mcl-PHA implant associated infection and inflammation has been developed.
10. We describe the strategy for *in vivo* monitoring of mcl-PHA implant infection development using bioluminescent strains.
11. We show the possibility of H-ICG sensor application for monitoring of early infection stages or stages when bacteria enters stationary growth phase.

VII. References

Adelmann R, Mennicken M, Popescu D, Heine E, Keul H , Moeller M. (2009). Functional polymethacrylates as bacteriostatic polymers. *European Polymer Journal*. 45: 3093–3107.

Agarwal G, Kapil A, Kabra SK, Das BK, Dwivedi SN. (2005). *In vitro* efficacy of ciprofloxacin and gentamicin against a biofilm of Pseudomonas aeruginosa and its free-living forms. *Natl Med J India*. 18:184–6.

Albert M, Feiertag P, Hayn G, Saf R, Honig H. (2003). Structure−Activity Relationships of OligoguanidinesInfluence of Counterion, Diamine, and Average Molecular Weight on Biocidal Activities. *Biomacromolecules*;4(6):1811–7.

Babu GN, Christopher SS, Copley BC, Overstreet TS. Radiation curable polyolefin pressure sensitive adhesive Número de patente: 5209971, 199.

Bäckström BT, Brockelbank JA, Rehm BHA. (2007). Recombinant Escherichia coli produces tailor-made biopolyester granules for applications in fluorescence activated cell sorting: functional display of the mouse interleukin-2 and myelin oligodendrocyte glycoprotein. *BMC Biotechnol*. 7, 3.

Banki MR, Gerngross TU, Wood DW. (2005). Novel and economical purification of recombinant proteins: intein-mediated protein purification using in vivo polyhydroxybutyrate (PHB) matrix association. *Protein Science*. 14, 1387–1395.

Benjamini Y, Hochberg Y. (1995). Controlling the false discovery rate: a practical and powerful approach to multiple testing. *J R Stat Soc B* 57: 289–300.

Bergsson G, Arnfinnsson J, Steingrimsson O, Thormar H. (2001). Killing of Gram-positive cocci by fatty acids and monoglycerides. *APMIS.* 109: 670–8.

Bustin M, Catez F, Jae-Hwan L. (2005). The dynamics of histone H1 function in chromatin. *Mol Cell* 17: 617-620.

C.A.L.S Approved standard M07-A8, in: Institute, methods for dilution antimicrobial susceptibility tests for bacteria that grow aerobically, Clinical and Laboratory Standards Institute, Wayne, PA, 2008.

Caserta E, Tomsic J, Spurio R, La Teana A, Pon CL, Gualerzi CO. (2006). Translation initiation factor IF2 interacts with the 30S ribosomal subunit via two separate binding sites. *J Mol Biol* 362: 787-99.

Chen GQ, Wu Q. (2005). The application of polyhydroxyalkanoates as tissue engineering materials. *Biomaterials*. 26: 6565.

Chen GQ. (2009). A microbial polyhydroxyalkanoates (PHA) based bio- and materials industry. *Chem. Soc. Rev.* 38: 2434–2446.

Cornell RJ, Donaruma LG. (1965). 2-Methacryloxytroponones. Intermediates for Synthesis of Biologically Active Polymers. *J. Med. Chem*., 8, 388-390.

Costerton JW, Cheng KJ. (1975). The role of the bacterial cell envelope in antibiotic resistance. *Journal of Antimicrobial Chemotherapy*. 1: 363-377.

Darouiche RO. (2004). Treatment of infections associated with surgical implants. N. *Engl. J. Med.* 350: 1422–1429.

de Eugenio LI, Escapa IF, Morales V, Dinjaski N, Galán B, García JL, Prieto MA. (2010a). The turnover of medium-chain length polyhydroxyalkanoates in *Pseudomonas putida* KT2442 and the fundamental role of PhaZ depolymerase for the metabolic balance. *Environ Microbiol* 12: 207-221.

de Eugenio LI, Galán B, Escapa IF, Maestro B, Sanz JM, García JL, Prieto MA. (2010b). The PhaD regulator controls the simultaneous expression of the *pha* genes involved in polyhydroxyalkanoate metabolism and turnover in *Pseudomonas putida* KT2442. *Environ Microbiol.* 12: 1591-1603.

de Eugenio LI, García P, Luengo JM, Sanz JM, Román JS, García JL, Prieto MA. (2007). Biochemical evidence that phaZ gene encodes a specific intracellular medium chain length polyhydroxyalkanoate depolymerase in Pseudomonas putida KT2442: characterization of a paradigmatic enzyme. *J. Biol. Chem*. 282: 4951-62.

de Lorenzo V, Eltis L, Kessler B, Timmis KN. (1993). Analysis of Pseudomonas gene products using lacIq/Ptrp-lac plasmids and transposons that confer conditional phenotypes. *Gene*. 123: 17-24.

de Lorenzo V, Timmis K. (1994). Analysis and construction of stable phenotypes in gram-negative bacteria with Tn5- and Tn10-derived minitransposons. *Methods in Enzymo.l* 235: 386-405.

Defoirdt T, Boon N, Sorgeloos P, Verstraete W, Bossier P. (2009.) Short-chain fatty acids and poly-β-hydroxyalkanoates: (New) Biocontrol agents for a sustainable animal production. *Biotechnology Advances*. 27: 680–685.

DeLeo FR, Chambers HF. (2009). Reemergence of antibiotic-resistant Staphylococcus aureus in the genomics era. *J. Clin. Invest*. 119: 2464–2474.

Deretic V, Hibler NS, Holt SC. (1992). Immunocytochemical analysis of AlgP (H_p1), a histonelike element participating in control of mucoidy in *Pseudomonas aeruginosa*. *J Bacteriol.* 174: 824-831.

Deretic V, Konyecsni WM. (1990). A prokaryotic regulatory factor with a histone H1-like carboxy-terminal domain: clonal variation of repeats within *algP*, a gene involved in regulation of mucoid in *Pseudomonas aeruginosa*. *J Bacterio.l* 172: 5544-5554.

Dinjaski N, Galan B, Vilches F, Siglez MÁ, Cebolla Á, Arévalo-Rodríguez M, García JL, Prieto MA. (2009). *New Biotechnology (Elsevier).* 25: S76. doi:10.1016/j.nbt.2009.06.327.

Epand RF, Sarig H, Mor A, Epand RM. (2009). Cell-wall interactions and the selective bacteriostatic activity of a miniature oligo-acyl-lysyl. *Biophys J*. 97:2250–2257.

Escapa IF, Morales V, Martino VP, Pollet E, Avérous L, García JL, Prieto MA. (2011). Disruption of β-oxidation pathway in Pseudomonas putida KT2442 to produce new functionalized PHAs with thioester groups, *Appl. Microbiol. Biotechnol.* 89: 1583–1598.

Fasman, G.D. (ed.). (1976). Handbook of biochemistry and molecular biology.Section A. Proteins, 3rd ed., vol. III. CRC Press, Inc., Cleveland, Ohio.

FDA U.S. Department of Health and Human Services, F.D.A. Guidance for Industry, 1997, Rockville, p.54.

Follonier S, Escapa IF, Fonseca PM, Henes B, Panke S, Zinn M, Prieto MA. (2013). New insights on the reorganization of gene transcription in Pseudomonas putida KT2440 at elevated pressure. *Microb. Cell Fact*., 12: 30.

Freitas S, Merkle HP, Gander B. (2005). Microencapsulation by solvent extraction/evaporation: reviewing the state of the art of microsphere preparation process technology. J. *Controlled Release*, 102(2): 313–332.

Furrera P, Panke S, Zinn M. (2007). Efficient recovery of low endotoxin medium-chain-length poly([R]-3-hydroxyalkanoate) from bacterial biomass*, Journal of Microbiological Methods*. 69(1): 206–213.

Galán B, Dinjaski N, Maestro B, de Eugenio LI, Escapa IF, Sanz JM, García JL, Prieto MA. (2011). Nucleoid-associated PhaF phasin drives intracellular location and segregation of polyhydroxyalkanoate granules in Pseudomonas putida KT2442.*Mol. Microbiol.*, 79: 402-18.

Gelman MA, Weisblum B, Lynn DM, Gellman SH. (2004). Biocidal activity of polystyrenes that are cationic by virtue of protonation. *Org Lett.* 6(4): 557–60.

Gerdes K, Howard M, Szardenings F. (2010). Pushing and pulling in prokaryotic DNA segregation. *Cell.* 141: 927-942.

Giacometti A, Cirioni O, Ghiselli R, et al. (2005). Comparative efficacies of quinupristin–dalfopristin, linezolid, vancomycin, and ciprofloxacin in treatment, using the antibiotic-lock technique, of experimental catheterrelated infection due to Staphylococcus aureus. *Antimicrob Agents Chemother.* 49: 4042–5.

Gibney K, Sovadinova I, Lopez AI, Urban M, Ridgway Z, Caputo GA, Kuroda K. (2012). Poly(ethylene imine)s as antimicrobial agents with selective activity. *Macromol Biosci*. 12: 1279–1289.

Gitai Z, Thanbichler M, Shapiro L. (2005). The choreographed dynamics of bacterial chromosomes. *Trends Microbiol.* 13: 221-228.

Gomes ME, Reis RL. (2004). *Int. Mater*. Rev. 49: 261.

Goyard S. (1996). Identification of BpH2, a novel histone H1 homolog in *Bordetella pertussis*. *J Bacteriol.* 178: 3066-3071.

Grage K, Jahns AC, Parlane N, Palanisamy R, Rasiah IA, Atwood JA, Rehm BH. (2009). Bacterial polyhydroxyalkanoate granules: biogenesis, structure, and potential use as nano-/micro-beads in biotechnological and biomedical applications. *Biomacromolecules.* 13: 660-669.

Grande D, Renard E, Babinot J, Ramier J, Langlois V, Harnessing Biopolyesters in the Design of Functional and Nanostructured Architectures, Book: Degradable Polymers and Materials: Principles and Practice (2nd Edition), Chapter 12, pp 187–199, Chapter DOI: 10.1021/bk-2012-1114.ch012, ACS Symposium Series, Vol. 1114, ISBN13: 9780841228221eISBN: 9780841228238, 14, 2012 American Chemical Society.

Griebel R, Smith Z, Merrick JM. (1968). Metabolism of poly-beta-hydroxybutyrate. I. Purification, composition, and properties of native poly-beta-hydroxybutyrate granules from Bacillus megaterium. *Biochemistry*. 7: 3676-3681.

Grundmann H, Aires-de-Sousa M, Boyce J, Tiemersma E. (2006). Emergence and resurgence of meticillin-resistant Staphylococcus aureus as a public-health threat. *Lancet.* 368: 874–85.

Hancock REW, Chapple DS. (1999). Peptide antibiotics. *Antimicrob Agents Chemother.* 43(6): 1317–23.

Hazer DB, Kılıçay E, Hazer B. (2012). Poly(3-hydroxyalkanoate)s: Diversification and biomedical applications A state of the art review. *Materials Science and Engineering* C 32: 637–647.

Herrero M, de Lorenzo V, Timmis KN. (1990). Transposon vectors containing non-antibiotic resistance selection markers for cloning and stable chromosomal insertion of foreign genes in gram-negative bacteria. *J. Bacteriol*. 172: 6557-67.

Huang CB, George BJ, Ebersole L. (2010). Antimicrobial activity of n-6, n-7 and n-9 fatty acids and their esters for oral microorganisms. *Archives of Oral Biology* 55 555 – 560.

Hugo WB,. Longworth AR. (1966). The effect of chlorhexidine on the electrophoretic mobility, cytoplasmic constituents, dehydrogenase activity and cell walls of Escherichia coli and Staphylococcus aureus, *Journal of Pharmacy and Pharmacology*. 18: 569-578.

Huijberts GN, Eggink G, de Waard P, Huisman GW, Witholt B. (1992). Pseudomonas putida KT2442 cultivated on glucose accumulates poly(3-hydroxyalkanoates) consisting of saturated and unsaturated monomers. *Appl Environ Microbiol.* 58(2):536–544.

Ihssen J, Magnani D, Thöny-Meyer L, Ren Q. (2009). Use of extracellular medium chain length polyhydroxyalkanoate depolymerase for targeted binding of proteins to artificial poly[(3-hydroxyoctanoate)-co-(3-hydroxyhexanoate)] granules. *Biomacromolecules*. 10: 1854-64.

Ikeda T, Ledwith A, Bamford CH, Hann RA. (1984). Interaction of a polymeric biguanide biocide with phospholipid membranes. *BBA – Biomembranes*. 769: 57-66.

Jendrossek D. (2009). Polyhydroxyalkanoate granules are complex subcellular organelles (carbonosomes). *J Bacteriol*. 191(10): 3195-202.

Jenssen H, Hamill P, Hancock REW. (2006). *Peptide Antimicrobial Agents, CLINICAL MICROBIOLOGY REVIEWS,* 19(3): 491–511.

Ji Y, Li XT, Chen GQ. (2008). Interactions between a poly (3-hydroxybutyrate-co-3-hydroxyvalerate-co-3-hydroxyhexanoate) terpolyester and human keratinocytes. *Biomaterials.* 29: 3807–17.

Johnson WCJr. (1988). Secondary structure of proteins through circular dichroism spectroscopy. *Annu Rev Biophys Biophys Chem.* 17: 145-166.

Kaniga K, Delor I, Cornelis GR. (1991). A wide-host-range suicide vector for improving reverse genetics in gram-negative bacteria: inactivation of the *blaA* gene of *Yersinia enterocolitica*. *Gene.* 109: 137-141.

Kasinsky H, Lewis J, Dacks J, Ausio J. (2001). Origin of H1 linker histones. *FASEB J.* 15: 34-42.

Kato J, Tapan M, Chakrabarty AM. (1990). AlgR3, a protein resembling eukaryotic histone H1, regulates alginate synthesis in *Pseudomonas aeruginosa*. *Proc Natl Acad Sci USA.* 87: 2887-2891.

Kaul R, Allen M, Bradbur EM, Wenman WM. (1996). Sequence specific binding of chlamydial histone H1-like protein. *Nucleic Acid Res.* 24: 2981-2989.

Kenawy ER, Abdel-Hay FI, El-Raheem A, El-Shanshoury R, El-Newehy MH. (1998). *J Controlled Release.* 50(1–3): 145–52.

Kenawy ER, Abdel-Hay FI, El-Shanshoury AERR, El-Newehy MH, (2002). Biologically active polymers. V. Synthesis and antimicrobial activity of modified poly(glycidyl methacrylate-co-2-hydroxyethyl methacrylate) derivatives with quaternary ammonium and phosphonium salts, Journal of Polymer Science, Part A: *Polymer Chemistry*. 40: 2384-2393.

Kiedrowski MR, Horswill AR. (2011). New approaches for treating staphylococcal biofilm infections. *Annals of the New York Academy of Sciences*. 1241: 104–121.

Kimberly NC, Gitai Z. (2010). Surface association and the MreB cytoskeleton regulate pilus production, localization and function in *Pseudomonas aeruginosa*. *Mol Microbiol.* 76: 1411-1426.

Klein E, Smith DL, (2009). Ramanan Laxminarayan Emerging Infectious Diseases, Vol. 15, No. 12, December Community-associated Methicillin-Resistant Staphylococcus aureus in Outpatients, United States,1999–2006

Kojima M, Morisaki T, Izuhara K, Uchiyama A, Matsunari Y, Katano M, Tanaka M. (2000). Lipopolysaccharide increases cyclo-oxygenase-2 expression in a colon carcinoma cell line through nuclear factor-kB activation. *Oncogene.* 19: 1225-1231.

Komeili A, Li Z, Newman DK, Jensen GJ. (2006). Magnetosomes are cell membrane invaginations organized by the actin-like protein MamK. *Science.* 311: 242-245.

Koyama Y, Katagiri S, Hanai S, Uchida K, Miwa M. (1999). Poly (ADP-ribose) polymerase interacts with novel ribosomal proteins, L22 and L23a, with a unique histone-like amino-terminal extensions. *Gene.* 226: 339-345.

Kundu K, Knight SF, Willett N, Lee S, Taylor WR, Murthy N. (2009). Hydrocyanines: a class of fluorescent sensors that can image reactive oxygen species in cell culture, tissue, and in vivo. *Angew Chem Int Ed Engl*. 48(2): 299-303.

Kuroda K,. Caputo GA. (2013). Antimicrobial polymers as synthetic mimics of host-defense peptides. *WIREs Nanomed Nanobiotechnol*. 5: 49–66.

Lee SB, Koepsel RR, Morley SW, Matyjaszewski K, Sun YJ, Russell AJ. (2004). Permanent, nonleaching antibacterial surfaces. 1. Synthesis by atom transfer radical polymerization. *Biomacromolecules*. 5(3): 877–82.

Lee SJ, Park JP, Park TJ, Lee SY, Lee S, Park JK. (2005). Selective immobilization of fusion proteins on poly(hydroxyalkanoate) microbeads. *Anal Chem*. 77: 5755-9.

Lewis JG, Rehm BHJ. (2009). ZZ polyester beads: an efficient and simple method for purifying IgG from mouse hybridoma supernatants. *Immunol. Methods*. 346: 71-4.

Lienkamp K, Madkour AE, Musante A, Nelson CF, Nusslein K, Tew GN. (2008). Antimicrobial polymers prepared by ROMP with unprecedented selectivity: a molecular construction kit approach. *J Am Chem Soc*. 130: 9836–9843.

Lin PW, Myers LE, Ray L, Song SC, Nasr TR, Berardinelli AJ, et al. (2009). Lactobacillus rhamnosus blocks inflammatory signaling in vivo via reactive oxygen species generation. *Free Radic Biol Med*. 47(8): 1205-11.

Lu G, Wu D, Fu R. (2007). Studies on the synthesis and antibacterial activities of polymeric quaternary ammonium salts from dimethylaminoethyl methacrylate, *Reactive and Functional Polymers.* 67: 355-366.

Madison LL, Huisman GW. (1999). Metabolic engineering of poly (3-hydroxyalkanoates): from DNA to plastic. *Microbio Mol Biol Rev.* 63: 21-53.

Maehara A, Taguchi S, Nishiyama T, Yamane T, Doi Y. (2002). A repressor protein, PhaR, regulates polyhydroxyalkanoate (PHA) synthesis via its direct interaction with PHA. *J Bacteriol.* 184: 3992-4002.

Maestro B, Galán B, Alfonso C, Rivas G, Prieto MA, Sanz JM. (2013). A new family of intrinsically disordered proteins: structural characterization of the major phasin PhaF from Pseudomonas putida KT2440. *PLoS One*. 8: 56904.

Mah TF, O'Toole GA. (2001). Mechanisms of biofilm resistance to antimicrobial agents. *Trends Microbiol*. 9:34.

Maria D, Hernandez MD, Mohammad D, Mansouri MS, Saima Aslam MD, Barry Zeluff MD, Rabih O, Darouiche MD. (2009). Efficacy of Combination of N-acetylcysteine, Gentamicin, and Amphotericin B for Prevention of Microbial Colonization of Ventricular Assist Devices infection control and hospital epidemiology. 30: 2.

Martínez V, García P, García JL, Prieto MA. (2011). Controlled autolysis facilitates the polyhydroxyalkanoate recovery in Pseudomonas putida KT2440. *Microbial Biotechnology.* 4: 533–547.

Mauclaire L, Brombacher E, Bünger JD, Zinn M. (2010). Factors controlling bacterial attachment and biofilm formation on medium-chain-length polyhydroxyalkanoates (mcl-PHAs). *Colloids and Surfaces B: Biointerfaces*. 76: 104–111.

McCool GJ, Cannon MC. (1999). Polyhydroxyalkanoate inclusion body-associated proteins and coding region in *Bacillus megaterium*. *J Bacteriol.* 181: 585-592.

Medvedkin VN, Permyakov EA, Klimenko LV, Mitin YV, Matsushima N, Nakayama S, Kretsinger RH. (1995). Interactions of (Ala*Ala*Lys*Pro)n and (Lys*Lys*Ser*Pro)n

with DNA. Proposed coiled-coil structure of AlgR3 and AlgP from *Pseudomonas aeruginosa*. *Protein Eng.* 8: 63-70.

Miller WG, Lindow SE. (1997). An improved GFP cloning cassette designed for prokaryotic transcriptional fusions. *Gene.* 191: 149-153.

Moldes C, Farinós GP, de Eugenio LI, García P, García JL, Ortego F, Hernández-Crespo P, Castañera P, Prieto MA. (2006). *Appl. Microbiol. Biotechnol.* 72: 88-93.

Moldes C, García P, García JL, Prieto MA. (2004). *In vivo* immobilization of fusion proteins on bioplastics by the novel tag BioF. *Appl Environ Microbiol.* 70: 3205-3012.

Moldes C. (2003). Desarrollo de nuevos sistemas para la producción de proteínas de fusión por fermentación. PhD Thesis. In: Departamento de Microbiología II. Madrid: Universidad Complutense de Madrid (UCM).

Moscoso M, García E, López R. (2006). Biofilm formation by Streptococcus pneumoniae: role of choline, extracellular DNA, and capsular polysaccharide in microbial accretion. *Bacterio*l. 188(22): 7785-95.

Mosmann T. (1983). Rapid colorimetric assay for cellular growth and survival: application to proliferation and cytotoxicity assays. *Journal of Immunological Methods*. 65: 55-63.

Nakayama GR, Caton MC, Nova MP, Parandoosh Z. (1997). Assessment of the Alamar Blue assay for cellular growth and viability in vitro. *J Immunol Methods*. 204: 205–208.

Nelson KE, Weinel C, Paulsen IT, Dodson RJ, Hilbert H, Martins dos Santos VAP, *et al*. (2002). Complete genome sequence and comparative analysis of the metabolically versatile *Pseudomonas putida* KT2440. *Environ Microbiol.* 4: 799–808.

Neumann L, Spinozzi F, Sinibaldi R, Rustichelli F, Pötter M, Steinbüchel A. (2008). Binding of the major phasin, PhaP1, from *Ralstonia eutropha* H16 to poly (3-hydroxybutyrate) granules. *J Bacteriol.* 190: 2911-2919.

Niki H, Yamaichi Y, Hiraga S. (2000). Dynamic organization of chromosomal DNA in *Escherichia coli*. *Genes Dev.* 14: 212–223.

Nogales J, Palsson BØ, Thiele I. (2008). A genome-scale metabolic reconstruction of Pseudomonas putida KT2440: iJN746 as a cell factory. *BMC Syst. Biol*., 2: 79.

O'Leary ND, O'Connor KE, Ward P, Goff M, Dobson AD. (2005). Genetic characterization of accumulation of polyhydroxyalkanoate from styrene in *Pseudomonas putida* CA-3. *Appl Environ Microbiol.* 71: 4380-4387.

Olivera ER, Carnicero D, Jodra R,Miñambres B, García B, Abraham GA, Gallardo A, Román JS, García JL, Naharro G, Luengo JM. (2001). Genetically engineered Pseudomonas: a factory of new bioplastics with broad applications. *Environ Microbiol.* 3(10): 612–618.

Olofsson AC, Hermansson M, Elwing H. (2003). N-acetyl-l-cysteine affects growth, extracellular polysaccharide production, and bacterial biofilm formation on solid surfaces. *Appl Environ Microbiol*. 69: 4814–22.

Parlane NA, Wedlock DN, Buddle BM, Rehm, BH. (2009). Bacterial polyester inclusions engineered to display vaccine candidate antigens for use as a novel class of safe and efficient vaccine delivery agents. *Appl. Environ. Microbiol*. 75: 7739-44.

Perez-Giraldo C, Rodriguez-Benito A, Moran FJ, Hurtado C, Blanco MT, Gomez-Garcia AC. (1997). Influence of N-acetylcysteine on the formation of biofilm by Staphylococcus epidermidis. *J Antimicrob Chemother*. 39: 643–6.

Pernak J, Sobaszkiewicz K, Mirska I. (2003). Anti-microbial activities of ionic liquids. *Green Chemistry*. 5: 52-56.

Peters V,Rehm BH. (2006). In vivo enzyme immobilization by use of engineered polyhydroxyalkanoate synthase. *Appl. Environ. Microbiol*. 72: 1777-83.

Pieper-Fürst U, Madkour MH, Mayer F, Steinbüchel A. (1995). Identification of the region of a 14-kilodalton protein of *Rhodococcus ruber* that is responsible for the binding of this phasin to polyhydroxyalkanoic acid granules. *J Bacteriol* 177: 2513–2523.

Poblete-Castro I, Becker J, Dohnt K, dos Santos VM, Wittmann C. (2012). Industrial biotechnology of Pseudomonas putida and related species. *Appl. Microbiol. Biotechnol.* 93: 2279-90.

Poblete-Castro I, Binger D, Rodrigues A, Becker J, Martins Dos Santos VA, Wittmann C. (2013). Poblete-Castro I, Binger D, Rodrigues A, Becker J, Martins Dos Santos VA, Wittmann C. (2013). Metab. Eng. 15: 113-23. *Metab. Eng*. 15: 113-23.

Poblete-Castro I, Escapa IF, Jäger C, Puchalka J, Lam CM, Schomburg D, Prieto MA, Martins dos Santos VA. (2012). The metabolic response of P. putida KT2442 producing high levels of polyhydroxyalkanoate under single- and multiple-nutrient-limited growth: highlights from a multi-level omics approach. *Microb. Cell. Fact*. 11: 34.

Popa A, Davidescu CM, Trif R, Ilia G, Iliescu S, Dehelean G. (2003). *React Funct Polym*. 55(2): 151–8.

Prieto MA, Bühler B, Jung K, Witholt B, Kessler B. (1999). PhaF, a polyhydroxyalkanoate-granule-associated protein of *Pseudomonas oleovorans* GPo1 involved in the regulatory expression system for *pha* genes. *J Bacteriol.* 181: 858-68.

Raafat D, von Bargen K, Haas A, Sahl H-G. (2008). Insights into the mode of action of chitosan as an antibacterial compound. *Appl Environ Microbiol*, 74: 3764–3773.

Raygada JL, Levine DP. (2009). "Managing CA-MRSA Infections: Current and Emerging Options". *Infections in Medicine.* 26 (2).

Rehm BH. (2006.) Genetics and biochemistry of polyhydroxyalkanoate granule self-assembly: The key role of polyester synthases. *Biotechnol Lett* 28: 207-213.

Reusch RN. (2000). Transmembrane ion transport by polyphosphate–poly-(R)-3-hydroxybutyrate complexes. *Biochem. Engl. Trans*. 65: 280–295.

Ruth K, Grubelnik A, Hartmann R, Egli T, Zinn M, Ren Q. (2007). Efficient production of (R)-3-hydroxycarboxylic acids by biotechnological conversion of polyhydroxyalkanoates and their purification. *Biomacromolecules*, 8(1): 279-86.

Ruth K, de Roo G, Egli T, Ren Q. (2008). Identification of two acyl-CoA synthetases from Pseudomonas putida GPo1: one is located at the surface of polyhydroxyalkanoates granules. *Biomacromolecules*. 9: 1652-1659.

Rutherford DR, Hammer WJ, Babu GN. (1997). Poly(β-hydroxyorganoate) pressure sensitive adhesive compositions, U.S. Patent 5614576, Fecha de presentación: 3 Feb 1992

Saad B, Neuenschwander P, Uhlschmid GK, Suter UW. (1999). New versatile, elastomeric, degradable polymeric materials for medicine. *Intern J Biol Macromol*. 25: 293-301.

Sambrook J, Russell DW. (2001). *Molecular Cloning. A Laboratory Manual*. Cold Spring Harbor, NY, USA: CSHL Press.

Sandoval A, Arias-Barrau E, Bermejo F, Cañedo L, Naharro G, Olivera ER, Luengo JM. (2005). Production of 3-hydroxy-n-phenylalkanoic acids by a genetically engineered strain of Pseudomonas putida. *Appl. Microbiol. Biotechnol*. 67(1): 97-105.

Schäfer A, Tauch A, Jäger W, Kalinowski J, Thierbach G. Pühler A. (1994). Small mobilizable multi-purpose cloning vectors derived from the Escherichia coli plasmids pK18 and pK19: selection of defined deletions in the chromosome of Corynebacterium glutamicum. *Gene.*, 145: 69-73.

Scheffel A, Gruska M, Faivre D, Linaroudis A, Plitzko JM, and Schuler D. (2006). An acidic protein aligns magnetosomes along a filamentous structure in magnetotactic bacteria. *Nature.* 440: 110-114.

Schirmer A, Jendrossek D. (1994). Molecular characterization of the extracellular poly(3-hydroxyoctanoic acid) [P(3HO)] depolymerase gene of Pseudomonas fluorescens GK13 and of its gene product. *J. Bacteriol.* 176: 7065–7073.

Schmidt HHHW, Kelm M. (1996). Determination of nitrite and nitrate by the Griess reaction, *Methods in Nitric Oxide Research.* 491-497.

Scholz C. (2010). Perspectives to produce positively or negatively charged polyhydroxyalkanoic acids. *Appl Microbiol Biotechno.l* 88(4): 829–837.

Scholz C, Wolk S, Lenz RW, Fuller RC. (1994). Growth and polyester production by Pseudomonas oleovorans on branched octanoic acid substrates. *Macromolecules* 27(22): 6358–6362.

Scopes RK. (1974). Measurement of protein by spectrophotometry at 205 nm. *Anal Biochem.* 59: 277-82.

Selvam S, Kundu K, Templeman KL, Murthy N, García AJ. (2011). Minimally invasive, longitudinal monitoring of biomaterial-associated inflammation by fluorescence imaging. *Biomaterials*. 32: 7785-7792.

Sherris JC. Staphylococci. In: Sherris JC, editor. Medical Microbiology. An Introduction to Infectious Diseases. New York: Elsevier Science Publishing Co., Inc., 1990:275–89.

Siedenbiedel F, Tiller JC. (2012). Antimicrobial Polymers in Solution and on Surfaces: Overview and Functional Principles. *Polymers*. 4: 46-71.

Silva-Queiroz SR, Silva LF, Pradella JG, Pereira EM, Gomez JG. (2009). PHA(MCL) biosynthesis systems in Pseudomonas aeruginosa and Pseudomonas putida strains show differences on monomer specificities. *J. Biotechnol.*, 143: 111-8.

Silva-Rocha R, Martínez-García E, Calles B, Chavarría M, Arce-Rodríguez A, de Las Heras A, Páez-Espino AD, Durante-Rodríguez G, Kim J, Nikel PI, Platero R, de Lorenzo V. (2013). *Nucleic Acids Res*., 41(Database issue):D666-75.

Smyth GK, Speed T. (2003). Normalization of cDNA microarray data. *Methods* 31: 265–273.

Smyth GK. (2004). Linear models and empirical Bayes methods for assessing differential expression in microarray experiments. *Stat Appl Genet Mol Biol* 3: Article 3.

Sodian R, Hoerstrup SP, Sperling JS, Daebritz S, Martin DP, Moran AM, Kim BS, Schoen FJ, Vacanti JP, Mayer JE. (2000). Early in vivo experience with tissue-engineered trileaflet heart valves. *Circulation*. 102(Suppl.):22–9.

Sodian R, Hoerstrup SP, Sperling JS, Daebritz SH, Martin DP, Schoen FJ, Vacanti JP, Mayer JE. (2000). Tissue engineering of heart valves: in vitro experiences. *Ann Thorac Surg*. 70: 140–4.

Sodian R, Hoerstrup SP, Sperling JS, Martin DP, Daebritz S, Mayer Jr JE, Vacanti JP. (2000). Evaluation of biodegradable, threedimensional matrices for tissue engineering of heart valves. *ASAIO J.* 46: 107–10.

Sodian R, Loebe M, Hein A, Martin DP, Hoerstrup SP, Potapov EV, Hausmann H, Lueth T, Hetzer R. (2002). Application of stereolithography for scaffold fabrication for tissue engineered heart valves. *ASAIO J*. 48: 12–6.

Sodian R, Sperling JS, Martin DP, Egozy A, StockU, Mayer Jr JE, Vacanti JP. (2000). Fabrication of a trileaflet heart valve scaffold from a polyhydroxyalkanoate biopolyester for use in tissue engineering. *Tissue Eng*. 6: 183–8.

Steinbuchel A, Aerts K, Babel W, Follner C, Liebergesell M, Madkour MH, Mayer F, Pieper-Furst U, Pries A, Valentin HE. (1995). Considerations on the structure and biochemistry of bacterial polyhydroxyalkanoic acid inclusions. *Can J Microbio* 41: 94-105.

Steinbüchel A, Hein S. (2001). Biochemical and molecular basis of microbial synthesis of polyhydroxyalkanoates in microorganisms. *Adv Biochem Eng Biotechnol.* 71: 81-123.

Steinbuchel A, Valentin HE. (1995). Diversity of bacterial poly-hydroxyalkanoic acids, *FEMS Microbiol*. Lett. 128:219–228.

Stock UA, Nagashima M, Khalil PN, Nollert GD, Herden T, Sperling JS, Moran A, Lien J, Martin DP, Schoen FJ, Vacanti JP, Mayer Jr JE. (2000). Tissue-engineered valved conduits in the pulmonary circulation. *J Thorac Cardiovasc Surg*. 119: 732–40.

Tashiro T. (2001). *Macromol Mater Eng*. 286(2):63–87.

Teleman AA, Graumann PL, Lin DC, Grossman AD, Losick R. (1998). Chromosome arrangement within a bacterium. *Curr Biol.* 8: 1102–1109.

Tian, J., Sinskey, A.J., and Stubbe, J. (2005) Kinetic studies of polyhydroxybutyrate granule formation in *Wautersia eutropha* H16 by transmission electron microscopy. *J Bacteriol* 187: 3814-3824.

Tiller JC, Liao CJ, Lewis K, Klibanov AM. (2001). Designing surfaces that kill bacteria on contact. *Proc Natl Acad Sci USA*. 98(11):5981–5.

Timm A, Steinbüchel A. (1992). Cloning and molecular analysis of the poly (3-hydroxyalkanoic acid) gene locus of *Pseudomonas aeruginosa* PAO1. *Eur J Biochem.* 209: 15-30.

Timofeeva L, Kleshcheva N. (2011). Antimicrobial polymers: mechanism of action, factors of activity, and applications. *Appl Microbiol Biotechnol.* 89: 475–492.

Toy KE, Zhou H, Stephanopoulos GN. (2006). High-throughput screen for poly-3-hydroxybutyrate in *Escherichia coli* and *Synechocystis* sp. strain PCC6803. *Appl Environ Microbio.l* 72: 3412-3417.

Valentin HE, Stuart ES, Fuller RC, Lenz RW, Dennis D. (1998). Investigation of the function of proteins associated to polyhydroxyalkanoate inclusions in *Pseudomonas putida* BMO1. *J Biotechnol*. 64: 145-157.

Viollier PH, Thanbichler M, McGrath PT, West L, Meewan M, McAdams HH, Shapiro L. (2004). Rapid and sequential movement of individual chromosomal loci to specific subcellular locations during bacterial DNA replication. *Proc Natl Acad Sci USA* 101: 9257-9262.

Wang SY, Lan XY, Xiao JH, Yang JC, Kao YT, Chang ST. (2008). Antiinflammatory activity of Lindera erythrocarpa fruits, *Phytotherapy Research.* 22: 213-216.

Wang Y, Bian YZ, Wu Q, Chen GQ. (2008). Evaluation of three-dimensional scaffolds prepared from poly(3-hydroxybutyrate-co-3-hydroxyhexanoate) for growth of allogeneic chondrocytes for cartilage repair in rabbits. *Biomaterials.* 29:2858–68.

Wang YW, Yang F, Wu Q, Cheng YC, Peter HF, Chen JC, et al. (2005). Effect of composition of poly(3-hydroxybutyrate-co-3-hydroxyhexanoate) on growth of fibroblast and osteoblast. *Biomaterials*. 26:755–61.

Wang Z, Wu H, Chen J, Zhang J, Yao Y, Chen GQ. (2008). A novel self-cleaving phasin tag for purification of recombinant proteins based on hydrophobic polyhydroxyalkanoate nanoparticles. *Lab Chip*., 8, 1957-62.

Waschinski CJ, Herdes V, Schueler F, Tiller JC. (2004). Influence of satellite groups on telechelic antimicrobial functions of polyoxazolines. *Macromol Biosci.*5(2):149–56.

Waschinski CJ, Tiller JC. (2005). Poly(oxazoline)s with telechelic antimicrobial functions. *Biomacromolecules.*6(1):235–43.

Wieczorek, R., Pries, A., Steinbüchel, A., and Mayer, F. (1995) Analysis of a 24-kilodalton protein associated with the polyhydroxyalkanoic acid granules in *Alcaligenes eutrophus*. *J Bacteriol* 177: 2425-2435.

Wiggam MI, O'Kane MJ, Harper R, Atkinson AB, Hadden DR, Trimble ER, Bell PM. (1997). Treatment of diabetic ketoacidosis using normalization of blood 3-hydroxy-butyrate concentration as the endpoint of emergency management, *Diabetes Care.* 20: 1347–1352.

Williams SF, Martin DP, Horowitz DM, Peoples OP. (1999). PHA applications: addressing the price performance issue I. Tissue engineering, *International Journal of Biological Macromolecules.* 25: 111–121.

Williams SF, Martin DP, Skraly FA. (2000). Medical devices and application of polyhydroxyalkanoate polymers. US Patent Appl 535146,

Wise DL, Trantolo DJ, Altobelli DE, Yaszemski MJ, Gresser JD, Schwartz ER, (1998). Encyclopaedic Handbook of Biomaterials and Bioengineering, Part A: Materials. New York: Marcel Dekker. 269–304.

Witholt B, Kessler B. (1999). Perspectives of medium chain length poly(hydroxyalkanoates), a versatile set of bacterial bioplastics. *Curr Opin Biotechnol.* 10(3): 279–285.

Worley SD, Sun G. (1996). *Trends Polym Sci*. 4(11): 364–70.

Xiao XQ, Zhao Y, Chen GQ. (2007). The effect of 3-hydroxybutyrate and its derivatives on the growth of glial cells. *Biomaterials*. 28: 3896–903.

Xu XY, Li XT, Peng SW, Xiao JF, Liu C, Fang G, Chen KC, Chen GQ. (2010). The behaviour of neural stem cells on polyhydroxyalkanoate nanofiber scaffolds. *Biomaterials*. 31(14): 3967-75.

Yang YH, Dudoit S, Luu P, Lin DM, Peng V, Ngai J, Speed TP. (2002). Normalization for cDNA microarray data: a robust composite method addressing single and multiple slide systematic variation. *Nucl Acids Res* 30:e15.

Yao YC, Zhan XY, Zhang J, Zou XH, Wang ZH, Xiong YC, Chen J,Chen GQ. (2008). A specific drug targeting system based on polyhydroxyalkanoate granule binding protein PhaP fused with targeted cell ligands. *Biomaterials*. 29: 4823-30.

Yuste L, Hervas AB, Canosa I, Tobes R, Jimenez JI, Nogales J, Perez-Perez MM, Santero E, Diaz E, Ramos JL, de Lorenzo V, Rojo F. (2006). Growth phase-dependent expression of the *Pseudomonas putida* KT2440 transcriptional machinery analyzed with a genome-wide DNA microarray. *Environ Microbiol* 8: 165–177.

Zasloff M. (2002). Antimicrobial peptides of multicellular organisms. *Nature*. 415(6870): 389–95.

Zlatanova J, Caiafa P, van Holde K. (2000). Linker histone binding and displacement: versatile mechanism for transcriptional regulation. *FASEB J* 14: 1697-1704.